Purdue University
Purdue e-Pubs

Open Access Dissertations | Theses and Dissertations

2013

Neuroprotection by Chitosan and Chitosan Nanoparticles

Bojun Chen
Purdue University

Follow this and additional works at: https://docs.lib.purdue.edu/open_access_dissertations

 Part of the Neuroscience and Neurobiology Commons

Recommended Citation
Chen, Bojun, "Neuroprotection by Chitosan and Chitosan Nanoparticles" (2013). *Open Access Dissertations*. 208.
https://docs.lib.purdue.edu/open_access_dissertations/208

This document has been made available through Purdue e-Pubs, a service of the Purdue University Libraries. Please contact epubs@purdue.edu for additional information.

Graduate School ETD Form 9
(Revised 12/07)

PURDUE UNIVERSITY
GRADUATE SCHOOL
Thesis/Dissertation Acceptance

This is to certify that the thesis/dissertation prepared

By BOJUN CHEN

Entitled
NEUROPROTECTION BY CHITOSAN AND CHITOSAN NANOPARTICLES

For the degree of Doctor of Philosophy

Is approved by the final examining committee:

Jianming Li	Co-chair	Linjie Pan	
Chair			
Richard Ben Borgens	Co-chair		
Stephen R. Byrn			
Youngnam Cho			

To the best of my knowledge and as understood by the student in the *Research Integrity and Copyright Disclaimer (Graduate School Form 20)*, this thesis/dissertation adheres to the provisions of Purdue University's "Policy on Integrity in Research" and the use of copyrighted material.

Approved by Major Professor(s): Richard Ben Borgens

Approved by: Laurie Jaeger 12/02/2013
Head of the Graduate Program Date

NEUROPROTECTION BY CHITOSAN AND CHITOSAN NANOPARTICLES

A Dissertation

Submitted to the Faculty

of

Purdue University

by

Bojun Chen

In Partial Fulfillment of the

Requirements for the Degree

of

Doctor of Philosophy

December 2013

Purdue University

West Lafayette, Indiana

This dissertation is dedicated to Christos Deligkaris, my parents, my grandparents, Alexis Chen, and Teddy.

ACKNOWLEDGMENTS

I express my gratitude to my major professor Dr. Richard B. Borgens. He gave me the opportunity to study and work at Purdue University. I appreciate his advice and support all these years. His enthusiasm, knowledge and constructive discussions inspired me and helped me to develop as a scientist. I appreciate the critical feedback on experimental designs and data analysis Dr. Li provided as my co-advisor. I thank Dr. Youngnam Cho for introducing me into the frontier field of Nano-Medicine. Special thanks to my committee members: Drs. Stephen Byrn and Linjie Pan for their constant support and willingness to help. I thank all of the members at Center for Paralysis Research, Debbie Bohnert, John Cirillo, Jennifer Danaher, Wen Gao, Judy Grimmer, Andrew Marquis, Elaine Mihelc, Michel Schweinsberg, for their friendliness, technical support and constant help during my graduate work. Finally, I thank Gloria, Graduate Coordinate of the Department of Basic Medical Sciences, for all of the help that she provided during these years.

TABLE OF CONTENTS

Page

Page

Page

Page

LIST OF TABLES

LIST OF FIGURES

Figure Page

Figure Page

Figure Page

Figure Page

Figure Page

Figure Page

ABBREVIATIONS

4-AP	4-Aminopyridine
AANS	The American Association of Neurological Surgeons
AFM	Atomic Force Microscopy
AP	Action Potential
AMP	Adenosine monophosphate
BDNF	Brain Derived Neurotrophic Factor
CAP	Compound Action Potential
Chi	Chitosan
Chi-DSNPs	Chitosan DextranSulfate Nanoparticles
Chi-TPPNPs	Chitosan Triphosphate Nanoparticles
Chi-NPs	Chitosan Nanoparticles
CNS	Central Nervous System
CSPG	Proteolycans Chondroitin Sulphate Proteoglycan
CTM	Cutaneous Trunci Muscle
DA	Degree of Acetylation
dbc-AMP	dibutyryl-cyclic Adenosine Monophosphate
DOPS	Dioleoyl phosphatidylserine
DPhPC	Diphytanoyl phosphatidylcholine
DPPC	Dipalmitoyl phosphatidylcholine
DNA	Deoxyribonucleic Acid
EPO	Erythropoetin
FBS	Fetal Bovine Serum
FDA	Food and Drug Administration
FITC	Fluorescein Isothiocyante

GAG	Glycosaminoglycan
rGCS	r-Glutamylcysteine Synthetase
GFAP	Glial Fibrillary Acidic Protein
GSHPx	Glutathione Peroxidase
HA	Hyaluronic Acid
LDH	Lactate Dehydrogenase
LPO	Lipid Peroxidation
MW	Molecular Weight
MP	Methylprednisolone
MS	Multiple Sclerosis
NAD	Nicotinamide Adenine Dinucleotide
NASCIS	The National Acute Spinal Cord Injury Studies
NGF	Nerve Growth Factor
NMDA	N-Methyl-D-Aspartate
NT3	Neurotrophin-3
P188	Poloxamer 188
PA	Phsphatidic Acid
PACUC	Purdue Univeristy Animal Care and Use Committee
PEO	Poly(ethylene oxide)
PEG	Polyethylene Glycol
PBCA	Poly(butyl cyanoacrylate)
PBS	Phosphate buffer saline
PLGA	Poly-Lactic-co-Glycolic Acid
PNS	Peripheral Nervous System
PPO	Poly(propylene oxide)
PSiNPs	PEG-Silica Nanoparticles
PtdCho	Phosphatidylcholine
PtdEtn	Phosphatidylethanolamine
PtdIns	Phsphatidylinsitol

PtdSer	Phosphatidylserine
ROS	Reactive Oxygen Species
SOD	Superoxide Dismutase
SCI	Spinal Cord Injury
SEM	Scanning Electron Microscope
SEMA3	Secreted Protein Semaphoring 3
SP	Surface Pressure
SSEP	Somatosensory Evoked Potential
TEOS	Tetraethyl Orthosilicate
TEM	Transmission Electron Microscopy
TMR	Tetramethylrhodamine
TPA	3-(Trimethoxysilyl) propyl aldehyde
v/v	volume/volume
v/w	volume/weight
XPS	X-ray Photoelectron Spectroscopy

ABSTRACT

Chen, Bojun Ph.D., Purdue University, December 2013. Neuroprotection by Chitosan and Chitosan Nanoparticles. Major Professor: Richard B. Borgens.

In the U.S., about 200,000 people are currently living with spinal cord injury (SCI). An estimated of 50%-70% of all SCI cases occurs in the range of ages between 15-35 years old. The destructive neurotrauma results in the majority of adult disability, even after patients suffering with SCI survived from the acute death. There are two stages involved in the progression of SCI, the primary stage and the secondary stage. The primary stage is mainly the mechanical damage to the central nervous system. The rapid collapse of the integrity of cell membrane and tissue is often one of the initial onsets. Centered by the cascade of biochemical disruption, such as aldehyde toxins, the secondary injury is responsible for the major clinical deficits in sensory and motor functions. Available pharmacological treatment for SCI includes high doses of steroids. However, the side effects of steroid therapy leave patients more susceptible for complications, such as infections, chronic pain and blood clots. The absence of "standard of care" have triggered waves of intense research leading to "finding a cure for SCI". Based on our previous successful explorations of the neuroprotection by chitosan and chitosan nanoparticles (Chi-NPs) in SCI related cell and tissue studies, we further investigated the neuroprotective effects based on two major characteristics of chitosan: (1) molecular weight (MW) and (2) degree of acetylation (DA). Our results demonstrated that chitosan polymer blocked the random exchange of a probe, tetramethyl-rodamine (TMR) and an endogenous protein, lactate dehydrogenase (LDH), across mechanically compromised cell membrane, while a significant difference of the membrane "sealing" effect was not suggested among different MWs and DAs of chitosan polymer. A similar affinity

of FITC-chitosan polymer at intact and injured spinal tissues was also suggested. To push the use of chitosan a step towards clinical tests, we incorporated the advantage of nanomedicine with our "promising chitosan material". Different factors were investigated during the formation and the storage of Chi-NPs. Two types of Chi-NPs (chitosan-triphosphate, Chi-TPPNPs and chitosan-dextran sulfate, Chi-DSNPs) were synthesized, with a range of size at 100-300nm and zeta-potentials of 30.65mV and -47.4mV, based on an ionic gelation method. Chi-DSNPs were shown to rescue necrotic BV-2 cells induced by a short incubation of hydrogen peroxide at 5.5mM. In addition, the conduction of somatosensory evoked potentials (SSEPs) through the lesion produced by the compression injury was partially restored after 1 week of the subcutaneous administration of Chi-DSNPs. We also found that polyethylene glycol (PEG)-coated silica NPs were significantly accumulated at the compression injured spinal tissues. The affinity of NPs at severed cell membranes was guided by PEG. Our experimental findings suggested that chitosan and ChiNPs provided neuroprotective effects using both in vitro and in vivo models.

1. INTRODUCTION

The central nervous system (CNS), as part of the nervous system, consists of the brain and spinal cord. The CNS serves as the command center that gives order and receives feedback from organs and limbs through neural pathways of peripheral nervous system (PNS). Extending from the brain, the spinal cord transmits motor (descending) and sensory (ascending) signals between the brain and the rest of the body. If the brain is considered as a hub for generating human motor, intellectual and emotional information, then, the spinal cord is the interconnecting network that coordinates nerve reflexes and transmits these motor and sensory signals in the body. In a sense, it is the spinal cord that acts as the informational highway that enables human behavior [1].

Spinal cord injury (SCI) occurs most commonly via compression, resulting from spinal fracture or dislocation by direct mechanical forces on the vertebral column. Based on the injury level at the vertebral columns, SCI can result in neurologic function deficits below the lesion, while normal functions are still preserved above the site of insult. In severe injury cases, SCI can lead to paralysis and even death. A succession of complications can follow SCI, such as neurologic deterioration, pressure sores, aspiration and pulmonary problems. Both SCI and its complications create tremendous financial burden on individuals and the society. The average annual medical cost for treating SCI is \$15,000-\$30,000. Among others, falls, violence and sports, motor vehicle accidents (46%) are the leading causes of SCI. The most frequently occurring age at injury is 19. The average estimated lifetime cost is more than \$3 million and injured persons can live close to a normal life span [2]. All these facts make SCI the most expensive and untreatable traumatic injury to the human body.

The history of SCI management can be traced to World War II, when people died from secondary complications [1]. The widespread development and use of antibiotics

changed these outcomes, but did not lead to functional returns. Unfortunately, compared with the breakthroughs and remarkable movements in burn control, fracture nonunions, and even cancer, there is still no way to reverse the damage in SCI. This is mainly derived from the complexity and multi-factorial nature of SCI. The only current therapy option is steroid therapy (Methylprednisolone, MP). The administration of MP in the acute phase of SCI was claimed to be useful in SCI by reducing the free radical mediated damage in the national acute spinal cord injury studies (The National Acute Spinal Cord Injury Studies, NASCIS) II and III clinical trials. However, this steroid therapy was not recommended by the Congress of Neurological Surgeons / the American Association of Neurological Surgeons (AANS) spelled out in 2013, due to the lack of placebo-controlled trial design and harmful side effects of infection and avascular necrosis [3, 4]. Moreover even earlier critics pointed out the exaggerated claims and dubious statistical comparisons used by NASCIS investigators [1]. The therapy thus was never taken as proven beneficial nor considered as any form of "standard of care". Other neuroprotective interventions have shown either no clear benefit for SCI or raised the concern of medical side effects: such as GM-1 ganglioside, the NMDA antagonist gacyclidine, Neotrofin, Prochord injection therapy, to name only a few [1, 5–7]. The lack of standard pharmacological protocol for SCI management and repair justified and triggered extensive investigations to new treatments.

This introduction will: 1) review the anatomy of spinal cord and pathophysiology of SCI; 2) emphasize the role of the distortion of the membrane integrity as an initiator in primary injury and as a critical turning point in SCI from primary injury to proceeding secondary injury; 3) summarize the advantages and disadvantages of different neuroprotective strategies and 4) discuss the opportunities for nanomedicine applications.

1.1 The anatomy of spinal cord

The human spinal cord is located in the vertebral column. It extends from the medulla oblongata which is a lower part of the brain stem, through the foramen magnum (one of the large openings in the base of the skull) and ends with the conus medullaris. Spinal cord is divided into 8 cervical (C), 12 thoracic (T), 5 lumbar (L), 5 sacral (S), and 3 coccygeal segments. At each segment, one pair of nerve (dorsal and ventral) roots which are located on the left or right side of the vertebral column extends away from spinal cord tissue, bundled together as one spinal nerve, and innervates end targets, organs and muscles to transmit mortor and sensory signals in an orderly manner. The level of spinal cord is named after the origins of the spinal nerves. The spinal cord is enveloped by three layers of membranes, also called as spinal meninges. From the outermost to the innermost, there are the dura matter, the arachnoid matter, and the pia matter.

At the central area of the spinal cord, it is the butterfly-shaped grey matter which consists of neuron cell bodies, dendrites and axons. The surrounding tissue is the white matter which is occupied solely by axons and glial cells. Neurons are the structure and function units in nervous tissue which are capable of generating (from the cell bodies, dendrites and nodes of Ranvier) and transmitting (axons) action potentials (AP), whereas, neuroglia cells are supporting cells which are critical for the survival and function of neurons. Glial cells account for half the total volume of CNS. They are smaller in size but outnumber the neurons by 5-10 times. The white color of white matter is due to the lipid-rich myelin wrapped axons. The major functions of myelin are to insulate axons from the dissipation of electrically charged molecules and stabilize the mature axons from randomly axon sprouts. Myelin sheath gaps, also called as nodes of Ranvier, are uninsulated areas, capable of generating AP [8]. AP is a transit discharge of many positive and negative ions through the cell membrane and occurs when excitable cells reach a potential threshold. Then the potentials across the membrane are reversed by opening of voltage-gated ion channels on the membrane.

AP is transmitted through myelinated spinal cord axons by jumping from one node to the next one. This conduction pattern is named saltatory conduction.

Axons are arranged symmetrically as nerve bundles or tracts to transmit somatosensory and motor orders. Ascending tracts including Dorsal Column Medial Lemniscus System, Spinocerebellar Tracts, and Anterolateral System, receive sensory signals from the rest of body and project these eventually to the sensory cortex in the brain. Descending tracts including Pyramidal Tracts and Extrapyramidal Tracts, send motor axons from the brain to the lower motor neurons in the cord, and to the muscles or organs [1]. Injuries to the spinal cord can impair the electrical conduction or even block nerve impulse through the damage site(s). It results in the conduction blockage below the level of the insult. Therefore, the brain is essentially disenfranchised from the body.

1.2 The pathophysiology of spinal cord injury (SCI)

SCI can happen to grey matter, white matter or both, but the insult most commonly occurs at the white matter. The grey matter damage usually leads to the weakening of the limbs due to the loss of neurons at a restricted vertebral segment. Since the limbs are innervated by motor neurons from several vertebral segments, the loss of motor neurons at one vertebral segment causes paresis, or weakening, but not paralysis [1]. The loss of gray matter is sometimes referred to as central cord syndrome. The grey matter damage in SCI does not closely associate with significant behavior loss in patients. Alternatively, SCI-induced paralysis is commonplace when the white matter is damaged. Injuries on the nerve tracts can destroy the myelin insulation or tether the axons. The discontinuity of the conduits for electrical conduction slows down or even blocks nerve impulses. SCI at the thoracic, lumbar, or sacral regions results in paraplegia, while at the cervical level, the outcome of SCI is quadriplegia. Paraplegia is the loss of motor and sensory functions at legs. Quadriple-

gia is the paralysis at arms, legs and torso. Therefore, the higher the level of SCI, the greater loss of function a person experiences.

1.2.1 Primary and secondary injury

In most cases, SCI is initiated when the spinal cord is under constant compression by damaged vertebral columns. Sometimes, the fragmented spine can penetrate the spinal meninges. The damage to the grey matter, which is more vascularized, results from the central manifestation of compression from the outside. Thus, cords degenerate from the center outwards and it is referred to in the clinic as central hemorrhagic destruction [9]. The white matter is also crushed and distorted. Complete spinal cord transection is rare. The localized insult, usually extends less than one vertebral segment, and is referred as the primary injury. Within hours, the localized damage can progress beyond the initial zone to neighboring healthy cell producing more tissue death. The self-propagating cell loss which is often centered by biochemical cascade is regarded as the secondary injury. In secondary injury of SCI, the disruption of membrane permeability and the following generation of endogenous toxins, such as free radicals and aldehydes, can form cycles that induce cellular destructions over many weeks to months [10].

1.2.2 The lipid composition of animal cell membranes

The cell membrane is a biological membrane, consisting of membrane lipids and membrane proteins. Membrane lipids are amphiphiles. Driven by hydrophobic interactions between the acyl tails of lipids and other weak forces (hydrogen-bonding and van der Waals), membrane lipids assemble as membrane lipid bilayers spontaneously. The core of the membrane is hydrophobic and the surfaces of the membrane are polar, surrounded by cytosol or extracellular fluid. Most of molecules and solutes are not capable of diffusing passively through the membrane due to the hydrophobic regions of the cell membrane. The major components of animal cell membrane

lipids are phospholipids, glycolipids, and cholesterol, with phospholipids the most abundant. A phospholipid molecule is an amphiphile. The hydrophobic groups are fatty acid chains, while the hydrophilic components consist of a glycerol or a sphingosine backbone, a phosphate and an alcohol. Due to the polar phosphate headgroups of phospholipids on the membrane bilayer, the membrane surface carries an overall negative charge. Based on the types of fatty acid chains, glycerophosphlipids can be classified further as phosphatidylcholine (PtdCho), phosphatidylethanolamine (PtdEtn), phosphatidylserine (PtdSer), phosphatidylinositol (PtdIns) and phosphatidic acid (PA). At the cell membrane plasma level, PtdCho is the most abundant membrane lipid on the extracellular side and it accounts for more than 40% of phospholipids. The PtdCho molecule is a zwitterion which carries neutral charge due to the anionic phosphate group and cationic choline [11].

1.2.3 The selective permeability of cell membranes

An intact animal cell membrane serves as a selective permeability barrier that regulates the passage of ions and molecules through the membrane. The resulted heterogeneous distribution of ions across the plasma membrane produces a voltage difference, which is called the membrane potential. The resting membrane potential is established by electrochemical equilibrium mainly via Na^+/ K^+ pumps and leaking K^+ ion channels imbedded on the cell membrane. In an axon hillock of a typical neuron, the resting membrane potential is around -70mV which is contributed mainly by intracellular potassium ions. Calcium ions and sodium ions are tightly regulated and are mostly excluded to the cell's exterior space. In a cardiac cell, there is a 25000 times difference of calcium ions across the membrane, which creates a strong electrochemical driving force for Ca^{2+} inward flow through the opening of voltage-gated calcium channels when the membrane is depolarized.

1.2.4 The role of the membrane distortion in SCI

In SCI, the cell membrane integrity is mostly impaired by mechanical forces. The distorted membrane is likely the earliest adverse response to primary injury. Mechanical forces can damage the integrity of the cell membrane by creating membrane defects, such as "holes". For instance, the tapping mode of an atomic force microscopy (AFM) was used to produce precise punctures through cell membranes in vitro (50 nm diameter, 500 nm in depth). The resulted leakage of cytoplasm out of the soma through the "holes" slowly led to the collapse of the cell morphology. An ever-growing pool was formed on the floor of the substrate over a period of 30 min [12].

It was suggested that the influx ions, particularly Ca^{2+} ions can activate the resealing strategies to block the "holes" by insulted cells spontaneously, if the membrane defects are limited [13–16]. However, more often, in the traumatic injury, the impact of unregulated ions is so overwhelming that it can deplete the membrane battery quickly and result in a conduction block [17]. Without the regulation of ions across the cell membrane, cells can be randomly excited or shut-down completely through dysfunctional voltage-gated transmembrane proteins. As a critical messenger ion, quickly increased intracellular Ca^{2+} then non-selectively and simultaneously activate downstream biochemical pathways. Cellular proteins that maintain the mechanical strength of the cell, such as the cytoskeleton, microfilaments and microtubules, will be destabilized by increasing Ca^{2+} which results in the collapse of regular cell morphology. Similarly, cascading down the electrochemical gradient, the influx of large amount of Na^{+} ions also trigger the release of the cytoplasmic pool of Ca^{2+} ions in the mitochondria which leads to mitochondria dysfunction. Moreover, the membrane disruption leaves cells susceptible to necrotic cell death. The dying necrotic cell will eventually burst and release deadly intracellular aldehydes, such as acrolein, into extracellular space, triggering inflammation and tissue swelling [18, 19].

1.2.5 Membrane disruption as the turning point from primary injury to secondary injury

Membrane disruption is also a critical link between primary and secondary injury. The mitochondria dysfunction in injured cells leads to unregulated generation of free-radicals, such as super oxide, hydroxyl ions and hydrogen peroxide. These free radicals can attack and oxidize plasma membrane lipids of cells. This chemical reaction is called lipid peroxidation (LPO) [20]. During LPO, membrane lipids are broken down and chemical aldehyde toxins, such as acrolein and 4-hydroxynoneanal, are generated as "by-products" [18]. These toxins can freely pass through membranes and attack cellular membrane and organelle membranes in nearby cells, producing a continuing process called "bystander damage", which results in the damage beyond the initial insult area.

Compression damage in white matter can progress in severity to tissue disconnection in some, but not all, spinal cord (or peripheral nerve tracts). The proximal segments (connected to the cell bodies) may remain intact but are permanently isolated from their target cells. The distal segments of these same axons completely degenerate and are lost in all mammals. This process is called Wallerian Degeneration. Wallerian degeneration was first described by a British neurophysiologist, Augustus Volney Waller. As a result, the previous impaired electrical conduction produced by the primary injury is forever lost as secondary injury processes continue. This process is variable in time. It may take hours to many weeks depending on many factors such as the severity of the primary injury, the axon's caliber, whether it is myelinated or not - to name but a few. It has been demonstrated that quickly restoring membrane integrity can preserve and enhance cell viability and attenuate both primary and secondary damage [1, 21–28].

1.2.6 Reactive gliosis and fibrous scar tissue developments in SCI

When the dura matter, located at the outermost layer of the meninges, is penetrated during SCI, the connective tissue elements, mainly fibroblast, can invade the lesion. These become knitted with each other through the production of non-functional extracellular matrix and also walled off by reactive astrocytes to form a multicellular and dense fibrous scar tissue. This is usually referred to as the fibroglia scar noting its two main cellular components. When the dura matter is not broken, the scar is occupied by reactive astrocytes only. The hypertrophic astrocytes produce dense intermediate filaments, glial fibrillary acidic protein (GFAP), and form a rubbery membrane at the tips of nerve fibers. Even though, there are disagreements of the gliosis and fibrous tissue as a possible physical barrier to CNS regeneration [1,29,30], both inhibitory molecules interfering with axon guidance and disfavoring nerve regeneration are demonstrated to be closely associated with the harsh environment of the "scar" tissue. NI-250 and N35 were the first clearly identified myelin associated inhibitory factors. Other inhibitory molecules are: 1) proteoglycans-chondroitin sulphate proteoglycan (PSPG)-generated by reactive astrocytes; 2) secreted protein semaphoring 3 (SEMA3), highly expressed by invading fibroblasts at the core of the lesion; 3) ephrin-B2 in astrocytes and its receptor EPHB2 , also associated with fibroblasts of the fibrous scar tissue; and 4) the slit proteins along with glypican 1 receptor in reactive astrocytes.

1.3 The pharmacological interventions of SCI

The pathophysiology of SCI can lay out several blueprints for pharmacological strategies to reduce the severity and consequences of SCI. The goals of current research are to facilitate the repair of existing damage and prevent new damage due to secondary injury in SCI. Promising neuroprotective agents under current investigations of clinical SCI trials are Riluzole, a sodium channel blocker, Methylprednisolone (MP), a ROS scavenger, Erythropoetin (EPO), a hormone, and Minocycline,

an anti-inflammatory agent (Table 1.1). However, the application of these therapeutic agents requires caution due to various side effects, such as infections and hepatotoxicity. Hepatotoxicity is defined as chemical-induced liver damage (discussed here as drugs) and is often difficult to diagnose in patients [31]. The liver acts as a "chemical factory" that detoxifies chemicals or drugs which makes the liver susceptible to chemical-induced toxicity. Other beneficial pharmacological agents investigated in experimental SCI animal models are summarized in Table 1.2. In order to pass these drug candidates to more advanced stages of human clinical trials, more investigations on drug safety need to be done at pre-clinical level. The beneficial effects derived from studies which are conducted using single type of laboratory animals (almost always rodents) need to be validated in other species of laboratory animals, because a drug may affect one species differently from another (Guidance for Industry, Animal Models-Essential Elements to Address Efficacy Under the Animal Rule).

1.3.1 Restoring membrane integrity by membrane fusion polymers: polyethylene glycol (PEG) and chitosan

PEG

The Borgens research group pioneered the application of polymers to restore injured spinal cord tissues. PEG is a hydrophilic polymer with different molecular weights (MW) depending on its chain length. PEG is the basis of many laxatives and PEG 3350 is FDA-approved. Borgens et al. thoroughly investigated the neuroprotective effects and limitations of PEG in both animal SCI and brain trauma [21–23,45,46]. They reported that brief administration of PEG within 8 hours of SCI can facilitate nerve conduction and functional recovery by restoring membrane integrity in vivo [24]. They also demonstrated that PEG can attenuate the production of ROS-induced by both compression spinal cord injury and acrolein-mediated PC12 neural death [25, 28, 47, 48]. On the other hand, the toxicity of PEG administration is also well established in vivo and ex vivo. The prolonged exposure (more than 5 mins)

Table 1.1
Pharmacological strategies for SCI in current clinical trials [32].

Agents	Functions	Trials (Phase)	Side Effects
Riluzole	Glutamate receptor [33] and Voltage-gated Na^+ channels blocker [35]	II and III	Hepatotoxicity [34] (rare and severe)
Methylprednisolone	ROS Scavenger [1] Anti- Inflammation [37]	III	Infection [36] avascular necrosis
Erythropoietin	Preserving white matter and myelin [38]	III	Thrombotic Risks
Minocycline	Anti-inflammatory agent [5]	III	Hepatotoxicity [34]

Table 1.2
Major neuroprotective agents in experimental SCI studies.

Target	Category	Agents	Limitations
Gliosis tissue and fibrous "scar" tissue			
Dystrophic environment	Protein neurotrophic factors	BDNF	Modest regeneration [39]
		NGF	fail to overcome myelin inhibition [1]
		NT3	off-target enhanced neuron functions [40]
PSGS	Protein enzyme	Chondroitinase-ABC	Incomplete digest of GAG chains [41]
Myelin inhibition	Small molecule	dbc-AMP	Not clear [42]
Myelin debris	Recombinant protein	Rho inhibitor	Not clear [43, 44]
Membrane defects			
	Polymers	Polyethylene Glycol (PEG)	High MW viscosity and monomer toxicity [21, 22, 24, 25]
	Polymer	Chitosan	Hemostasis [26]

of PEG on healthy spinal cord tissues was found to cause axon fusion and cavitation [1]. PEG is not biodegradable and the excretion pathway of PEG is mainly through kidney filtration. High doses of PEG have the potential to cause kidney failure. In addition, low MW (such as 300Da) PEG, or the impurity of injected PEG with monomers, or the breakdown products of long PEG chains, such as monomers and dimers, can also produce PEG toxicity.

Chitosan

Another polymer investigated in the Borgens group that also has neuroreparative potential is chitosan, a natural cationic polysaccharide [26,27,49]. Due to the polarity and biodegradability of chitosan, it is extensively used in many applications, such as water filtration, food industry, wound management and drug/gene delivery [50–53]. In addition, Cho et al recently reported that chitosan can seal membrane breaches produced by transection and compression injuries in the white matter of spinal cords. The main mechanism was suggested through electrostatic interactions between the amino groups of chitosan and phosphate headgroups of the membrane lipids [26].

1.3.2 Considerations

Many promising neuroprotective agents are based on successful cell and animal studies. However, the transition from pre-clinical to clinical stage is filled with obstacles, mainly because of the inherent complexity of human body on drug enzymatic metabolism.

As we know, the therapeutic effect of a drug mainly depends on the local concentration at the sites of action. Once a drug enters the human body, the activity and life-time of the drug are challenged by different physiological systems, simultaneously or subsequently: the blood, the immune system, the filtration system, the blood brain barrier and the digestive tract (based on the route of administration). Fast drug metabolism or a short-life time in the circulation system results in the reduction of

the local drug concentration, which can lead to a possibly compromised therapeutic effect and unnecessary drug accumulation in sensitive organs. However, simply increasing the dosage might not enhance the desired outcome. More commonly, this could induce side effects in a dose-dependent manner, especially in pre-compromised organs. When the safety window of the drug is narrow, the side effects can sometimes overwhelm the desired outcome and lead to fatal conditions. 4-Aminopyridine (4-AP) is such an example. 4-AP is a potassium channel blocker. It was shown to restore the conduction block in demyelinated nerve fibers in SCI. However, this therapy can induce peripheral vasospasms, which is the most hazardous complication of this drug [1]. In addition, since most candidate drugs used in CNS Injury are based on proteins or molecules, (summarized in Tables 1.2 and 1.1), the systemic circulation of these "bare" and "bulk" materials (candidate drugs) in the body makes them vulnerable for antibody opsonization and phagocytosis. Opsonization describes the process of non-specific binding of "invaders" (discussed here as therapeutic agents) with antibodies which can in turn attract the phagocytes for ingestion and destruction. Phagocytosis as one of the major body innate immune responses protects the body by direct internalization of the foreign objects for destruction. Phagocytosis is size dependent and it is sensitive to the object with the size larger than 0.5μm [54]. The initiation of phagocytosis is also enhanced by small contact angles (less than $45°$) [55]. The contact angle is defined as the angle between the average tangential line at the spreading surface of a phagocyte on an object and the membrane normal line at the site of attachment. In other words, an object with irregular shape is susceptible to phagocytosis. One liter of human blood contains about six billion white blood cells in which macrophages are the most competent phagocytes. Therefore, the biocompatibility of therapeutic agents in the physiological fluid is highly important.

1.4 Nanomedicine

Advanced nanomedicine technology brings opportunities for innovative drug development and drug delivery methods. Nanomaterials are materials with the size scale of a billionth part, generally less than a micron [56]. The nano-scale size is similar as the size of biological molecules - even viruses - which increases the bioavailability and protects nanoparticles from phagocytosis. Moreover, the large surface area on/inside the nanoparticles (NPs) can be viewed as a great reservoir for small molecules, drugs, genes and even stem cells. The core materials of the nanoparticles can be inorganic or organic (like silica and chitosan). Therefore, the functions of the nanoparticles can vary. For instance, gold nanoparticles were used as contrast agents for in vivo tumor imaging with photoacoustic tomography technology [57]. Iron oxide nanoparticles were proven to be highly effective for magnetic resonance imaging [58]. Silica nanoparticles were capable of loading and releasing drugs (hydralazine) in a time-dependent manner [25]. Nanoparticles are referred as theranostic nanomedicines when they combine both diagnostic (imaging) and therapeutic (drug delivery) properties together. For instance, magnetic nanoparticles were used to trace the tumor location and the induced hyperthermia was used as a treatment to kill tumor cells in a mouse xenograft model by alternating magnetic fields [59]. The surface functionalization of mesoporous silica nanoparticles enabled nanoparticles with both drug/gene delivery and sensing applications [60]. One successful example of nanomedicine application is the FDA approved cancer drug Abraxane, which is a paclitaxel-albumin nanoparticle. Major nanomedicine studies in CNS are summarized in Table 1.3.

A new generation of nanoparticles enhances the retention of nanoparticles at a specific group of cells using targeting strategies by attaching antibodies and small peptides on the exterior of the nanoparticles, which are referred as engineered nanoparticles [65].

Table 1.3
Major NPs' studies in CNS injury (animal and cell studies)

Nanoparticles	Functions (Delivery,D)	Routes of administration	Conjugation (Drugs/Molecules)	CNS Damage
Poly(glycidyl methacrylate)-Polyethylenimine	Imaging Molecule-D	Intravitreal	Iron oxide, Rhodamine B	Optic nerve transection [61]
Poly-lactic-co-glycolic acid (PLGA)	Drug-D	Local	MP	SCI contusion [62]
Poly(butyl cyanoacrylate) (PBCA)	Drug-D	Incubation	SOD NMDA antibody	Superoxide-cells [63]
Silica (without drug)	Membrane Restoration	Subcutaneous	PEG coating	SCI compression and transection, PC12 cells [25]
Silica (with drug)	Drug-D	Incubation	Hydralazine	Acrolein-PC12 cells [28]
Magnetic	Toxicity and uptake	Intravenous	Neil red	SCI transection [64]
Chitosan	Drug-D	Incubation	Hydralazine	Acrolein-PC12 cells [27]

1.5 Goals of this work

Our previous work showed that brief incubation of damaged spinal cord with chitosan polymer solution can significantly inhibit the random exchanges of intracellular and extracellular molecules and restore the signal conduction through the injury site [26].

This work was based off the previous observations, and pushed forward to continue to investigate the neuroprotective effects derived from intrinsic factors of chitosan polymer. The purpose of this work is to provide insights for the mechanisms of the neuroprotection by chitosan polymer. Two major factors investigated were molecular weight (MW) and degree of acetylation (DA). Nanofabrication technology was utilized to preserve the neuroprotective effect of chitosan and increase its performance in physiological fluids. Chitosan nanoparticles were synthesized by an ionic gelation method. Different parameters were investigated to provide insights on the mechanisms of nanoparticle formation and optimize the performance of chitosan nanoparticles. The neuroprotective effect by chitosan nanoparticles in a hydrogen peroxide challenged cell model was tested. Finally, the signal conduction profiles of both healthy and compression injured animals were established. The functional recovery after the administration of chitosan nanoparticle was investigated. In addition, the affinity of PEG-coated silica nanoparticles at the compression injury sites of spinal cord tissues was investigated as a parallel study.

2. AFFINITY OF POLYETHYLENE GLYCOL (PEG) - SILICA-NPS FOR DAMAGE SITES OF MEMBRANES AFTER SPINAL CORD INJURY

2.1 Introduction

Spinal cord injury (SCI) is a complex pathological process. It is generally initiated by a mechanical force and progresses as a secondary injury, primarily via biochemical cascades [10, 66]. Damage to the integrity of cell membranes is a direct and dangerous consequence of SCI [21–23]. When the lipid bilayer structure is impaired, the regulated ion gradients across the membrane are lost and leave the cells vulnerable to necrosis. Even though membrane self-repair can be activated by Ca^{2+} influx, spontaneous repair often fails to keep pace with the self-propagating and ever enlarging scope of membrane disruption after traumatic injuries [13, 15]. Consequently, unregulated Ca^{2+}/Na^{+} influx can lead to structural protein destabilization, reactive oxygen species (ROS) generation, and subsequent lipid peroxidation (LPO) [15, 67]. Promising strategies for controlling cellular and tissue damages after SCI include neuroprotective agents against ROS production, stem cell therapies. Among all therapies, restoring membrane integrity rapidly and effectively after injury would be critical to interfering with progressive secondary injury and further deterioration of the tissues of the central nervous system (CNS) [21–23].

It has been shown that locally applying membrane fusion polymers such as polyethylene glycol (PEG) soon after SCI can reduce cell death, attenuate secondary injury, and partially restore signal conduction through the region of damage [24,47,48]. PEG is a polyether compound. The degree of polymerization determines the chain length or polymer MW, which also affect the physical properties of PEG, such as viscosity, when it is prepared as solution. In high MW PEG, the increased inter-

molecular interactions result in higher viscosity. Due to its hydrophilicity and low toxicity, PEG can be used as laxatives, tablet excipients and as well as coupled with hydrophobic molecules to form surfactants.

PEG is also a well-known cell membrane fusion agent [68–70]. The first PEG induced membrane fusion was discovered in plant protoplasts in 1974 [71]. Later, PEG-induced membrane fusion was recognized between different types of cells such as hen erythrocytes and yeast protoplasts [72]. The mechanism of PEG-induced membrane fusion was first suggested to be due to a dehydration effect and followed by a volume-exclusion effect which induces the aggregation of lipids between closely contact membranes [14, 73]. The dehydration effect by PEG is to exclude water from the regions of disorganized and disrupted membranes. The volume-exclusion effect describes the dynamic adaptation of membrane lipids towards the hydrophobic environment in the regions of disorganized and disrupted membrane by driving the re-aggregation of the neighboring membrane lipids. According to the fluid mosaic model of S.J.Singer and G.L. Nicolson (1972), the structure of membrane lipids and proteins is dynamic [74]. In order to minimize the energy cost and stabilize the structure, closely contacted lipids are reorganized into single bilayer through lateral diffusion, aggregation, and re-assemblage of neighboring lipids.

The membrane fusion function of PEG also serves as the basis for each neuroprotective effect. Borgens et al. reported that a brief administration of PEG within 8 hours of SCI facilitated nerve conduction and motor recovery in an in vivo study [21]. PEG also attenuated acrolein-mediated PC12 neural death [75]. However, PEG is not a ROS scavenger. The beneficial effects of PEG are due to the restoration of the membrane integrity. This significantly reduces or eliminates the pathological exchange of ions and molecules between the cytoplasm and external milieu. This unregulated exchange is the impetus for ROS production. The routes of administration of PEG were also tested in topical, intravenous, intraperitoneal, and subcutaneous applications [21, 22, 45, 46, 76, 77]. All applications provided significant benefit in anatomi-

cal, physiological, and functional outcomes measured in adult guinea pig models of SCI [21, 22, 45, 46, 76, 77].

On the other hand, the toxicity of PEG administration was also investigated both in vivo and ex vivo. The prolonged exposure (>5mins) of PEG on healthy spinal cord tissues was found to cause axon fusion [1]. PEG is non-biodegradable and is excreted from the body via kidney filtration. Therefore, high doses of PEG might increase the stress of kidney function and potentially induce kidney failure. In addition, low MW (such as 300 Da) or the impurity of PEG with monomers can produce ethylene glycol toxicity [78, 79]. The high viscosity in high MW PEG also increases the injection pressure through syringes during the delivery of PEG solutions [80–83].

Therefore, the administration of PEG inside the human being has to be tailored to keep the therapeutic effects and minimize the toxicity induced by systemical circulations. Our previous study showed that PEG-functionalized silica NPs (PSINPS) exhibited neurprotective effects on the spinal cord tissues subsequent to experimentally induced traumatic injuries [25]. The subcutaneous administration of PEG in animals with spinal cord compression injury also provided statistically significant beneficial effects on the restoration of somatosensory evoked potentials (SSEP) compared with saline control treatment groups [22]. The presence of SSEP in post-injury groups indicates the conduction of nerve impulses through the lesion. To summarize, the advantages of PSINPs are: (1) the surface areas on the NPs are large and sufficient to carry enough PEG polymers to produce a therapeutic effect, (2) the segregation of PEG polymers as nano-scaled packages reduces the viscosity of PEG for the intravenous application by increasing the distance between PEG molecules and the potential toxicity induced by the accumulation of bulk materials in the human being, (3) the nano-carrier provides new benefits by conjugating with therapeutic drugs or imaging molecules, (4) PEG coating enhances the biocompatibility and the half-life of nano-carriers in the body by acting as a stealth layer on the nano-carrier. PEG coating reduces antibody opsonization by reducing non-specific bindings of nano-carrier with serum proteins, which in turn decreases the chance of the nano-carrier being

engulfed and cleared by phagocytes from the blood circulation [25, 84]. Opsonization describes the process where a foreign object is marked by antibodies for the destruction by phagocytes, which are a type of cell protecting the body from harmful particles.

In this work, we utilized a nanomedicine based labeling system to evaluate the distribution of PEG polymer on damaged spinal cord tissues. Based on the membrane fusion capability of PEG polymer, our hypothesis was that PSINPs accumulated in sites of membrane damage spinal cord tissues. The ex vivo injury model was produced by a standardized compression injury using a pair of modified forceps on isolated spinal cord segments. Dye loaded PSINPs were applied to both damaged and intact cords. The uptake of Dye-PSINPs was evaluated by fluorescence microscopy and scanning electron microscopy.

2.2 Methods and materials

2.2.1 Spinal cord isolation

All animals used in this study were handled in accordance with, and prior approval by, the Purdue University Animal Care and Use Committee (PACUC). In this study, every effort was made to reduce the number and suffering of the animals used. Adult female guinea pigs (Hartely strain), weighing 300-400g, were anesthetized deeply with an intraperitoneal injection of a mixture of ketamine (60mg/kg) and xylazine (10mg/kg). Toe-pinch method was used to test the depth of anesthesia. They were then perfused through the heart with 500ml sterile lactate ringer solution (25°C) or until blood completely removed. The vertebral column was excised by performing a midline incision in the mid-thoracic region and a complete laminectomy. The spinal cord was extracted and immersed in cold oxygenated Kreb's solution for at least an hour to ensure recovery from the surgical procedure before experimentation. The composition of Krebs's solution (pH7.2) was as follows: NaCl 124 mM, KH_2PO_4 1.2

mM,$MgSO_4$ 1.3 mM, KCl 2 mM, $NaHCO_3$ 26 mM, $CaCl_2$ 2 mM, dextrose 20 mM, bubbling with 95% O_2/5%CO_2 throughout the duration of the experiment.

2.2.2 Compression injury ex vivo

A 15-s compression injury was induced using a pair of modified forceps processing a 0.8mm spacer (Figure 2.1). Previous investigation showed that a complete block of the compound action potential (CAP) conduction through guinea pig spinal cord was resulted from the compression injury performed as above [22]. The compression injury was named as site 0. The proximal areas with a distance of 1cm, 2cm, and 3cm away from the site0 were named as site1, site 2, site 3.

2.2.3 Synthesis and functionalization of TMR-doped, PEG-functionalized silica NPs (TMR-PSiNPs)

TMR-PSiNPs were synthesized (Figure 2.2). Briefly, the formation of silica NPs was based on water-in-oil method with sol-gel technology. 4ml 0.3M tetraethyl orthosilicate (TEOS), served as a water phase, was slowly added to a mixture of oil phase chemical solutions with 1h vigorous stirring. The oil phase contained 1.77 mL of Triton X-100, 1.8 mL of n-hexanol, 7.5 mL of cyclohexane, and 0.5 mL of 1% aqueous tetramethyl rhodamine-dextran, where pH was adjusted at 2.0. 60 μL of NH_4OH was added to to terminate polymerization reaction. Silica NPs were precipitated by acetone and washed with ethanol and acetone several times via centrifugation. Then, the NPs were dried under vacuum at 100°C for 12 hr. The surface modification of NPs by PEG-NH_2 (MW 3KDa) was conducted via a reactive schiff's base linkage. The pre-hydrolyzed silanol group by 3-(trimethoxysilyl) propyl aldehyde (TPA) provided an aldehyde group to react with amino group on PEG.

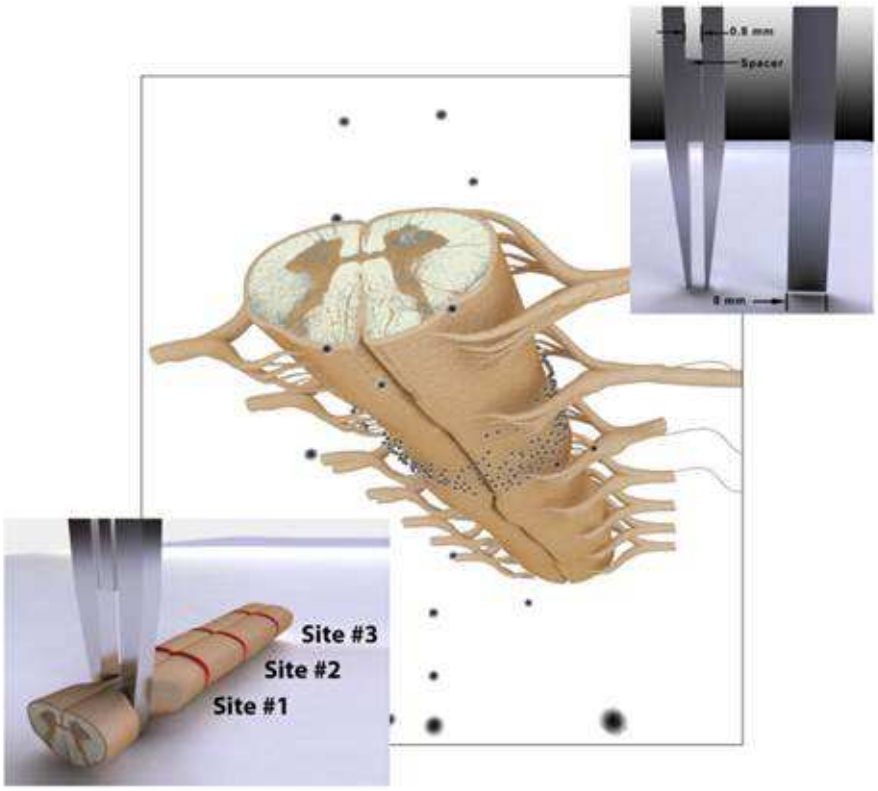

Fig. 2.1. Schematic illustration of the compression injury to an ex vivo spinal cord tissue. The top right shows a pair of modified forceps processing a 0.8mm spacer. The central image illustrates the isolated spinal cord tissue incubated in the PEG-Silica NP suspension. The dark spots represent the NPs. The lower left image demonstrates the compression injury induced by the forceps at Site 0. The red regions at Site1, Site2, and Site3 are indicated as intact segments with a distance of 1-cm, 2-cm, and 3-cm away from the compression site 0.

2.2.4 Evaluation of the affinity of TMR-PSiNPs at the damage sites of spinal cord tissues

Fluorescence microscopy

A 8-cm spinal cord segment was used at each experiment. A 5s constant mechanical compression injury was induced at 2-cm away from one end of the segment by a pair of modified forceps processing a spacer. Three intact areas were located 1-cm,

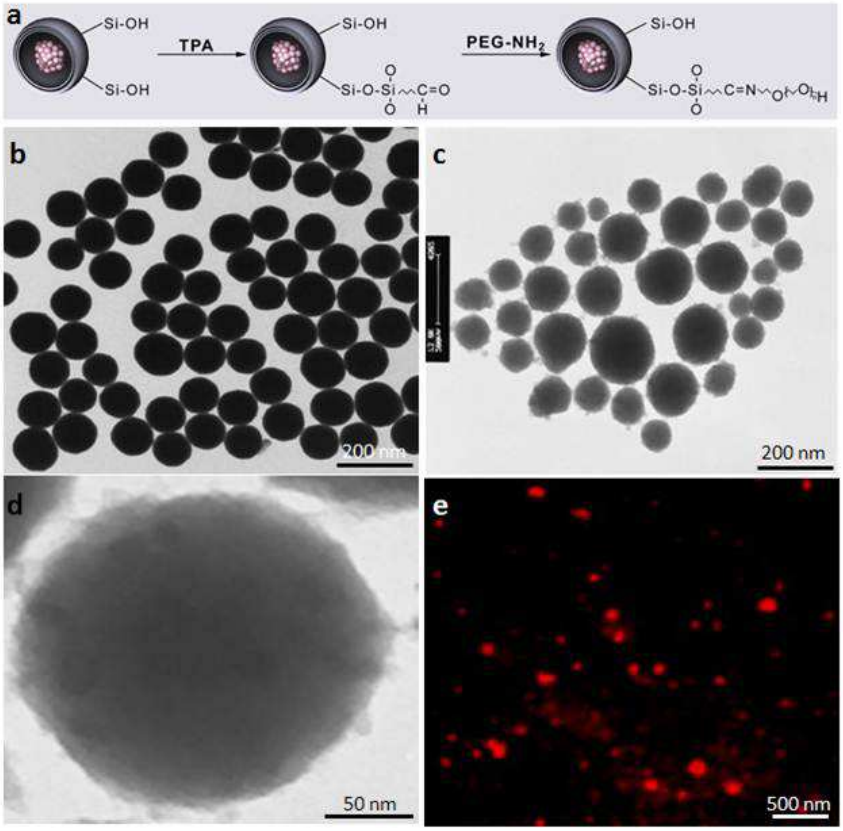

Fig. 2.2. TMR-PSINPs. (a) The illustration of PEGylation of TMR-doped Silica NPs. The NPs were loaded with 0.1% TMR and synthesized by a reverse-microemulsion method. TPA was used to functionalize the silanol group on the surface of silica NPs. PEG was coated through a schiff's base linkage with aldehyde group immobilized on NPs. (b-d) TEM images of bare-silica NPs (b), PEGylated silica NPs (c), and a magnified image of PEGylated silica NPs (d). The fluffy surface of the silica NPs demonstrated the present of PEG polymers on the surface. (e) The image of TMR-PSINPs captured with the Rhodamine channel of a Fluorescent microscopy.

2-cm, and 3-cm away from the compression site (Figure 2.1). The whole cord was incubated in the TMR-PSINPs solution (1mg/ml) for 15mins in the dark at room temperature to allow the interaction of NPs with both lesion and intact areas. The cord was further incubated in the Kreb solution for another 5mins to remove the loosely attached fluorescence probes on the tissue surface. The cord was carefully

dissected as 1cm segments with lesion or intact areas exposed to one end. Then the segments were fixed in 4% paraformaldehyde for 4-5hours in the dark. After fixation, the segments were embedded in Tissue Tek OCT compound, frozen in liquid nitrogen. Sections were cut at 50μm thickness using a freezing microtome (Thermo Electron, Waltham, MA, USA). Then, the sections were visualized by epi-fluorescence on an Olympus BX61 microscope with a standard rhodamine cube (545nm and 590nm of excitation filter and emission filter, Olympus). Rhodamine fluorescence images were captured at a 2x objective. At this magnification, the whole section was captured within one image. The images were saved for further analysis. All parameters of the fluorescence microscope were kept constant during the experiment. Quantification of the fluorescence intensity was measured by using Image J software (NIH). Four sections or images were randomly recorded from the target zone for each treatment at each experiment. Triplicates were performed for each treatment. The imaging zone was defined as the thickness within 1-2mm of the site of lesion or intact area. 12 data points were measured to produce the average intensity value for each treatment. The florescence intensity of white matter in each section was taken after outlining the boundary of the white matter manually. The value of the fluorescence intensity was expressed in arbitrary units, generated from the software.

Scanning electron microscope (SEM)

Spinal cord tissue segments treated with PSINP were fixed in 2.5% glutaraldehyde at 4°C overnight. The fixed tissue samples underwent continuous dehydration by different concentrations of ethanol. The ethanol incubation time was 15-30mins from 30% to 100% ethanol. The tissue can be stored in the 100% ethanol until it was read to be visualized by SEM. After dried by critical point drying method, the PSINP imbedded tissue segments were coated with a thin layer of conductive material with a JEOL JFC-110 ion sputtering (Tokyo, Japan) and the images of samples were recorded by a JEOL JSM-840 SEM .

2.2.5 Materials

TMR-dextran was purchased from Invitrogen (Life Technologies). Ketamine and xylazine were purchased from Purdue Veterinary School Pharmacy. All other chemicals used were purchased from Sigma Aldrich (St.Louis, MO). SEM is located at Purdue Life Science Microscopy Facility. Microtome is located in Center for Paralysis Research (CPR) at Purdue University (Thermo Electron, Waltham, MA). Adult guinea pigs were purchased from Hilltop and housed at Purdue animal holding facility.

2.2.6 Statistics

All data were represented as means±standard deviation. Statistical analysis was conducted using one-way ANOVA for comparison among more than 2groups and Tukey-Kramer Multiple Comparisons test for comparison between experiment groups (InStat^{TM} software). Values were accepted as being statistically significant difference if the P value was less than 0.05.

2.3 Results

2.3.1 The Distribution of TMR-PSiNPs at Both Damaged and Intact Sites Revealed by Fluorescence Microscopy

The distribution of TMR-PSiNPs at both the compression site (site 0) and proximal intact sites (site 1-3) was captured by epi-fluorescence microscopy and measured by ImageJ software. Figure 2.3 shows the fluorescence images of spinal cord cross-sections. At site 0, the morphology of grey matter was distorted by the compression injury which was not observed in other intact samples. It was found that grey matter was extensively labeled by the TMR probe in all groups, indicating that PEG-Silica NPs had a non-specific uptake by neurons of gray matter. However, the TMR intensity in white matter was reduced in all sites, at distance from the epicenter of the lesion. Figure 2.4 showed the quantitative analysis of the fluorescence intensity

recorded by fluorescent microscopy. Three animals were used here. Four cross-section images were randomly selected from the target zone. The fluorescent signal intensity was recorded solely in white matter, excluding the central gray matter. In sites 1-3, there was an average of 20% reduction of signal intensity compared with site 0 (Injured site). These reductions were statistically significant in both site1 ($P<0.05$) and site3 ($P<0.01$). Similar accumulations of PEGylated silica NPs were found among intact sites1-3 ($P>0.05$). When the animal number used for this work was increased to 5, the reduction of TMR-PSINPs was observed as a function of distance away from the compression injury regions ($P<0.05$) (Figure2.5).

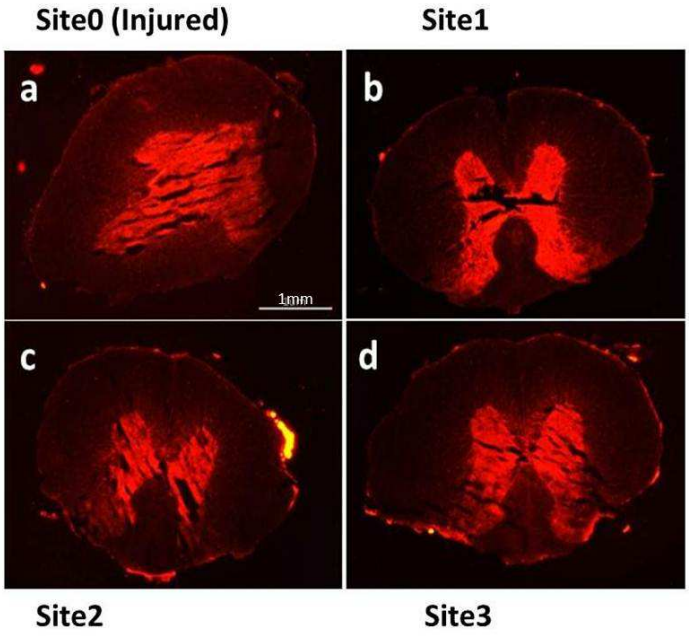

Fig. 2.3. The distribution of TMR-PSINPs in both compressed and intact spinal cord segments. TMR fluorophores stained the regions of grey matter equally in all samples. The intensity of the red fluorescent signal in white matter was reduced in intact segments (b-d), compared to the intensity in white matter of the compressed cord (a). a) The compressed cord (Injured, site 0), where the morphology of the grey matter was most distorted by the compression injury. b) Intact cord, 1cm-away from the compression site (site 1). c) Intact cord, 2cm-away from the compression site (site 2). d) Intact cord, 3cam-away from the compression site (site 3). Scale bar is 1mm, indicated in (a).

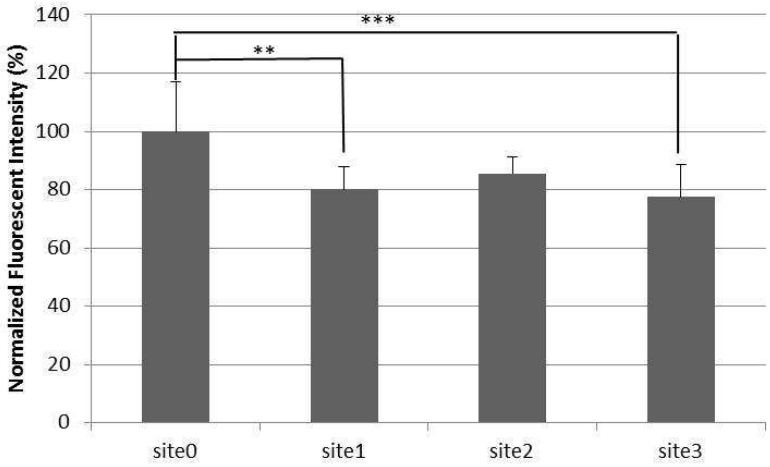

Fig. 2.4. Quantitative analysis of the distribution of TMR-PSINPs in both compressed and intact spinal cord segments-1. The fluorescence probe signals of intact cords in white matter were normalized against the signals recorded from compressed cords. Data was expressed as a percent of the intensity at site 0. Site enumeration as above. Compared with site 0, the intensity was statistically significantly reduced at site 1($P<0.05$) and site 3 ($P<0.01$). At site 2, a reduction of the intensity of the signal was observed as well, but the significance of the difference was not reached. (n=3). Data was expressed as mean±SD.

2.3.2 The accumulation of PSiNPs at both damaged and intact sites revealed by SEM

The accumulation of PEG-Silica NPs at both the compression site (site 0) and proximal intact sites (site 1-3) was evaluated by SEM. Figure 2.6 shows the SEM images of spinal cord cross-sections. Due to the compression injury, a difference in morphology was observed between site 0 and the intact sites (site 1-3). The surface accumulation of dense PEGylated particles was noticed at the compression injury site. As the distance away from the lesion increased, the deposition of NPs was decreased respectively. Both individual particles and the aggregation of NPs were observed in these samples.

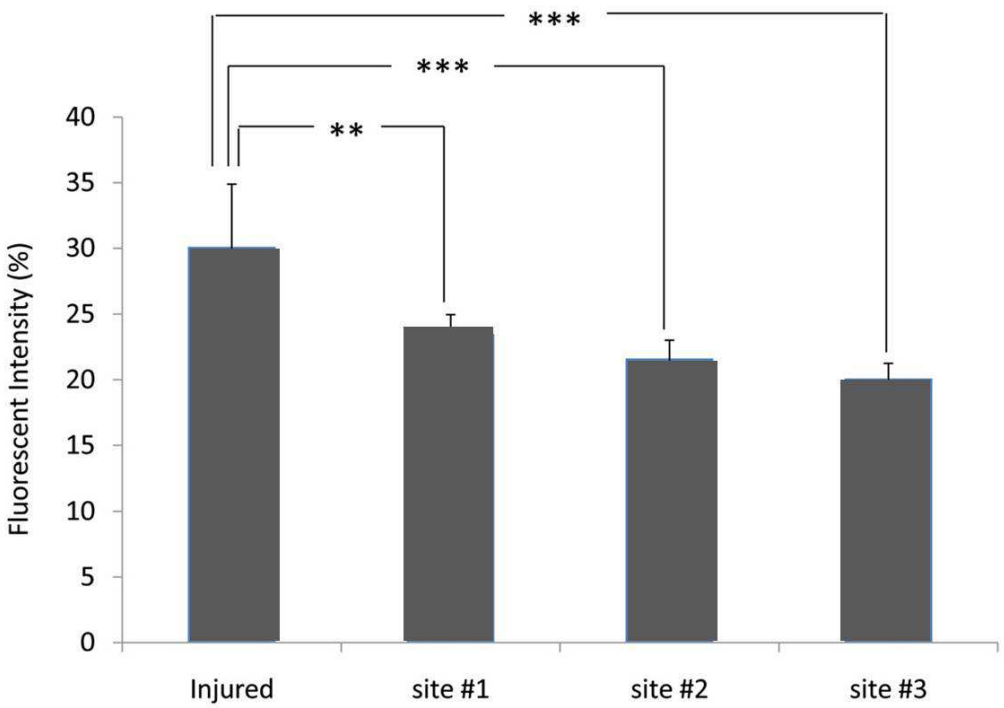

Fig. 2.5. Quantitative analysis of the distribution of TMR-PSINPs in both compressed and intact spinal cord segments-2. Injured (Site 0) is the site of compression as above. Site enumeration as above. Compared with injured (site 0), the intensity of TMR-PSINPs was reduced at site 1, site2, and site3 significantly ($P<0.01$). Results are expressed as a percent of the uninjured values ±SD (n=5). **$P<0.01$, ***$P<0.001$.

2.4 Discussion

In this work, we addressed the issue of the affinity of PEG for damaged regions using isolated spinal cord segments. The work was based on beneficial effects of PEG application induced by the strategy of membrane sealing.

2.4.1 Cell membrane "resealing" and cell functions

"Resealing" of the membrane is critical for a free living cell and multicellular organisms. It was suggested as an adaptive strategy for early eukaryotic cells to

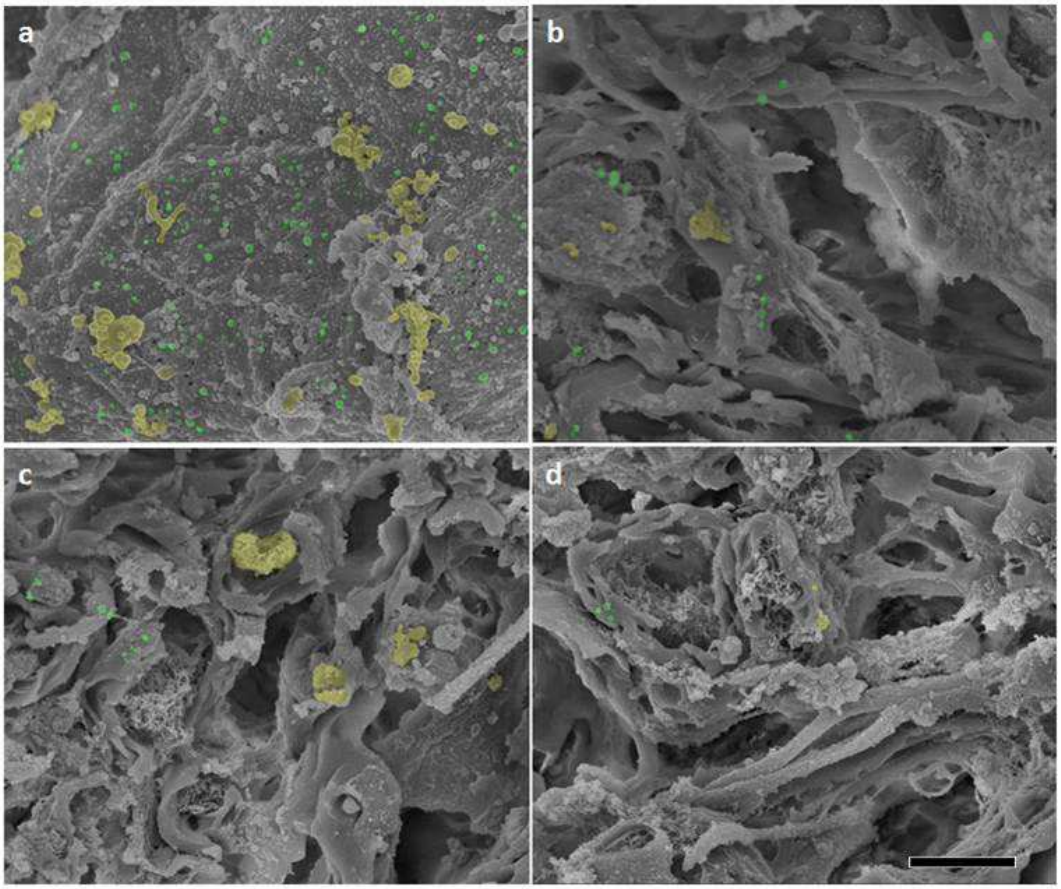

Fig. 2.6. Qualitative evaluation of PSINPs in both compressed and intact spinal cord segments by SEM. Spinal cord segments incubated with PSINPs were examined at the compression injury, site 0(a) and the proximal intact sites 1(b), site 2(c), and site 3(d). The dense accumulation of PSINPs was observed in (a), the compressed spinal cord sample, whereas uptake of PSINPs was minimized in site 1(b), site 2(c), and site 3(d), the intact spinal cord segments. Individual and aggregated NPs were partially indicated with green and yellow color in post-analysis.

survive in many mechanically challenged environments, after the loss of cell wall during the evolution from prokaryotes [13, 15]. The acquisition of endosomal/lysosomal organelles in a eukaryotic cell may enable the evolution of fusion-based resealing. The resealing of membrane is common and essential in many mammalian cellular processes, such as endocytosis, exocytosis, and cell division, where the presence of

$Ca^{2+}$is often required and necessary in nucleated cells. The disruption of cell membrane in traumatic injuries might also initiate these self-resealing processes [16, 85]. Based on the size of the wound area, the suggested resealing processes can be: (1) lateral diffusion and aggregation of the free ends of membrane lipids, if the size of the wound is smaller than 1nm. (2) exocytosis of lipid molecules at the adjacent intact membrane regions to reduce the wound areas, if the size is smaller than 1μm. (3) fusion of local vesicles and exocytosis of membrane batches directly at the wound areas, which serve as "plugs" at the "holes" of the membrane, if the size is smaller than 10μm. The time required for these resealing strategies to block the random exchange of materials across the membrane is size and cell type-dependent, varied from 30s-90mins. In severe cases, the self-resealing strategy might fail to overcome the unregulated rapid ion exchange and the ensuing destruction of cellular contents.

2.4.2 The affinity of PSiNPs at the damaged regions of spinal cord segments

Our previous studies showed that the membrane fusion property of PEG was preserved in PSINPs which were shown to provide beneficial effects on cell viability and functional recovery in both ex vivo tissue and animal studies with traumatic injury models [25]. In this work, we pursued the same line of study and further tested the affinity of PSINPs at the damage and intact regions of spinal cord segments. Our results suggested that PSINPs accumulated at the compression injury sites of the spinal cord tissue (Figure 2.6) and a subtle reduction of fluorophores was observed in the injury sites compared with the intact sites (Figure 2.5) ($P<0.05$). However, when SINPs were administered without a PEG coating, there was no significant difference of the distributions between injured and intact tissue samples ($P> 0.05$). Therefore, it is clear the selective distribution of NPs at damaged regions derived from the PEG coating. Our additional data of X-ray photoemission microscopy (XPS) evaluation of PSINPs distribution also agreed with both fluorescence imaging and SEM studies. A

high peak of Si 2p was generated in XPS surface deconvolution analysis confirming the existence of PSINPs in the compression injured spinal cord sample, whereas a similar peak was not observed in intact samples [86].

The affinity of PEG with damaged membranes was also discussed using simplified membrane models, such as Langmuir monolayers of phospholipids [87]. The lipid monolayer at the air-liquid interface was compressed to a certain surface pressure (SP) by applying a lateral pressure. The lipid packing density mimics the outer surface of a cell membrane when SP is 30 mN/m. The impaired membrane organization was indicated as loosely packed lipids. PEG was suggested to insert into the membrane lipids at the region with low membrane SP and be expelled out at high SP (for instance, SP at 46mN/m). The preference of PEG at the damage regions was shown in zwitterionic (diphytanoyl phosphatidylcholine (DPhPC) and dipalmitoyl phosphatidylcholine (DPPC)) and polar lipids (dioleoyl phosphatidylserine (DOPS)). Similar results were also observed in the interaction between Poloxamer 188 (P188) with membrane models [88]. P188 is capable of inserting into the model membrane lipids when SP is several mN/m lower than the SP of cell membrane bilayer equivalent pressure. When the lipids are packed tightly, P188 is not stable and excluded from the bilayer structure. P188 belongs to a class of hydrophilic triblock copolymers. It contains the hydrophilic chains (PPO) centered with hydrophobic chains (PEO).

2.4.3 Other benefits of PEG coating and PEGylation

PEG and PEG derivatives are also applied as coatings by linking with other chemical groups to enable multi-function capabilities of the conjugates in drug delivery in nanomedicine [84]. PEGylation is the act of covalently attaching PEG chains on the surface of other chemical structures, such as peptides, drugs, proteins or NPs (NPs). PEGylation was first described by Davies and Abuchowsky in the 1970s [89, 90]. The first PEGylation targeted amino groups. Now, the conjugation of PEG to thiol, hydroxyl or amide groups are also possible. There are several advantages of PEG modifi-

cation. PEG modified surface can protect the therapeutic agents from degradation by proteolytic enzymes, unspecific attachment with antibodies, and phagocytosis by the mononuclear phagocytic system [91]. Therefore, the circulation period for the agent is prolonged. PEGylation can also increase the solubility of hydrophobic agents, such as imaging tracers, and alter the distribution of agents (NPs) in vitro and in vivo, which results in less toxicity [92, 93]. However, the binding affinity for the target receptor or enzyme is accordingly reduced [94].

2.4.4 The strategy of fluorescence labeling

In order to trace the distribution of PEG in the biological tissues, PEG polymers are required to tightly bond with dye molecules. An ideal dye molecule needs to have large quantum yield which describes the efficiency of florescence process, high photostability and insignificant toxicity. However, the poor performance of traditional organic or inorganic dyes in physiological fluid limits in vivo applications. Significant advancements in nanotechnology led to new nanomaterial based labeling agents, such as Au-NP, quantum dots, Lanthanide (Ln^{3+}) NPs [95]. Compared with other polymer-based NPs, silica NPs have been used widely in bioanalysis and labeling with less aggregation and little dye leakage [25]. The easy surface chemistry of silica also enables the conjugation of other functional groups for multi-task activities. Even though static quenching occurs when a large amount of fluorophores are enveloped in a nano-sized volume, the benefit of largely enhanced quantum yield (large surface area) of a dye-doped silica nanoparticle than a single fluorescent molecule is a still significant gain. Silica nanoparticle also increases the photostability and decreases the toxicity of loaded fluorophores in the physiological fluid. Therefore, in this work, PSINPs were used to load fluorophores, TMR to represent the location of PEG polymers in both damaged and intact regions.

2.5 Conclusion

We constructed PSINPs, enveloped doped with TMR fluorophores. The selective affinity of TMR-PSINPs at the damaged sites of the spinal cord tissues was proven by SEM and quantitative fluorescence imaging. In addition, the reduction of PSINPs accumulation is inversely related as a function of distance from the epicenter of the spinal cord lesion.

3. THE NEUROPROTECTION BY CHITOSAN POLYMER - THE EFFECT OF THE DEGREES OF ACETYLATION AND THE MOLECULAR WEIGHTS OF CHITOSAN POLYMER

3.1 Introduction

A polymer is a macromolecule that consists of a number of repeated units (monomers). Based on the sources of polymer, it can be natural (protein and deoxyribonucleic acid (DNA)) or synthetic polymers (synthetic plastics). The application history of polymer as pharmaceutical delivery systems and biomedical devices has been dated since the last decade [96]. Even though each medical application requires highly specialized physico-chemical properties of the polymeric material, good biocompatibility must be met. Polysaccharides, such as cellulose, dextran, starch, hyaluronic acid, alginate, chitin and chitosan, display both biocompatibility and biodegradability. In addition, biodegradable polymers are perfect candidates for therapeutic devices such as temporary prostheses, scaffolds for tissue engineering, surgical dressings, and drug delivery vehicles, because of the superiority in in vivo metabolism, availability and minimum toxicity [97].

A biodegradable polymer is a type of material placed inside a biological system that will be degraded in biochemical ways at a certain time rate. Both chitin and chitosan are biodegradable. They are degraded enzymatically by chitinases and chitosanases in bacteria and lysozyme in mammals [98, 99]. The hydrolysis products of chitin and chitosan are its monomers, N-aceytl-D-gluocosamine and D-glucosamine (Figure 3.1). Glucosamine is suggested to produce anti-inflammatory, hepatoprotective, anti-reactive effects.

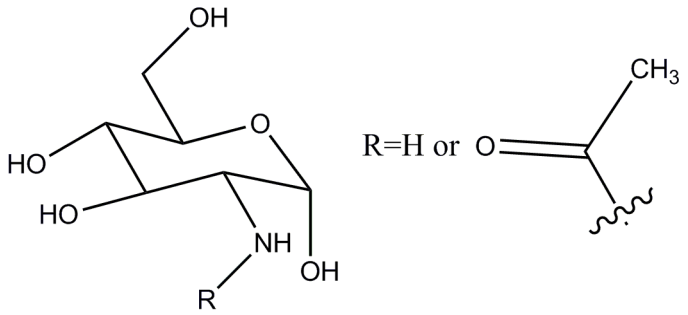

Fig. 3.1. The chemical compositions of gluocosamine and aceytl-glucosamine. The monomer is defined as glucosamine if R position is occupied by a proton. The monomer is defined as acetyl-glucosamine if R position is occupied as an acetyl group.

Chitin is the second most abundant polysaccharides in the biosphere, after cellulose. The discovery of chitin is attributed to Frenchman Braconnot in 1811 who found an alkali-resistant material from fungi [99]. The name "chitin" was derived from the Greek word "chiton", meaning cuticle by Odier in 1823, after he obtained the same material from the cuticle of beetles. The primary structure of chitin is N-acetyl-gluocosamine. It is also the major component in crustacean shells. Triggered by the increasing abundant shellfish waste in seafood industry in 1950's, extensive research targeted at converting chitin from waste to promising biomaterials. However, the poor solubility in aqueous and organic solutions limits the practical applications of chitin in industry.

As the principal derivative of chitin, chitosan is a naturally cationic polysaccharide which highly increases its solubility in a weak acid solution. Chitosan is produced by deacetylation of its parent polymer chitin with alkali and it naturally occurs in certain fungi (Mucoraceae). Chitosan was first isolated by Rouget treating chitin with potassium hydroxide in 1859. It was named as chitosan by HoppeSeyler in 1894. Then, the structure of chitosan was finally solved as a linear copolymer, consisting of β (1-4) linked 2-acetamido-2-deoxy-β-D-glycopyranose (acetylated glucosamine monomer)

and 2-amino-2-deoxy-β-D-glycopyranose (deacetylated glucosamine monomer) (Figure 3.2.).

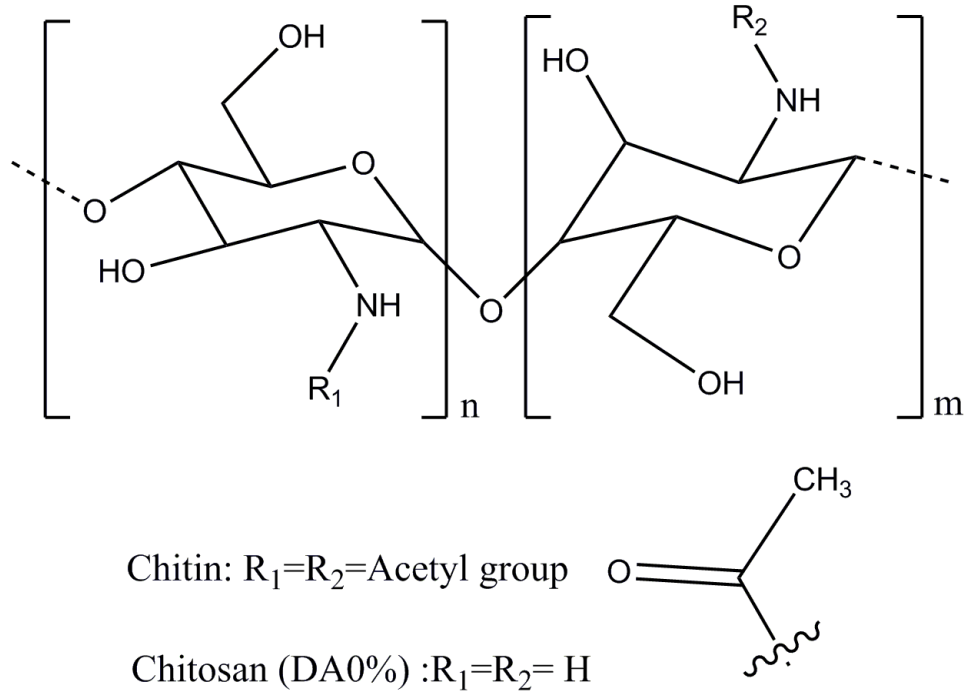

Fig. 3.2. The chemical compositions of chitin and chitosan. Chitin is defined when R1 and R2 positions are occupied by acetyl groups. Chitosan is defined if a part of positions (R1 and R2) is occupied by protons. The percent can be varied from 0%-100%. n and m represent the number of monomers in the polymer.

Chitosan has a pKa 6.5. It can be protonated at the deacetylated sites in weak acid solution. Based on the chemical processing, chitosan is usually defined by two major characteristics: 1). degree of acetylation (DA) which is the number of the fraction of acetylated unit per polymer molecule; and 2). molecular weight (MW) which is the number of sugar units per polymer molecule. The protonation degree of chitosan is proportional to DA. The higher the DA, the higher amount of charges that chitosan can carry. In addition, higher MW results in higher viscosity of the suspension of chitosan. This is due to inter-and intra-molecular interactions, especially hydrogen-bonds. The morphology tends to be coil-like as well. Ideally, chitin is defined as fully

acetylated form and chitosan is defined as fully de-acetylated form. In this work, Chitin is referred as the polymer with DA 100%. Chitosan is the polymer with DA less than 100%.

Chitosan has become one of the most interesting biopolymers because of its abundant renewable resource and its various biological activities. Due to the active primary amino groups on the polymer, chitosan can be used as an absorption enhancer, pharmaceutical excipient, metal recovering agent, hypocholesterolemic agent, film-forming agent, coagulant, polymeric scaffolds, and wound healing areas [50–53]. Global Industry Analysts, Inc., (GIA) predicted that the global market of chitosan would reach US$21.4 billion by the year 2015 with a surging demand in agrochemicals and healthcare fields [100]. Chitosan and its derivatives also have neuroprotective effects (Table 3.1), mainly contributed by the activity of free primary amino groups. The electrostatic interactions are suggested to be one of the major mechanisms of neuroprotection. However there is no consistent opinion on the optimum MW and DA in terms of potential therapeutic effects by chitosan polymer.

In traumatic spinal cord injury (SCI), the integrity of the cell membrane is directly compromised by mechanical forces. The animal cell membrane consists of membrane lipids and trans-membrane proteins and serves as a selective permeable barrier to regulate the exchange of molecules at both cytosol and extracellular environments. Phospholipids, glycolipids, and cholesterol are major components of animal cell membrane lipids, with phospholipids being the most abundant. A phospholipid molecule is an amphiphile. It contains both hydrophobic (fatty acid chains) and hydrophilic components (a backbone, a phosphate and an alcohol molecule). When the backbone of a phospholipid is a glycerol molecule, it is called as glycerophspholipid. When the backbone is sphingoid, the lipid molecule is sphingolipids . The anionic character of the cell membrane surface is contributed mainly by phosphate headgroups of phospholipids on the membrane bilayer (Figure 3.3). Based on the types of fatty acid chains, glycerophosphlipids can be classified further as phosphatidylcholine (PtdCho), phosphatidylethanolamine (PtdEtn), phos-phatidylserine (PtdSer), phosphatidylinositol

Table 3.1
In vivo neuroprotective properties of chitosan and chitosan derivatives.

Diseases	Applications	Chitosan (Chi) Chi-derivatives	DA	MW(Da)
Alzheimer's	Suppressing β -Amyloid Formation	Aminoethyl-Chi, Dimethylaminoethyl-Chi,	50%, 25%, 10%	Oligo
Alzheimer's	Inhibiting Acetylcholinesterase	Diethylaminotheyl-Chi, Chi	50%, 10%	10K,5K,<1K
Pathogen Infections or Irritations	Anti-inflammation	Water soluble Chi		
Serum Deprivation	Inhibiting Apoptosis	Water soluble Chi	10%	300K
Acrolein	Suppressing ROS	Chi, Chi-Nanoparticles	15%-20%	200K [27]
SCI	Sealing Membrane Breaches	Chi	15%-20%	200K [26]

(PtdIns) and phosphatidic acid (PA). At the cell membrane plasma level, PtdCho is the most abundant membrane lipid on the luminal side and it accounts for more than 40% of phospholipids. A PtdCho molecule is zwitterion which carries neutral charge due to the anionic phosphate group and cationic choline [11].

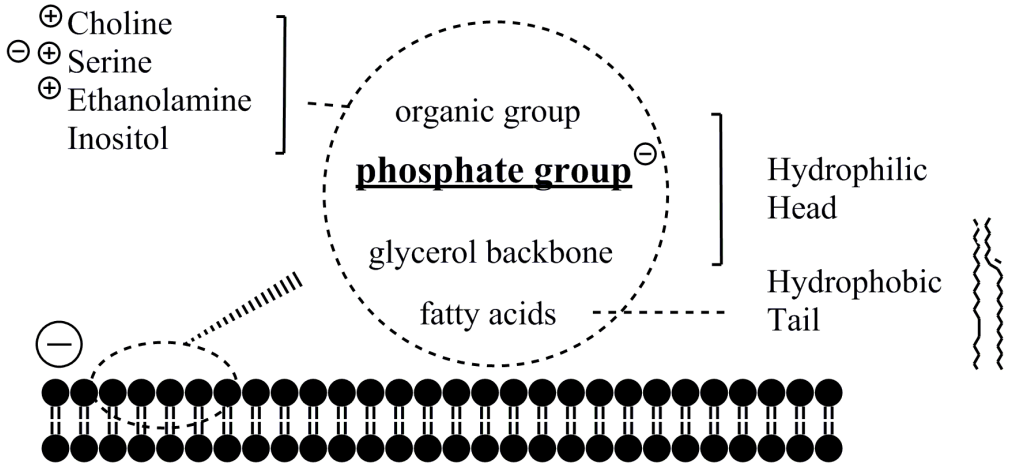

Fig. 3.3. The illustration of a phospholipid molecule on the cell membrane. A phospholipid molecule is composed of the hydrophilic head (an organic group, a phosphate group, and a glycerol backbone) and the hydrophobic tail (fatty acids). The organic groups of a phospholipid can be choline, serine, ethanolamine, and inositol. The cell membrane is charged negatively overall which is contributed mainly by the anionic phosphate groups.

A previous study showed that the administration of chitosan successfully inhibited the exchange of molecules (an endogenous enzyme, lactate dehydrogenase (LDH) and a fluorophore) between the cytosol and extracellular medium [26]. Since chitosan is cationic, a possible mechanism was suggested primarily through electrostatic interactions between the cationic amino groups of chitosan and anionic phosphate groups on the membrane lipids. Consequently, the compromised membrane holes were blocked and, furthermore, the partial recovery of electrical conduction through the lesions of isolated spinal cord tissue was also observed, while the absence of response persisted in control groups. Therefore, the number of amino groups, also referred as charged density or DA, should play a critical role in the chemical properties of chitosan. In

addition, Quemeneur indicated the profound effect of MW of chitosan polymers on the interactions with membrane lipids [101].

In this work, we further investigated the effects of DAs and MWs of chitosan polymer on specifically its neuroprotective effects. We utilized a standard compression injury model on isolated spinal cord tissues to study the capabilities of chitosan polymer with different MWs and DAs. Dye-exclusion and leakage of endogenous enzyme tests were performed to evaluate sealing by chitosan polymer with different MWs and DAs. The distribution of chitosan polymer on both damaged and intact spinal cord segments was also investigated.

3.2 Methods and materials

3.2.1 Spinal cord isolation

We followed the method as described previously (section 2.2.1 on page 21).

3.2.2 Transection and compression injury procedures ex vivo

1cm spinal cord strips were carefully dissected from each isolated spinal cord using a miniature scalpel-like cutting tool (#10315-12 microscaple). The segments were randomly divided into two groups: injured-untreated and injured-treated segments. Two types of injury models were used in this study: compression injury and transection injury. After additional incubation of dissected segments in Kreb's solution, the compression injury was induced by a 15s constant mechanical compression at the center of each segment by a modified forcep processing a spacer. The transection injury at ends of each segment was a requisite of the initial dissection. Therefore, no further incubation was performed. In the injured-treated group, samples were incubated with different DAs (0%, 10%, 20%, 100%) and MWs (oligo-chitosan 5kDa, low-chitosan 100kDa and medium-chitosan 200kDa) of chitosan aqueous solutions (Table 3.2). The injured-untreated samples were incubated in a freshly prepared

Table 3.2
Chitosan polymer with different DAs and MWs.

	#	Abbreviation	Chitosan(Chi) Samples	DA(%)	MW(Da)
MW	1	Low	Low MW Chi	15-25	100K
	2	Medium	Medium MW Chi		200K
	3	Oligo	Oligo MW Chi		5000
DA	4	DA0	DA0%Chi	0	
	5	DA10	DA10%Chi	10	
	6	DA20	DA20%Chi	20	
	7	DA100	DA100%Chi (Chitin)	100	

phosphate-buffer saline solution (PBS). 0.1% (w/v) chitosan solutions were prepared in 1% acetic acid and underwent overnight magnetic stirring to achieve a complete dissolution. All solution samples were bubbled with 95% O_2, 5%CO_2 throughout the duration of the experiment.

3.2.3 Detecting membrane integrity using a biochemical assay: Lactate Dehydrogenase (LDH) cytotoxicity assay

A large endogenous enzyme, Lactate Dehydrogenase (LDH, 140 kDa) was used as a membrane breach indicator. The leakage of this large enzyme into the extracellular space was a gauge of how severe such breaches were. The reduction of nicotinamide adenine dinucleotide (NAD) to NADH by LDH in extra-celluar medium can be specifically detected by colorimetric assay at 450nm. The compression injury was performed on equally weighted fresh spinal cord strips using a modified forceps processing a spacer. Then, segments were treated immediately with different DA and MW chitosan aqueous solutions and PBS solutions (negative control) respectively for 15 mins. After rinsing with PBS solution for three times to remove any leaked

LDH extra-cellularly, spinal cord strips were incubated in 1ml fresh PBS solution for additional 45mins to allow LDH leakage from un-repaired membrane breaches. 600μl bathing solution was tested using the TOX-7 kit (Sigma-Aldrich, Inc, USA). The absorbance was read at 490nm and 690nm using a multi-well plate reader on a spectrophotometer (plate reader). The final value was calculated by subtracting the background value (at 690nm) from the primary wavelength measurement (at 490nm). Six replicates were applied in this study.

3.2.4 Detecting membrane breaches using fluorescence microscopy with a Tetramethylrhodamine (TMR) fluorophore

we used a membrane impermeable fluorescent dye, tetramethylrhodamine (TMR)-dextran (10kDa), to indicate the degree of membrane damage and fluorescent microscope to measure fluorescence intensity. Transection injury was used since this would be the most extreme test of membrane sealing-even though transection of white or gray matter is clinically uncommon. Transection was performed on 1-cm segments of spinal cord strips. The damaged strips were immediately treated with 0.1% (w/v) different DA and MW chitosan aqueous solutions and PBS solution, respectively for 15mins. Then, all segments were transferred and incubated in 0.1%TMR-dextran solution for 15 mins in the dark. After rinsing with 0.1 mol/L fresh PBS solution three times, samples were fixed in 4% paraformaldehyde for 5h at 4°C in the dark. After fixation, the segments were embedded in Tissue Tek OCT compound, frozen in liquid nitrogen. Sections were cut at 50μm thickness using a freezing microtome and visualized by epi-fluorescence on an Olympus BX61 microscope with a standard rhodamine cube (excitation filter, 545nm and emission filter, 590nm, Olympus). Rhodamine fluorescence images were captured at a 2x objective. At this magnification, the whole section was captured within one image. The images were saved for further analysis. All parameters of the fluorescence microscope were kept constant during the experiment. Quantification of the fluorescence intensity was measured by using Im-

age J software (NIH). Five sections or images were randomly selected from the injury zone for each treatment at each experiment. Six replicates were conducted for each treatment in this test. The injury zone was defined as the area within 1-2mm of the exact plane of transection. 30 images were measured to produce the average intensity value for each treatment. The fluorescence intensity of white matter in each section was taken after manually outlining the boundary of the white matter manually. The value of the fluorescence intensity was expressed in arbitrary units, generated from the software.

3.2.5 Tracing the locations of chitosan polymer (DA0) using fluorescence microscopy with a fluorescein Isothiocyante (FITC)-dextran fluorophore

In order to trace chitosan polymer in damaged and un-damaged spinal cord strips, fluorescein isothiocyanate (FITC)-labeled chitosan DA0 was used to identify the location of chitosan in tissue segments. FITC-chitosan conjugation was prepared according to the method of Qaqish et al. [25, 102]. The procedure was as follows: 1%(w/v) chitosan DA0 was dissolved in 0.1M acetic acid by magnetic stirring overnight. 0.1% FITC in methanol was slowly added to the dissolved chitosan solution. The isothiocynate group (N=C=S) reacted with the primary amine group ($-NH_3^+$) of the chitosan polymer to form chitosan-FITC conjugation (Figure 3.4).

We allowed the reaction to proceed for 1h in the dark at room temperature. Then FITC conjugated chitosan solution was treated with 0.1M sodium hydroxide solution. The precipitation was formed at the bottom and collected by washing with de-ionized water for at least 3times to remove any free FITC molecules from the mixture. The polymer then was air-dried and stored in-20°C for further applications. It was documented that 2.3% of the amino groups of chitosan were modified in this reaction without altering the actual basic structure of the polysaccharide which was determined by elemental analysis. 0.1% FITC-chitosan solution was freshly prepared

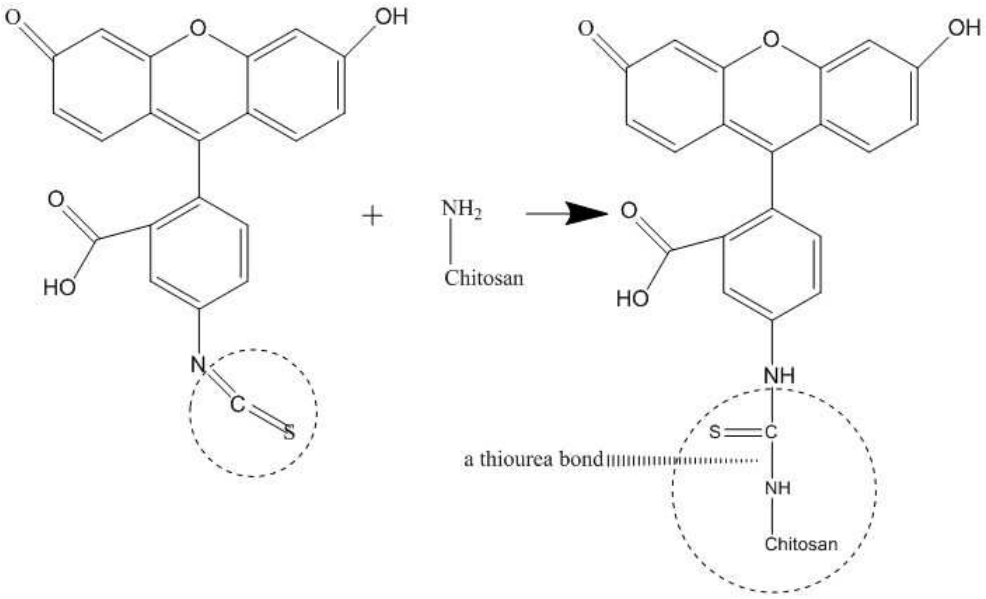

Fig. 3.4. The illustration of the conjugation of FITC-chitosan. A thiourea bond is formed between the isothiocyanate reactive group (-N=C=S) of a FITC molecule and the amino-group of chitosan polymer.

in PBS. The compression injury was performed in the middle of isolated spinal cords as describe. The intact segments located 2cm away from the compression site were served as self-controls. The whole cord was immediately incubated in the FITC-chitosan solution for 15mins in the dark to allow the sufficient fluorescence labeling at the potential areas. Then the cord was rinsed with Kreb's solution for three times to remove any free FITC-chitosan extracellularly. 1-cm segments were dissected from the injury site and intact sites and fixed in 4% paraformaldehyde for 5hrs at 4°C in the dark. The methods for the fixation and epi-fluorescence quantification were the same as described above in method of TMR. The difference is that the excitation and barrier wavelengths for FITC were 490 and 520nm respectively. Five replicates were used in this study.

3.2.6 Chemicals and reagents

TMR-dextran and FITC-dextran were purchased from invitrogen (life technologies). Chitosan (DA0%, DA10%, and DA20%) was purchased from CarboMer Inc. Chitosan (oligo lactate, low, medium MW and chitin), LDH cytotoxicity assay kit and all other chemicals used were purchased from Sigma Aldrich (St.Louis, MO). Microtome was purchased from Thermo Electron (Waltham, MA). Olympus BX61 microscope is located at Center for Paralysis Research (CPR) at Purdue University. #10315-12 microscaple was purchased from fine science tools (Foster City, CA).

3.2.7 Statistics

All data were represented as means±standard deviation (SD). Statistical analysis was conducted using one-way ANOVA (SAS 9.2, SAS institute inc., NC, USA). The comparison between untreated (PBS) and treated (different DA and MW chitosan) groups were subjected to Dunnett's test. The comparison among different chitosan treatment groups were subjected to Tukey's test. Values were accepted as being statistically significant difference if the P value was less than 0.05.

3.3 Results

Membrane permeability with treatments of different DA and MW chitosan was evaluated by TMR dye exclusive test and LDH assay.

3.3.1 The inhibition of TMR uptake in transection injured spinal cord by chitosan polymers

Data was normalized by the value of PBS groups and presented as decimals, where 1 was equivalent as 100%. Strong fluorescence intensity of TMR in controls indicated the intensive uptake of fluorophores through the compromised membrane at the damaged tissue sections (Figure 3.5). In contrast, the fluorescence intensity

in groups with chitosan treatments decreased significantly regardless of MW and DA ($P<0.05$) (Figure 3.6). Except for DA100, more than a 20% decrease of fluorescence intensity was observed in other chitosan treatments ($P<0.01$). However, no obvious DA or MW dependent effect was observed ($P>0.05$).

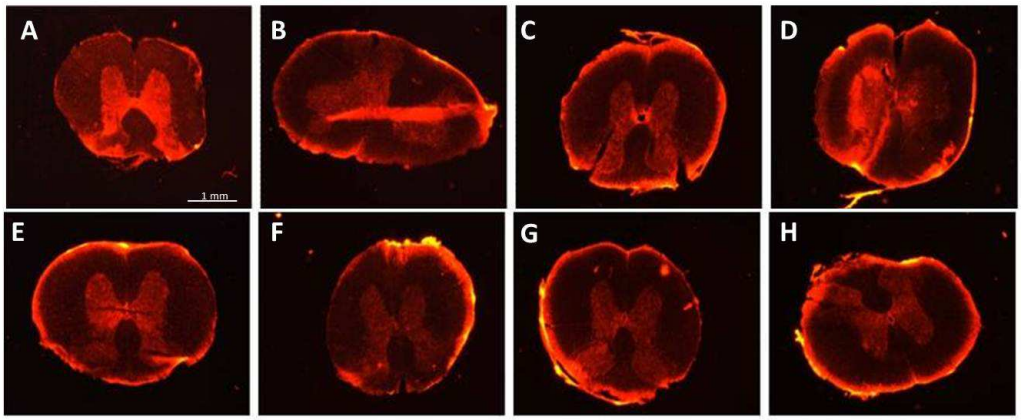

Fig. 3.5. The fluorescence intensity of TMR uptake after transection injury and its inhibition by different chitosan treatments. (A) Fluorescence intensity of TMR uptake in a cross-section of spinal cord given transection injury with PBS treatment (control). (B-H) Cross-section graphs showing different degrees of decreasing fluorescence intensity of TMR labeling in transected spinal cord with chitosan treatments. (B) Transection injury with DA100 treatment. (C) Transection injury with DA20 treatment.(D) Transection injury with DA10 treatment.(E) Transection injury with DA0 treatment.(F) Transection injury with Low MW treatment. (G) Transection injury with Medium MW treatment.(H) Transection injury with Oligo MW treatment.

3.3.2 The inhibition of LDH leakage at the compression injured spinal cord by chitosan polymers

The membrane sealing effect of chitosan was further confirmed by the inhibition of the leakage of the intracellular enzyme Lactate Dehydrogenase (LDH) (Figure 3.7). The signal intensity was proportional to the amount of LDH present in the bathing solution and inversely related to the condition of the membrane. More than a 60%

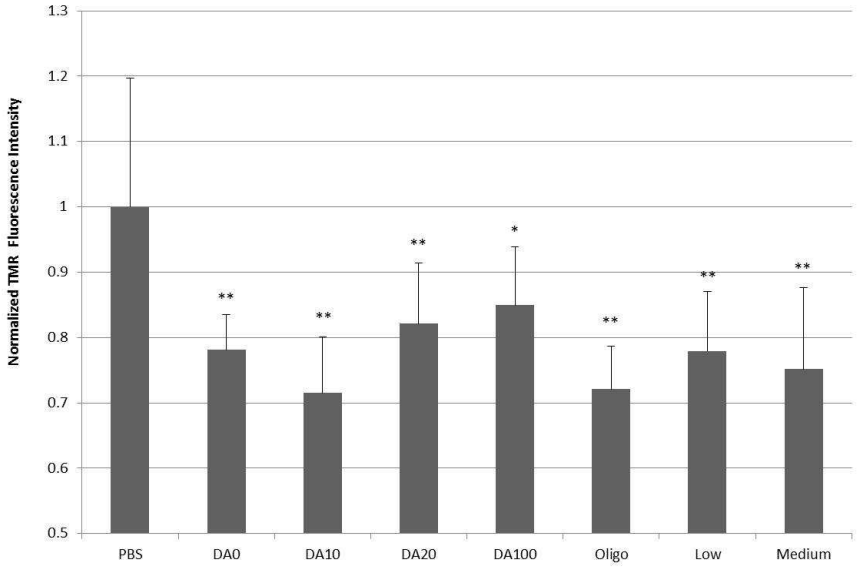

Fig. 3.6. Quantification of normalized fluorescence intensity of TMR uptake as a function of chitosan treatments. The fluorescence intensity in PBS group used as the control. Note that all chitosan treatments significantly decreased the fluorescence intensity of TMR uptake following the transection injury, *P<0.05 , ** P<0.01 (Dunnett test). N=6.

decrease of the signal intensity with the treatments of all chitosan strongly indicated the sealing effects of chitosan ($P < 0.05$). Similar to the Tetramethylrhodamine (TMR) test, we did not observe any correlation with the result and the composition (MW and DA) of chitosan.

3.3.3 The distribution of FITC-chitosan polymers in both intact and compressed spinal cord segments

To investigate the affinity of chitosan polymer at damaged tissue, the intensity of FITC-chitosan was measured in both compressed and intact spinal cord segments. A significant difference of intensity of FITC-Chi (DA0) labeling between the compression regions and intact regions was not detected (P>0.05) (Figure 3.8).

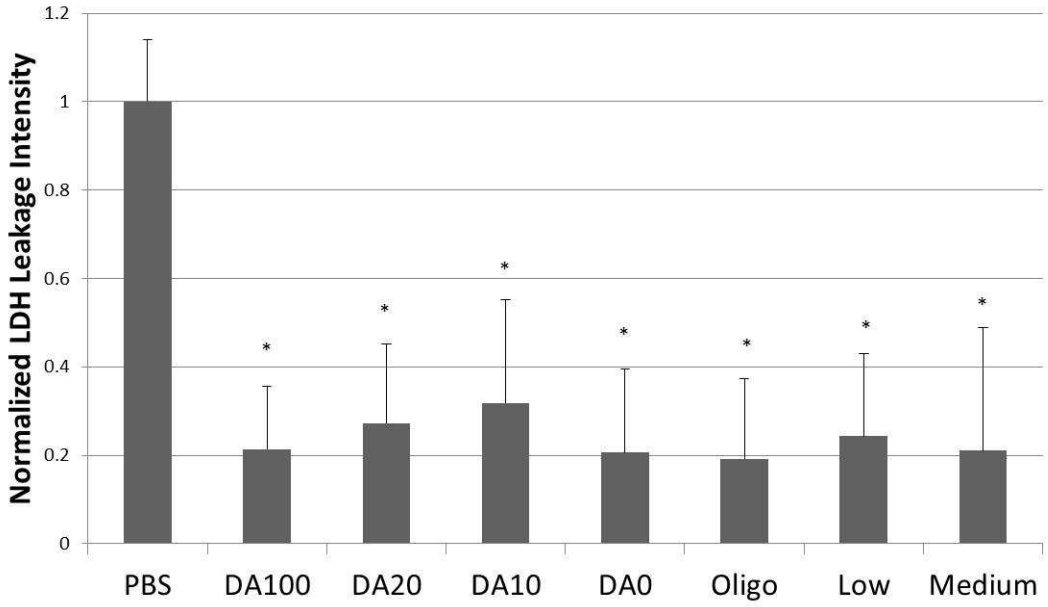

Fig. 3.7. Quantification of normalized fluorescence intensity of LDH leakage as a function of chitosan treatments. The fluorescence intensity in PBS group was used as the control. Note that all chitosan treatments significantly decreased the fluorescence intensity of LDH leakage following the compression injury, *P<0.05 (Dunnett test). N=6.

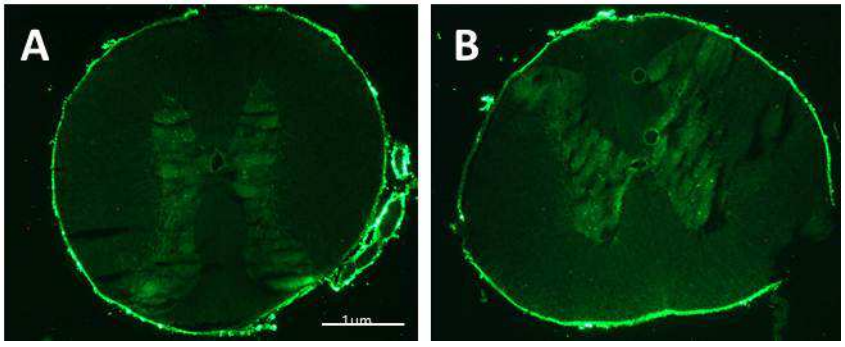

Fig. 3.8. The distribution of FITC-Chitosan on injured (compression injury) and intact spinal cord segments. No obvious difference of the labeling of FITC-Chitosan was observed between the injured and intact cords. (A). The cord with the compression injury. (B). The cord without the compression injury.

3.4 Discussion

3.4.1 Membrane resealing mechanisms

Membrane resealing can be achieved through different mechanisms based on the size and properties of the components that interact. When the size of the membrane disruption is relatively small, rapid membrane resealing can be accomplished through the lateral diffusion of continuous bilayers. The exposure of hydrophobic domains of membrane to the physiological fluid creates an energetically unfavorable area which acts as a driving force to induce the spontaneous aggregation of neighboring membrane lipids via hydrophobic interactions and hydrogen bondings. In nucleated animal cells, Ca^{2+} influx triggered-exocytosis is a key step in the membrane self-sealing. Membrane lipid molecules can be inserted at the continuous bilayer which indirectly reduce the size of the "hole". In the case of the larger "hole" in the membrane, a patch of lipids are accumulated and fused together at the disrupted region to block the random exchange of materials across the membrane.

Surfactant polymers such as polyethylene glycol (PEG) and Poloxamer 188 (P188) are well-known as membrane fusion agents. PEG is a hydrophilic molecule. Each ethylene oxide unit of PEG molecule typically react with 2-3 water molecules [103]. By associating with water molecules, PEG brings adjacent membrane lipids into close physical contact which results in the re-organization of membrane lipids via hydrophobic interactions. On the other hand, P188 is an amphiphilic macromolecule. It mimics behaviors of phospholipids and is incorporated into membrane structure at the low packing density of lipids. Chitosan is a cationic polysaccharide. Chitosan is suggested to interact with membrane lipids by electrostatic interactions between the free primary amino groups and the negatively charged phosphate groups. The insertion of chitosan polymer at the bilayer is also indicated via hydrogen bonding and hydrophobic interactions with acyl chains.

Our results revealed that chitosan indeed functioned as an important intervention in acute spinal cord injury, regardless of its DA and MW. Specifically, the TMR and

LDH study confirmed the significant effect of chitosan on inhibiting i.) the intrusion of an exogenous applied dye into damaged spinal cord cells ($P<0.05$); ii.) as well as escape of a large endogenous enzyme LDH.

3.4.2 The effect of degree of acetylation (DA)

The different DA represents different strengths of electrostatic interaction between the cationic chitosan and anionic lipids. Specifically, the lower the DA, the higher the number of positive ions a chitosan molecule carries. In turn, the higher concentration of surface charges on chitosan enables a more extended conformation due to electrostatic repulsion among charged amines on the chitosan backbone. Therefore, the polarity of the molecules is greatly enhanced. Since the lipid head-groups are negatively charged, molecules with lower DA might have a greater opportunity to diffuse close to the membrane breaches, and thus adsorb and seal the membrane through electrostatic interactions. This mechanism is consistent with previous studies in which chitosan polymers incorporated with artificial membrane films and vesicles. These physical attractions and interactions were a result of membrane adsorption [101, 104–106]. Our data however, did not reveal a hint of an improvement in function of chitosan when the DA is decreasing. Possible reasons might be due to (1) the concentration of chitosan polymer was too high which masked the DA effect, since the available binding sites on the membrane might be over-saturated with chitosan polymer, (2) the neuroprotective effect of chitin might suggest a different mechanism other than electrostatic interactions with the membrane. However, those hypothesis need further tests to prove.

3.4.3 The effect of molecular weight (MW)

Here, equivalent sealing effects using different MW chitosan treatments was suggested in both TMR and LDH tests, and in both transection and compression ex vivo injury models. Based on the fact that different MW chitosan in our study shared a

similar DA, one possible reason for the consistency of data found in different MW chitosan treatments might be the predominant role of DA over chitosan MW in initiating membrane repair. The chitosan bioactivity on the membrane lipids was suggested not only due to the electrostatic interactions [104]. A similar result is also observed in the zeta-potential evaluation of the influence of different MWs of chitosan on membrane adsorption [101]. The data shown in Figure 3.6 reveals that all tests showed a statistically significant reduction in TMR fluorescent intensity. There was little difference between them however - with the exception of DA100 which revealed a possible lower capability for sealing, but this difference did not reach statistical significance. The MW of chitosan is closely related with the morphological structure of chitosan presented in the aqueous solution. Typically, the two most common structures are 1.) rope-like and 2.) coil-like polymeric shapes. The most likely shape in an oligochitosan solution would be rope-like due to the relatively few numbers of monomers existing in the chitosan. The less folded main chains of this polymer require less energy to diffuse close to the cell membrane and fit near or into its breaches. MW is also proportional to the viscosity of the aqueous solution, which reflects the hydrodynamic diameter of chitosan molecules; refer back to Figure 3.7 and Figure 3.6 [107]. The degree of the intermingling entanglement of chitosan polymer is proportional to the chain length, in other words - the MW. Considering the higher MW of Medium chitosan which is 40 times the size of the oligomer, this might result in the reduced mobility of the polymer. This is likely to enhance polymer adhesion by increasing the contact area between chitosan molecules and lipids [108]. However, our results did not show the differences of MW induced function of chitosan based on dye exclusion (TMR) and protein leakage (LDH) tests.

3.4.4 The effect of targeting

In our study, Chitosan (DA0) polymers were covalently linked with FITC fluorophores. The distribution of chitosan polymer (DA0) at both damaged and intact

regions of spinal cord tissues was represented by the localization of FITC signal. A significant difference of the distribution of chitosan polymer (DA0) was not detected between the damaged and intact regions ($P>0.05$). Similar conclusions were suggested in the interaction of chitosan polymer with membrane models, such as Langmuir films [104]. Even though chitosan polymer is not surface active, it can interact with phospholipid monolayers through electrostatic interactions, hydrogen-bonding and hydrophobic forces [104–106]. Based on the packing density of the phospholipids, chitosan can either insert between membrane lipids or attach on the subsurface of the monolayer. However, our result was shown to be inconsistent with the previous report which indicated the affinity of chitosan polymer at the sites of the compromised membrane lipids in Cho's work [26]. The disagreement of the targeting of chitosan polymer at the sites of the compromised lipids might be due to using chitosan polymers with different MW and DA. In order to illustrate the preference effect of chitosan polymer on compromised membrane lipids, further test needs to be developed.

3.4.5 Restoration or disturbance of cell membrane

The interaction of chitosan polymer with membrane lipids is confirmed by both model and biological membrane lipids [105, 106]. The neuroprotective effects of chitosasn (nanoparticles) observed in PC12 cells, isolated spinal cord tissues and whole animals studies were suggested to be mediated through membrane restoration [27]. Other neuroprotective effects of chitosan are also observed in applications (Table 3.1). On the other hand, the strong binding capability of chitosan polymer with model membrane lipids which were "squeezed" at high lateral pressure suggested the potential of membrane incorporation or even disturbance among tightly packed lipid molecules [105, 106]. The disturbance of chitosan on cell viability, presumably through membrane disturbance, was observed in high concentration (>1mg/ml), cell types (primary cardiomyocytes), and incubation period (>24hours) (data not shown).

Chitosan is also suggested to be used to "digest" bacteria cells by interacting with phosphoryl groups of E.Coli [109]. In addition, the amino groups on chitosan polymers can interact with blood cells and initiate haemostasis [110]. Chitosan patches have also been developed to quickly stop the bleeding. Therefore, the beneficial effect of the systemic circulation of chitosan polymers might be counteracted and the unnecessary interactions with serum protein might lead to the quick clearance by phagocytosis. Chitosan derivatives and chitosan based nanoparticles are developed to increase the solubility in the physiological conditions, reduce the hemostasis effect and other side effects based on bulk materials.

3.5 Conclusion

Chitosan reduced the exchange of large endogenous enzymes and fluorescent probes across the membrane damage. A significant difference of DA and MW dependent sealing effects of chitosan was not detected in the isolated spinal cord segments. A significant difference of affinity of chitosan at damaged or intact tissues was not observed as well.

4. INVESTIGATING AND OPTIMIZING THE SYNTHESIS OF CHITOSAN NANOPARTICLES (CHI-NPS)

4.1 Introduction

Nanomedicine is the application of nanotechnology to medicine. Advanced nanomedicine technology brings opportunities for innovative drug development and drug delivery methods. Medicinal nanoparticles (NPs) are constructed at the size scale of a billionth part, generally less than a micron. Why does the size of particles matter in medicine? The size of NPs is similar to the size of biological molecules - even viruses - which increases their biocompatibility and reduces the chance of being phagocytized [56]. Phagocytes, such as neutrophils, monocytes, and macrophages function as part of the innate immune system. Phagocytosis is an endocytosis process where phagocytes engulf and destroy any foreign objects in the body. Phagocytosis is sensitive to objects with a size larger than 0.5μm [54]. NPs with 10-500nm sizes are suggested to remain in the circulation for an extended period of time with the intravenous administration [111]. Objects with irregular morphologies can also enhance the initiation of phagocytosis [55]. Materials with nano-structures also exhibit fundamental different properties from simple chemicals and these unique characteristics are not derived from the elemental composition alone. To name a couple of examples, carbon nanotubes and "quantum dots" or nano crystals. Carbon nanotubes have unique and remarkable electronic and mechanical properties which give rise to many applications: flat panel displays, gas storage devices, conduction paints and others [112]. Semiconductor "quantum dots" are particles with nanometer scale and capable of emitting size-tunable light. The light emission is significantly brighter

and more resistant to photobleaching than other dyes (organic dyes and fluorescent proteins) [113].

There are many advantages of using nanocarriers in drug delivery [56]. Nanocarriers with large surface/volume ratios can serve as a great reservoir for drugs, genes and stem cells. The releasing profile can also be tailored according to the physicochemical properties of the nano-carriers. In addition, packing therapeutic compounds into small (nano-scale) "envelopes" preserves the activity of the compounds from opsonization which in turn suppress opsonization-induced phagocytosis and increase the retention time of the drug (with the nano-carrier) in the blood circulation [114–116]. Opsonization describes the process that antibodies label the foreign objects for destruction by phagocytosis. Nanocarriers can also enhance the solubility of hydrophobic drugs in physiological fluids. The affinity of nanocarriers with different types of cells can be modified by attaching targeting moieties. For example, AP peptides were linked on the glycol chitosan NPs to direct the sufficient accumulation of NPs at the tumors [117]. Hyaluronic acid (HA) acted as targeting molecules for cancer cells where HA receptor CD44 was overexpressed on cancer cells [118]. Folic acid-NP conjugation was developed to induce folate receptor-mediated cancer cell specific gene delivery [119]. Interleukin-4 receptor binding peptide was successfully attached on the glycol chitosan NPs to increase the retention of the NPs at the tumor site [117]. Therefore, the increasing accumulation of NPs on defined groups of cells minimizes non-specific binding induced harmful side effects.

Nanomedicine can be developed as either a "permanent" nanodevice which acts as a supportive structure, such as artificial heart valves, or a "temporary" nanodelivery system for diagnostic, therapeutic, or theranostic purposes. Theranosis describes the combination of diagnostic and therapeutic modalities by one system for the treatment of the disease. Based on the purpose of the applications of the nanomedicine, the choices of nanomaterials are varied. NPs are developed based on quantum dots, gold, silver, iron oxideNPs (imaging), liposomes, carbon nanotubes, fullerenes, silica, polyethylene glycol, chitosan (drug delivery), and their composites (Theranosis) [56].

The "permanent" nanodevices require nanomaterials with superior mechanical properties to counteract the fatigue or collapse of the material in the body long term. Whereas, the "temporary" delivery system, commonly implemented by NPs, requires an exit strategy for the excretion of nanomedicine from the human body after drug delivery. Meanwhile, the toxicity of both the accumulation of nanomaterials and the generated by-products during the process of the enzymatic metabolism of the nanomaterials needs to be minimized.

The next question is why do biodegradable materials matter in therapeutic NPs? A biodegradable material is a type of material that when placed inside a biological system will be degraded via biochemical pathways at a certain time rate [99]. Using biodegradable nanomaterials as drugs or drug delivery systems is the most ideal strategy for combining multiple goals in current medicine research and development, as introducing "biodegradable foreign materials" inside the human body causes no stress or harm [97]. The journey of a biodegradable nanomaterial inside the human body is to perform the therapeutic task by delivering the content in a quantized way, to be "digested" and excreted as harmless by-products or residues out of the body.

Chitosan is a naturally cationic polysaccharide. It is a biodegradable polymer in nature and is suggested to be degraded by hydrolases, lysosomes in the human body. Chitosan has a variety of biological functions. It can be used as a membrane "fusion" agent, an absorption enhancer, pharmaceutical excipient, metal recovering agent, hypocholesterolemic agent, film-forming agent, coagulant, polymeric scaffolds, and wound healing agent [50–53]. Due to the flexible mechanical properties, it can also be processed into different forms, such as: film, hydrogel, and tablets. However, the biological applications of chitosan face a few obstacles. With a pKa of 6.5, the solubility of chitosan in physiological condition (pH7.3) is greatly reduced. Hemostasis can also be induced by the interaction between the primary amino groups with blood cells [110, 120].

As a biodegradable polymer, chitosan is one of the popular candidates for nanodelivery or NP applications [117]. The primary amino groups of chitosan can be

masked by reacting with anionic molecules to form Chitosan nanoparticle (Chi-NPs) complexes. Meanwhile, the solubility of chitosan polymer is also enhanced. The major methods of chitosan nanoparticle formation are summarized in Table 4.1. Among all, the ionic gelation method is suitable for biological applications where no harsh chemicals are involved [121,122]. It is based on the electrostatic interactions between cationic amino groups of chitosan and anionic groups of participants, such as triphosphate (TPP) and dextran sulfate (DS). Chi-NPs have shown neuroprotective effects on PC12-cells which were challenged with acrolein, an endogenous aldehyde generated highly after neurotrauma [27]. Chi-NPs are also capable of carrying and delivering different types of therapeutic drugs, for instance anticancer drugs (paclitaxel, cisplatin, docetaxel, and camptothecin), aldehyde-scavenger (hydralazine), anti-tumor peptides and genes [27, 123–126].

The major characteristics of nanomedicines are size and zeta-potential. The hydrodynamic size is more closely associate with the behavior of NPs in a biological fluid system which includes both the solvent layer and the dynamic layer. The solvent layer is the immobilized water on the surface of the bare NPs due to the hydration effect that includes hydrogen-bonding with water molecules. The dynamic layer is due to the thermal motion of submicron molecules, which is also referred as Brownian motion. The zeta potential describes the net effect of surface charges that NP carriers and the adsorption of counter-ions at the hydration layer of the NP. The surface charges of dried bare NPs are determined by the surface chemical properties of NPs, which also affect the distribution of ions in the medium. The accumulation of counter-ions on the surface of the NPs leads to the formation of electrical layers. By definition, zeta-potential is the potential at the surface of the hydrodynamic layer where ions are associated with the movement of NPs Figure 4.1. The magnitude of the zeta-potential and size indicate the potential stability of the NP suspension. A stable colloidal system will generally have a zeta-potential of $\pm$30mV or greater. Systems with zeta potentials less than that, may be stable, however, this is not certain.

Table 4.1
Methods of chitosan nanoparticle (Chi-NPs) formation. Methods based on chitosan derivatives are not included.

Methods	Pros	Cons
Emulsion cross-linking	Broad Size Range >200nm	Harsh crosslinking agents (glutaraldehyde)
Coacervation precipitation	Narrow size range (adjusting the nozzle size and air pressure)	Cross-linking agents (drug loading)
Spray-drying	Microparticles	Not for NPs formation
Emulsion-droplet Coalescence	High loading efficiency (without cross-linking agents)	Loading efficiency inversely affected by size
Ionic gelation	Mild and simple (no harsh chemicals)	
Reverse micellar	Narrow size range	Need surfactants
Sieving	Microparticles (500-700μm)	Not for NPs formation

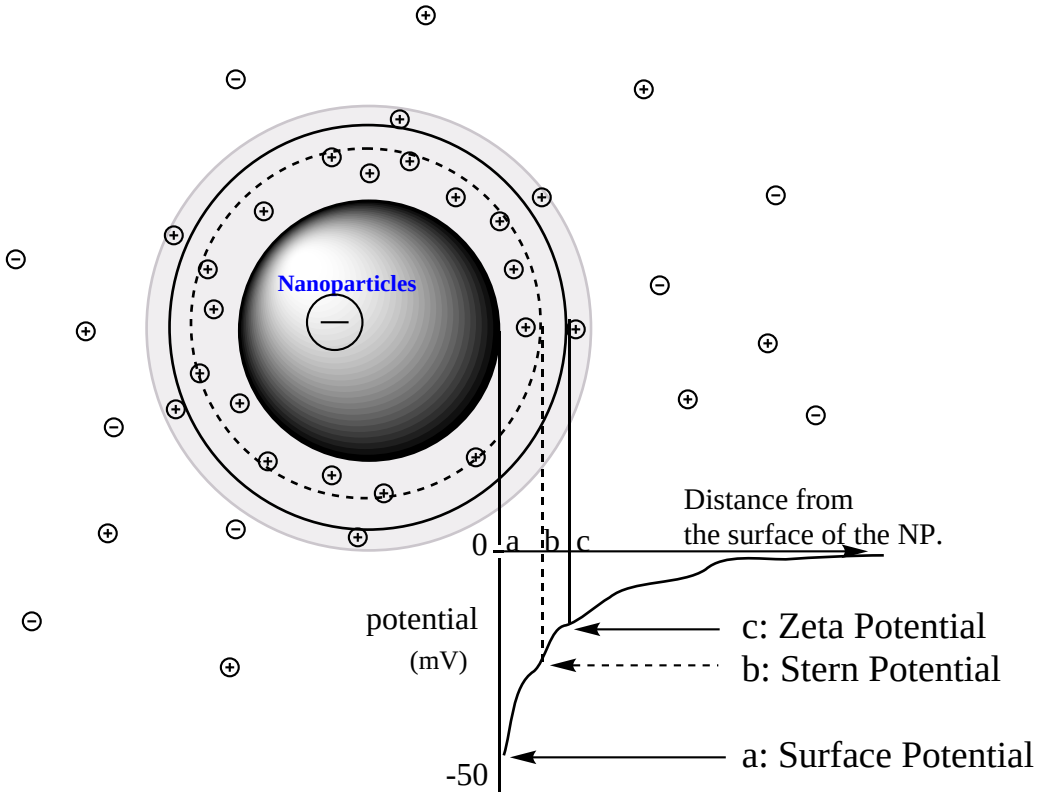

Fig. 4.1. The illustration of zeta-potential. A nanoparticle (NP) is shown to be incubated in the buffer solution. (a) Surface potential indicates the potential at the surface of the NP. If the surface potential of a NP is negative, it means that the NP carries anionic groups, such as RCOO-. (b) Stern potential indicates the potential at the stern layer. Due to the electrostatic interactions, counterions (cationic ions) in the buffer solution accumulate at the hydrated surface of the NP and these counterions tightly bind with NPs. As the distance from the surface of the NP is increasing, the attraction force between ions in the solution and the NP is decreasing. (c) Zeta potential indicates the potential at the slipping plate (next to the Stern layer) where the ions in the buffer solution are associated with the movement of the NP.

In this work, we synthesized and optimized the formation of ChiNPs based on the ionic gelation method. We formed two types of ChiNPs, namely Chi-TPPNPs and Chi-DSNPs. We measured the hydrodynamic size and zeta-potential during different pH and ionic strength environments to investigate the stability of NPs.

Since measurements of the size and zeta potentials do not guarantee NP formation, we used transmission electron microscopy to study the morphology changes of NPs with different preparation factors.

4.2 Methods and Materials

4.2.1 Chi-NPs prepared by an ionic gelation method

Chitosan nanoparticles were prepared using an ionic gelation method. The assembly relied on the electrostatic interactions between cationic chitosan polymer (200kDa) and anionic molecules chitosan-dextran sulfate (DS)(10kDa) and triphosphate (TPP) (387Da). The polymer reaction was highly susceptible to the pH change and dust accumulation. All reaction glasswares were autoclaved before sample preparations. Two types of chitosan nanoparticles were prepared in this study, chitosan-DS nanoparticles (Chi-DSNPs) and chitosan-TPP nanoparticles (Chi-TPPNPs). 0.1% chitosan was dissolved in 1% acetic acid solution and stirred overnight to achieve the complete dissolution and homogeneous distribution. 0.1% DS and 0.05% TPP in de-ionized water were freshly prepared and filtered through 0.45μm sterile syringe filters. DS or TPP solution was added dropwisely into chitosan solution under magnetic stirring with a rate of 2-3s/drop for 1h. The volume ratio were 5:3, 5:5, 5:8.5 for chitosan-DSNP and 5:1.5, 5:2 for chitosan-TPPNP formations. For DS-chitosan formation, the solution turned cloudy when the volume ratio was above 5:3. For TPP-chitosan formation, the solution was clear throughout the experiment. The nanoparticle solutions were kept in 4 °C until further analysis or experiment.

4.2.2 The purification of Chi-NPs by membrane dialysis

Regenerated cellulose dialysis membrane (300kDa) was soaked and rinsed with de-ionized water for 15mins to remove the remaining sodium azide. ChiNPs were carefully pipetted inside the membrane pocket. The pocket was sealed tightly with

dialysis closures on both ends. The dialysis membrane was placed in nano-pure de-ionized water with gentle magnetic stirring. The ratio of the loading solution and dialysis buffer was at least 1:100 to achieve the sufficient removal of un-reacted chemicals and salt ions. The buffer solution was changed every 2-3h for a total of 3 times before leaving it dialysis overnight. At the end of the dialysis procedure, the solution was retrieved from the dialysis pocket and kept in 4 °C until further analysis or experiment.

4.2.3 The morphology of ChiNPs by Transmission Electron Microscopy (TEM)

In order to confirm the synthesis of ChiNPs, the NPs were imaged with negative staining TEM. One drop of chitosan nanoparticle dispersion was placed on a carbon grid and allowed to settle for 2mins. Grid was swished through 2% uranyl acetate stain droplet and excess solution was removed with a filter paper. All samples were prepared in the method described above. Samples were imaged using a Philips CM-100 TEM operated at 100kV, spot3, 200μm condenser aperture and 70μm objective aperture. Images were captured using an SIA L3-C digital camera (Scientific Instruments and Application, Duluth, GA). Magnification was varied based on the quality of the results. Images were saved for further analysis.

4.2.4 The hydrodynamic size and zeta-potential measurements by zeta-sizer

Hydrodynamic size and zeta-potential were measured using a zetasizer (Zetasizer Nano ZS, Malvern Instruments Ltd, USA). The software affiliated to the instrument generated size quality report, z-avg, intensity and polydispersity indices (PDIs), and z-potential. The zeta-potentials were estimated from the electrophoretic mobility measurements using the Smoluchowski model. To minimize the fluctuation caused by temperature change and transfer samples, all samples were equilibrated 1-2h before

each measurement at room temperature. 1ml NP suspension was loaded to the disposable cuvette carefully to avoid bubble formation. Each measurement was repeated at least three times. Data was saved for further analysis.

4.2.5 The effects of ionic strengths on the hydrodynamic size and zeta-potential by zetasizer

Hydrodynamic size and zeta-potential were essential factors to evaluate stability of ChiNPs in different salt concentrations. The measurements were conducted as described in the above measurements. For higher ionic strength buffers (> 50mM NaCl), only two measurements were conducted in zeta-potential test to minimize the erosion of the cuvette. ChiNPs were incubated in different ionic strength buffers (0.01 XPBS-1 XPBS) at room temperature for 2 h or 24 h. Samples were loaded in cuvettes for measurements. Data was saved for further analysis.

4.2.6 Materials

Chemicals were purchased from Sigma-Aldrich. Syringes were purchased from Becton Dickison (BD) company. Cellulose Ester (CE) Dialysis membrane was purchased from Spectra/Pro Biotech. Syringe filters were purchased from Pall Corporation (Life Sciences), GE healthcare (Life Sciences, Whatman), and Corning Inc.. The freeze dryer (VirTis Benchtop K) is located at Center for Paralysis Research (CPR) at Purdue University. The Zetasizer (Zetasizer Nano ZS, Malvern Instruments Ltd, USA) is located in Birck Nanotechnology Center at Purdue University. The TEM is located at Life Science Microscopy Facility at Purdue University.

4.2.7 Statistics

All data were represented as means ±SD. Statistical analysis was conducted using one-way ANOVA (SAS 9.2, SAS institute inc., NC, USA). Values were accepted as being statistically significant difference if the P value was less than 0.05.

4.3 Results

4.3.1 Transmission Electron Microscopy (TEM)

The effect of pH on ChiNP formations

The morphologies of ChiNPs were observed by TEM negative staining technique. As shown in Figure 4.2, MC-TPPNPs were formed in both pH 4.3 (Figure 4.2 A) and pH 9.1 (Figure 4.2 B). ChiNPs appeared as dark spheres which were stained by uranyl acetate. After 2 week's air dried at room temperature, the global shape of all NPs was still preserved (Figure 4.2C,D). No distinct difference of the morphology and size distributions of Chi-TPPNPs was observed between two pH conditions.

MC-DSNPs were formed as dark spheres only in acidic pH(DS) environment (Figure 4.3 A). When the pH of DS solution increased from 4.6 to 6, only fiber-like aggregation was formed (Figure 4.3 B).

The effect of volume ratios on the formation of MC-DSNPs

The morphologies of MC-DSNPs with different volume ratios: 5:3, 5:5, 5:8.5 are shown in Figure 4.4. The edges of MC-DSNPs were found to be smoother when the Chi/DS volume ratio was above 5:3 (Figure 4.4 A). Large NPs (size more than 200nm) were both found in volume ratio at 5:5 and 5:8.5 preparations (Figure 4.4 B-2 and C-2).

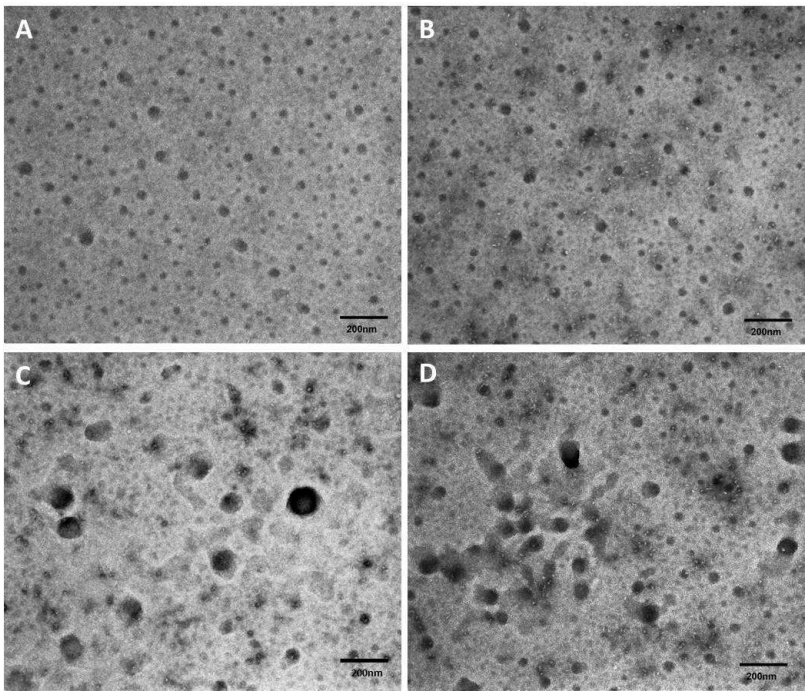

Fig. 4.2. The morphologies of MC-TPPNPs by TEM. MC-TPPNPs were synthesized when pH (TPP) was adjusted as 9.1 (A, C) or 4.3 (B, D). The MC-TPPNPs were successfully synthesized and appeared as dark spheres due to stain with 2% uranyl acetate. The sizes were accumulated in two ranges: around 50nm and 150nm. No obvious difference of morphology or size was noticed between two pH conditions of TPP. However, in 2 weeks, more MC-TPPNPs with lager size were observed. (A) NPs -TPP (pH9.1) Day 1, (B) NPs -TPP (pH4.3) Day 1, (C) NPs -TPP (pH9.1) Day 14, (D) NPs -TPP (pH4.3) Day 14. The scale bar equals 200nm.

The effect of purification methods on the morphology of ChiNPs

The morphology changes of MC-TPPNPs (pH 4.3) after dialysis, lyophilization, and re-suspension in the PBS were recorded by TEM in Figure 4.5. After 24 h dialysis, NPs and heterogeneous aggregations were co-existed (Figure 4.5 A). NPs were identified as dark spheres in all figures. The large heterogeneous aggregations were likely due to insufficient dialysis. Unreacted chitosan polymers were not dissolved at neutral pH. NPs were filtered at 0.45 μm and then subjected to dialysis. In Figure

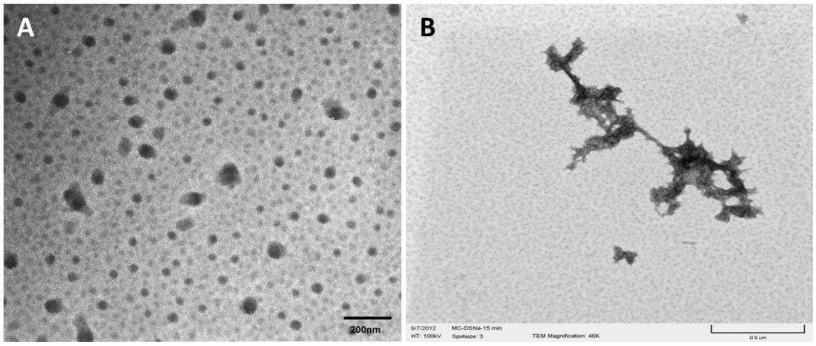

Fig. 4.3. The morphology of MC-DSNPs and aggregations. The morphology of MC-DSNPS synthesized at DS at pH 4.6 (A) and pH at 6 (B). MC-DSNPs were successfully formed as dark spheres in (A). However, (B) only fiber-like aggregations were formed when DS pH was increased to 6. The scale bar equals 200nm (A) and 0.5um (B).

4.5 B, much less aggregation was observed. After lyophilization (Figure 4.5 C), NPs were preserved and no distinct morphology change was noticed. However, NPs tended to aggregate after being re-suspended in PBS (Figure 4.5 D).

The morphology changes of MC-DSNPs (v/v, 5:8.5) after dialysis, lyophilization, and re-suspension in the PBS were monitored in Figure 4.6. NPs were filtered at 1.2 μm and then subjected to dialysis for 24 hours. The morphology of NPs was preserved in both dialysis and lyophilization. However, NPs tended to aggregate after being re-suspended in PBS (Figure 4.6).

The effect of drug loading on the morphology of ChiNPs

Two types of drugs, DEX and HY were incorporated into MC-TPP and MC-DSNP formations. All NPs appeared as dark spheres. Some of dark spheres had a couple of tiny white defects (dots) close to the edges. Those tiny white defects were likely air bubbles induced by vigorous stirring during the NPs formation, which was in agreement with the fact that only electron dense materials were shown as dark object in TEM. There was no distinct difference of morphology observed in Figure 4.7.

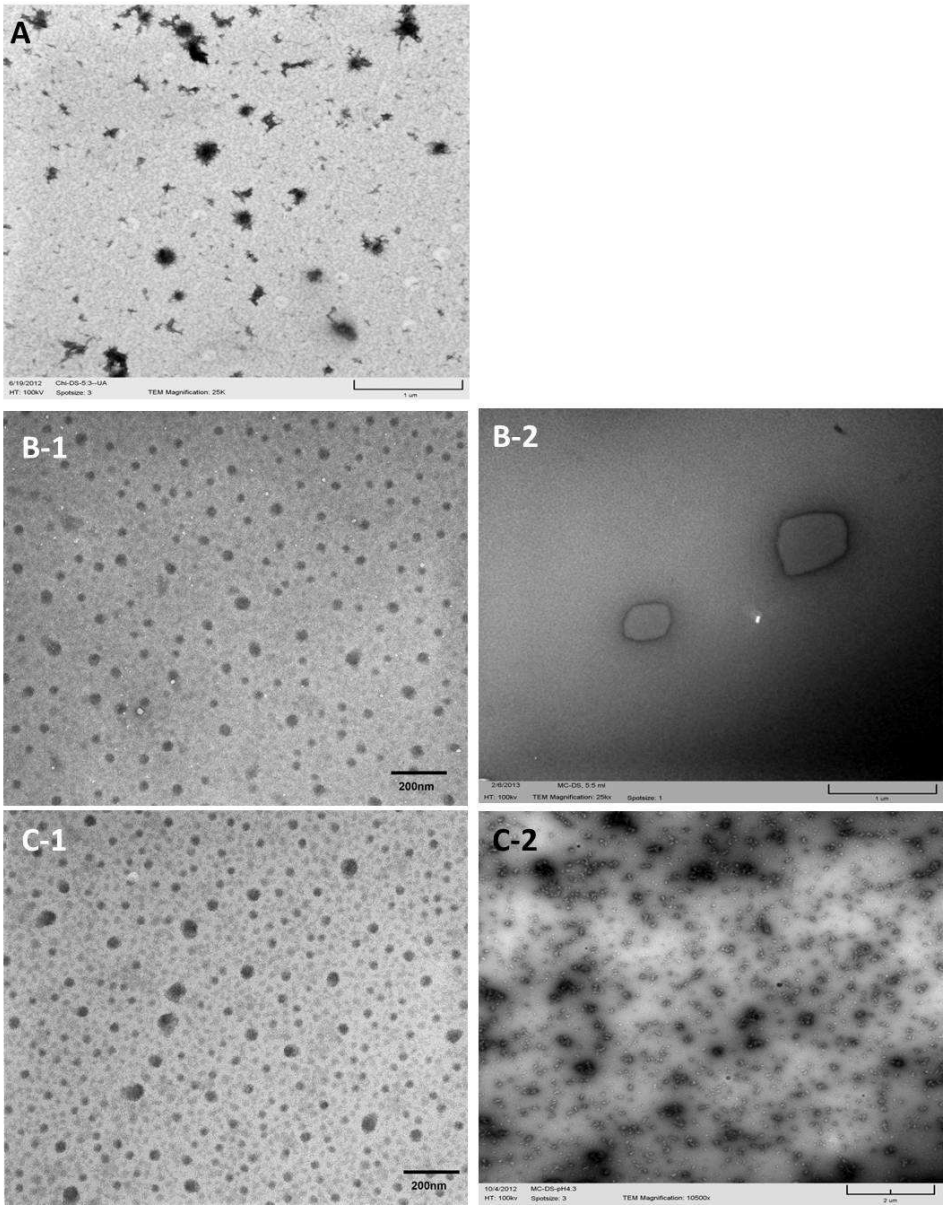

Fig. 4.4. The morphology of MC-DSNPs prepared with different volumes of DS. The MC-DSNPs were successfully formed in all preparations. The edges of NPs became smoother when the DS volume was increased. (A) MC: DS-5: 3(v/v). (B-1, B-2) MC: DS- 5: 5(v/v). (C-1, C-2) MC: DS- 5: 8.5(v/v). In MC/DS(5: 5, 5: 8.5) larger sizes were also observed(B-2, C-2). The scale bar equals 1um (A, B-2), 200nm (B-1, C-1), and 2um (C-2).

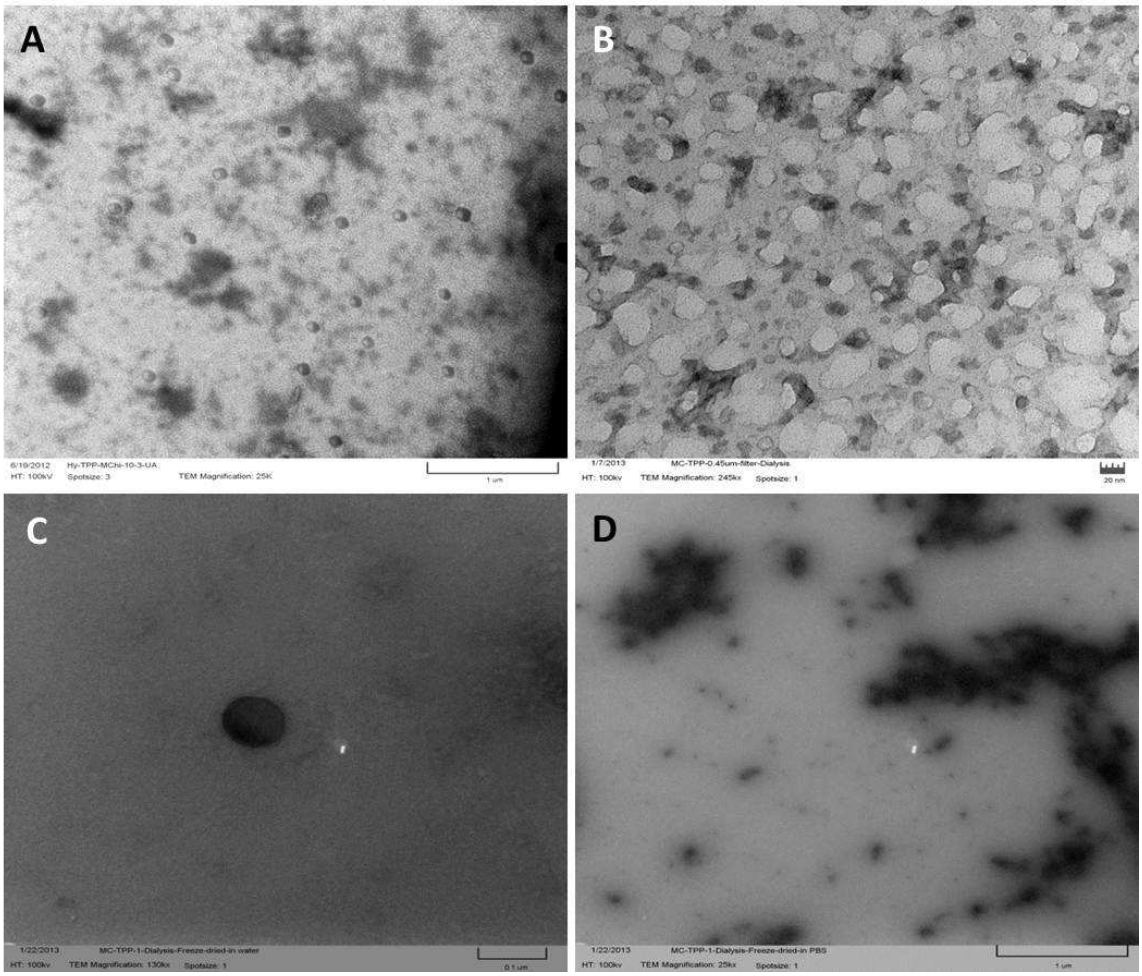

Fig. 4.5. The morphology of MC-TPPNPs (pH4.3) subjected to different purification methods. MC-TPPNPs (pH4.3) appeared as dark spheres. During dialysis, some extra chitosan polymers were insoluble in deionized water and appeared as cloudy aggregations (A). After removing large aggregations by filters, the morphologies of MC-TPPNPs were preserved in post-dialysis samples (B). The lyophilization did not affect the morphology of the NPs (C). The re-suspension of NPs in PBS caused some aggregations. (A) MC-TPPNPs post-dialysis in deionized water. (B)MC-TPP filtered with syringe filters and then subjected to dialysis in deionized water (C) MC-TPPNPs post-freeze-drying and re-suspended in deionized water (D) MC-TPPNPs post-freeze-drying and re-suspended in PBS. The scale bar (A, D) 1μm, (B) 20nm, (C) 0.1μm.

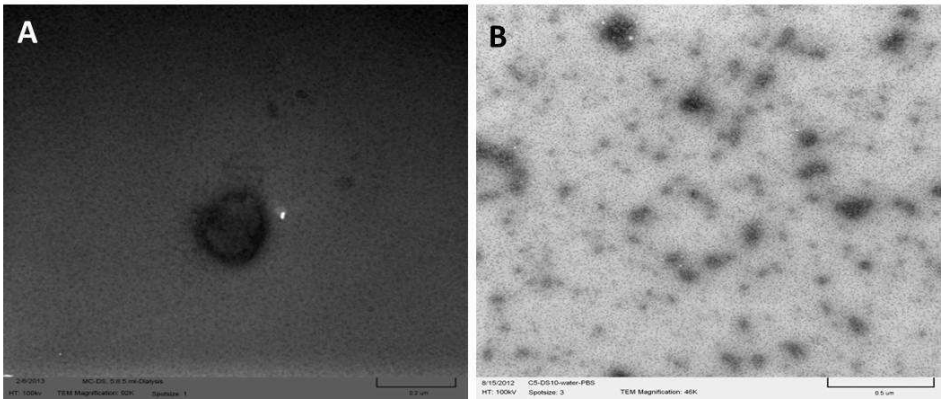

Fig. 4.6. The morphologies of MC-DSNPs after lyophilization. The morphologies of MC-DSNPs subjected to lyophilization and resuspended in deionized water (A) and PBS (B) were preserved. But some aggregation was observed in PBS suspensions (B). The scale bar (A) equals 0.2μm, (B) equals 0.5μm.

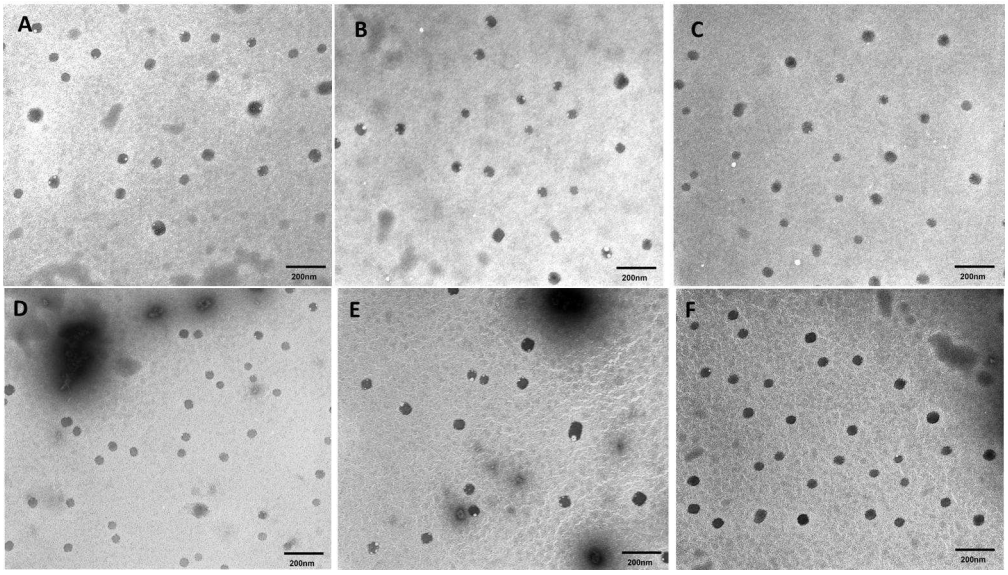

Fig. 4.7. The morphologies of MCNPs loaded with drugs. No obvious morphology changes of MCNPs were observed between pre-loading and post-loading. (A) MC-TPPNPs pre-loading, (B) MC-TPP post-loading with DEX 1mg. (C) MC-TPP post-loading with HY 1mg, (D) MC-DS pre-loading, (E) MC-DS post-loading with DEX 1mg (F) MC-DS post-loading with HY 1mg. Particles loaded with drugs appeared darker than the pre-loading conditions. The scale bar equals 200nm.

4.3.2 Size and zeta-potential results

Figure 4.8 showed a representative figure of size distribution by intensity data obtained with the measurement of MC-TPPNPs where pH (TPP) was 4.3. Two major size populations in MC-TPPNPs were indicated as two peaks in the intensity figure which were 28.9 nm and 151.15 nm, separately. A similar bimodal size distribution in the intensity profile was also observed in MC-TPPNPs where pH (TPP) was 9.1 (data not shown). The size of MC-TPPNPs were in the range of 100-200nm and the zeta-potential was in the range of 20-35mV. As the pH (TPP) increased from 4.3 to 9.1, the sizes of NPs decreased from 38.91± 2.1nm to 24.17±10.9nm and from 151.15±7.707nm to 128.15±21.14nm. By increasing 30% the volume (TPP), the sizes of NPs decreased 3%-15%. Both higher pH (TPP) and volume (TPP) suggested a trend of tighter binding between Chi and TPP molecules. However, no significant difference was observed among different preparations (Table 4.2, P>0.05).

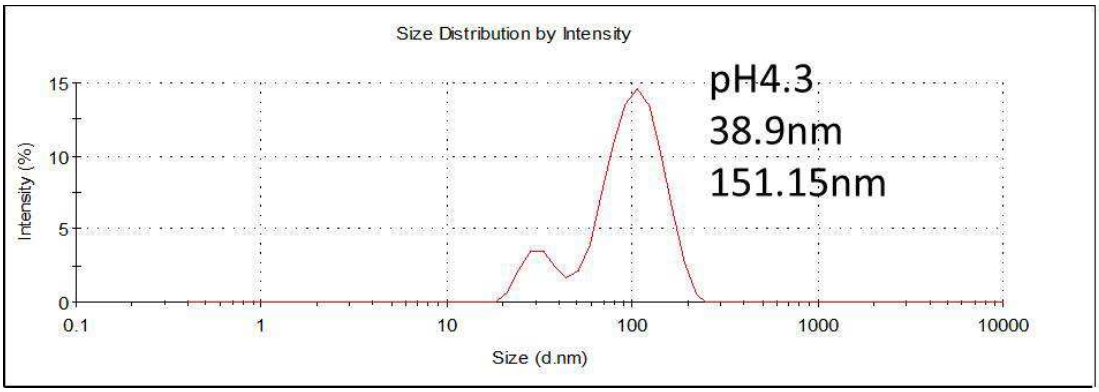

Fig. 4.8. The representative size distribution of MC-TPPNPs by intensity. A bimodal size distribution by intensity of MC-TPPNPs was observed when NPs prepared at pH4.3 of TPP.

Chi-DSNPs were prepared with different volume ratios (5:3, 5:5, and 5:8.5). In Figure 4.9, the average size of Chi-DSNPs was 217.76±12.97nm. Two size peaks were detected and shown as intensity 1 and intensity 2. As the volume ratio decreased from

Table 4.2

The size distribution and zeta-potential of MC-TPPNPs synthesized in different pH conditions. The size of MC-TPPNPs were in the range of 100-200 nm and the zeta-potential was in the range of 20-35 mV. MC-TPPNPs were positively charged which indicated the free amine groups of chitosan polymers spared on the surface of the NPs. No statistical significance was observed between different pH or v/v groups ($P>0.05$). The trend of the size decreasing was noticed with increasing TPP volumes and decreasing pH of TPP.

size	pH 4.3		pH 9.1	
MC/TPP (v/v)	5:2	5:1.5	5:2	5:1.5
intensity1 (nm)	147.43±22.45	151.15±7.707	119.5±11.74	128.15±21.14
intensity2 (nm)	32.94±8.35	38.91±2.1	26.82±7.12	24.17±10.9
z-p (mV)	27.7±5.52	31.13±9.26	30.91±3.68	28.81±4.059

5:3 to 5:5 and 5:8.5, the size (intensity 1) decreased significantly from 274.8±16.83 nm to 227.6±26.86nm (5:5) and 218.9±26.51nm (5:8.5) ($P<0.05$). No significant difference was found in intensity2 ($P>0.05$). Zeta-potentials of MC-DSNPs were significantly decreased as DS volume increased ($P<0.05$). The polarity was switched from positive to negative when the volume ratio was lower than 5:5.

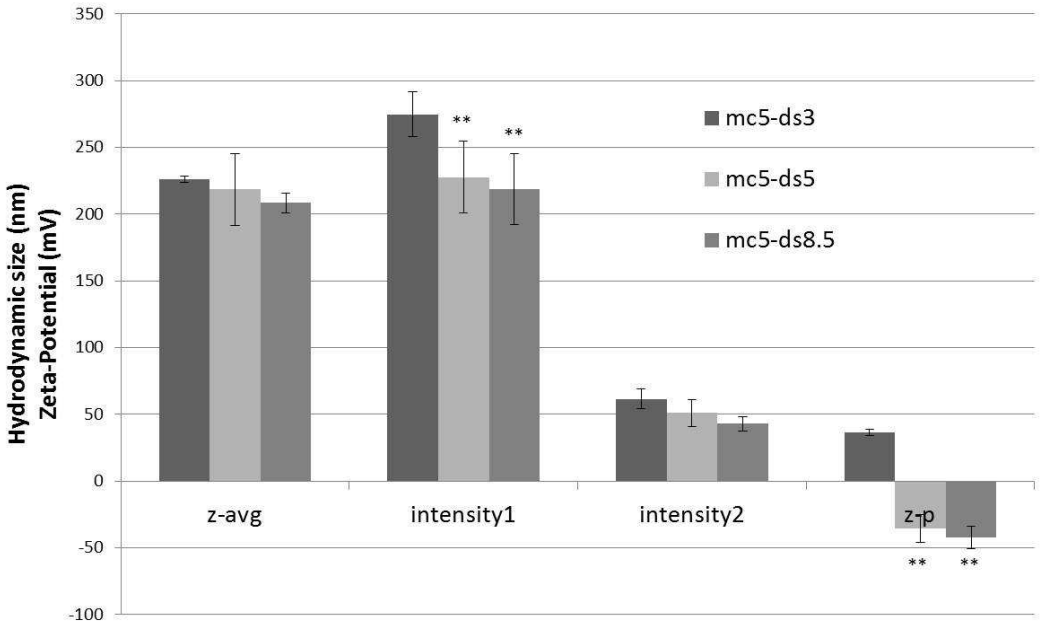

Fig. 4.9. The hydrodynamic sizes and z-potentials of MC-DSNPs synthesized with different volume ratios. MC-DSNPs had a bimodal size distribution which was represented as intensity 1 (around 200 nm-300 nm) and intensity 2 (40-60 nm). As volume ratio increased from 5:3 to 5:5 or 5:8.5, the size decreased significantly which were shown in intensity1 ($P<0.05$). Z-avg described the overall average size of NPs. All MC-DSNPs were around 210 nm (Z-avg). Zeta-potential was switched significantly from positive to negative as the volume of DS increasing from 3 ml to 5 ml or 8.5 ml ($P<0.05$). All data was represented as mean ± SD.

The effect of ionic strength on the size and zeta-potential of MCNPs

In Figure 4.10, MC5-TPP2NPs were diluted with different ionic strengths buffers: 0-1 XPBS at room temperature for 24h. No obvious difference in the hydrodynamic size was observed in NPs buffered with low ionic strengths between 0-0.1X PBS ($P>0.05$). In higher ionic strength buffers (0.3-1 XPBS), the size of NPs increased 5 times ($P<0.05$) which indicated that large aggregations were induced. The larger SDs of NPs in stronger ionic strengths (0.3 X-1X PBS) indicated that NPs were in-stable and therefore variable sizes were detected. The significant less cationic charge of NPs in higher ionic strength (less than 0.03 XPBS) was observed, which indicated the neutralizing effects produced by polarized salt ions on the surface of NPs ($P<0.05$).

In Figure 4.11, MC-DSNPs (v/v: 5/5) were diluted with different ionic strengths buffers: deionized water, 0.1 XPBS, 0.5 XPBS, and 1 XPBS at room temperature for 2 h and 24 h. No obvious difference in the hydrodynamic size was observed in NPs buffered with different ionic strengths ($P>0.05$). But the SDs in high ionic strengths (0.5 X and 1 XPBS) were much higher than the lower ones (0 and 0.1 XPBS), which indicated that the aggregation of NPs might be formed and precipitations might be anticipated. Indeed, the concentrated MC-DSNPs samples showed obvious precipitation quickly after diluting gently with concentrated salt ions (data not shown). The zeta-potential (post-24h) was significantly more negative after dialysis, indicating the removal of unreacted positively charged chitosan polymer in the suspension via dialysis. Significantly less anionic NPs in higher ionic strength (0.5 XPBS and 1X PBS) were observed, which indicated the neutralizing effects produced by polarized salt ions on the surface of NPs ($P<0.05$).

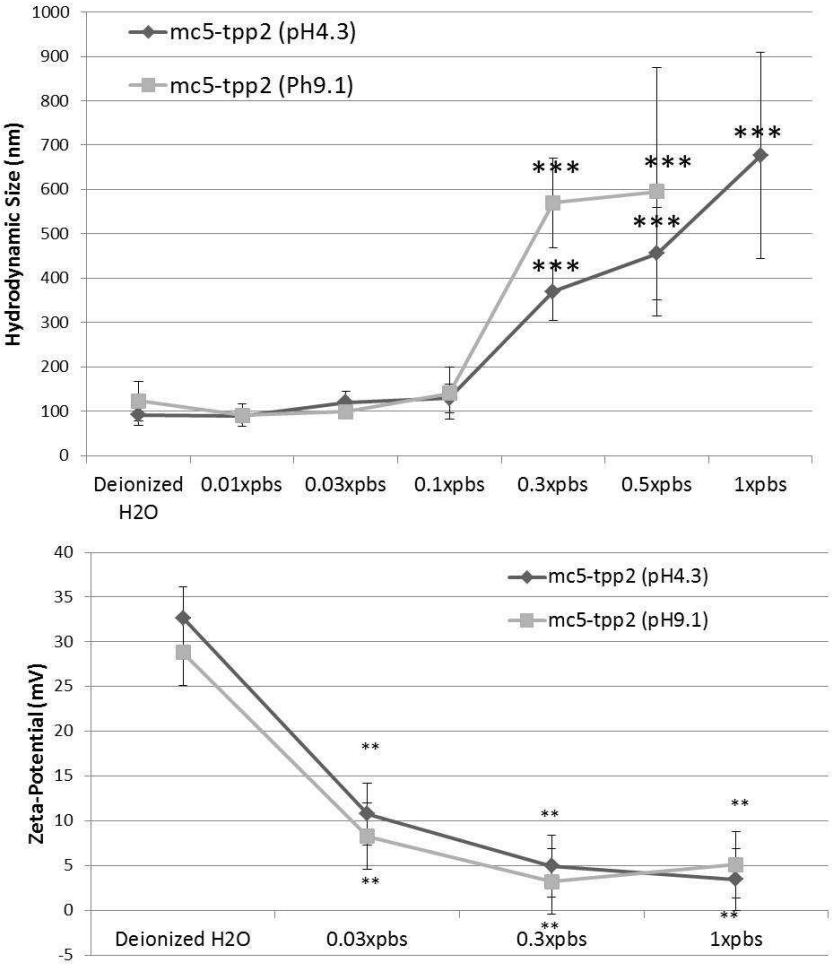

Fig. 4.10. The hydrodynamic sizes and zeta-potentials of MC-TPPNPs buffered with different ionic strengths. No obvious difference in the hydrodynamic size was observed in NPs buffered with low ionic strengths (less than 0.3 XPBS) ($P>0.05$). In high ionic strengths (0.3-1 XPBS), the size increased significantly, prepared in both pH conditions ($P<0.05$). The zeta-potential of NPs decreased significantly as the ionic strength increased (0.03 XPBS-1 XPBS), indicating the neutralizing effects produced by polarized salt ions on the surface of NPs. All data was compared with the results obtained in deionized water. N=3. The data was represented as mean ± SD.

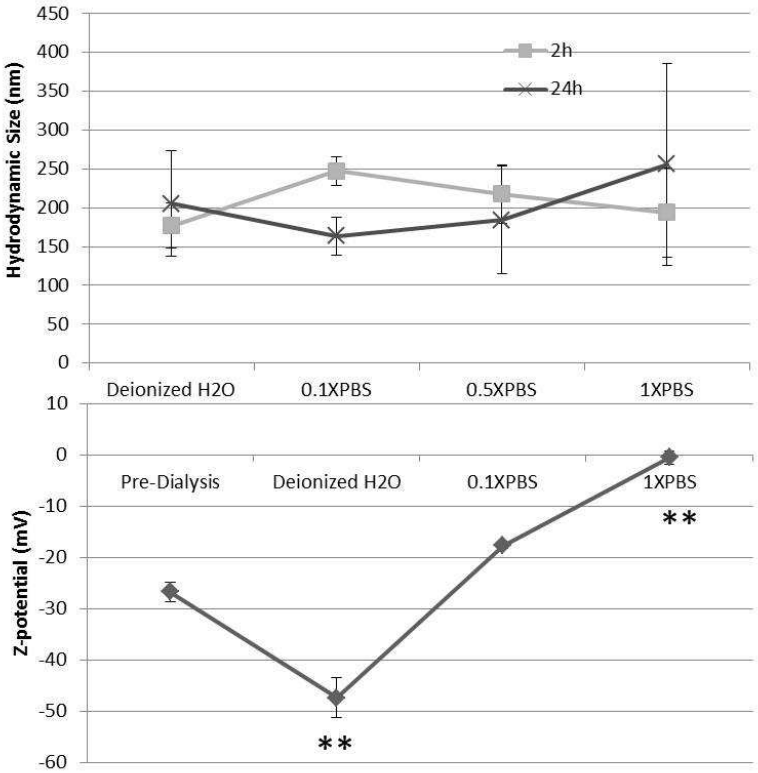

Fig. 4.11. The hydrodynamic sizes and zeta-potentials of MC5-DS5NPs buffered with different ionic strengths. MC-DSNPs (v/v: 5/5) were subjected to different ionic strengths buffers (deionized water, 0.1 XPBS, 0.5 XPBS, and 1 XPBS). No obvious difference in the hydrodynamic size was observed in NPs buffered with different ionic strengths ($P>0.05$). But the SDs in high ionic strengths (0.5 X and 1 XPBS) appeared much higher than the lower ones (0, 0.1 XPBS) indicated that the aggregation of NPs might be formed and precipitations might be anticipated. The zeta-potential (post-24h) increased significantly after dialysis, indicating the removal of extra positive charged chitosan polymer in the suspension via dialysis. The significant decrease of zeta-potential in higher ionic strength (0.5 XPBS and 1 XPBS) was observed ($P<0.05$) and indicated the neutralizing effects produced by polarized salt ions on the surface of NPs. Size values were compared with the results in deionized H_2O. Potential values were compared with results in the pre-dialysis condition. N=3. The data was represented as mean±SD.

4.4 Discussion

4.4.1 The impact of pH value

In this work, two types of ChiNPs were synthesized, Chi-TPPNPs and Chi-DSNPs. Based on the ionic gelation method, the protonated chitosan polymer acted as a backbone, providing binding sites for anionic molecules (DS/TPP) [127, 128]. With a pKa value of 6.5, chitosan can be protonated at the free amino groups which is dependent on the DA of chitosan and the pH value of the buffer. The base titration curve describes the change of pH as a function of the volume of bases, usually with sodium hydroxide (NaOH) added. The base titration curve of chitosan solution with 2 M NaOH added drop-wise, showed a sharp increase of pH value both at the range of pH less than 4 and higher than 6. However, at the range of pH (4 to 6), the rate of the pH increased much slower as NaOH was added (data not shown). When the pH was less than 4, there were many free protons provided by acetic acid in the chitosan solution that reacted with the hydroxyl groups in NaOH and this resulted in a higher pH value of the solution. When all free protons were interacting with hydroxyl groups, adding more NaOH led to the competition of binding with protons between the hydroxyl groups and the amino groups of chitosan. Therefore, it was observed as a slow increasing of pH at the range between 4 and 6. When the pH was greater than 6, almost all chitosan polymers might be deprotonated. Adding more NaOH meant the net increase of the number of hydroxyl groups. Then, the sharp increase of pH was observed again. In high pH environment, chitosan became less soluble and the solution appeared cloudy which indicated polymer aggregation and precipitation. It was also observed in Shu and Zhu's study where chitosan (DA14% and MW 400KDa) was suggested to be completely protonated at pH 4.7 and deprotonated at pH 8 [129, 130]. Therefore, to ensure the solubility of chitosan, with sufficient repulsion between protonated chitosan polymers and minimization of the number of free protons, the pH was adjusted between 4-5. A large number of free protons in the solution can

weaken the electrostatic interactions between chitosan polymers and TPP or DS and prevent the formation of the NPs.

The formation of Chi-TPPNPs was suggested to be independent of the pH value of TPP (Figure 4.2), which, however, was not applicable for the formation of Chi-DSNPs. The NP formation was largely influenced by the pH of the mix solution, which needs to be monitored and controlled at the range of 4-5 to ensure the solubility of chitosan, mainly because both TPP and DS were in the forms of sodium salt and they were water-soluble. When the pH of the mix was higher than 5, the effects of the intra-/inter-molecular attractions of chitosan polymer became dominant due to the decreased degree of protonation of chitosan. Therefore, it often resulted in a fiber-like aggregation (Figure 4.3 B) or the aggregation of microparticles [131]. The primary attraction forces were H-bonding and hydrophobic interactions between acetyl chains of chitosan.

In our work, the increase of the volume of TPP did not result in a significant difference (decrease) of the size of MC-TPPNPs, due to the choice of the volume/ratio selected (Table 4.2). Fan reported a TPP mass-dependent effect on NP size [127]. When more TPP was available to bind with higher amount of amino groups in the solution, the density of cross-linking increased; therefore, the size of single NP was expected to decrease. However, extra TPP can also bridge adjacent small NPs or chitosan polymers together forming large aggregations. Moreover, the protonation of TPP is pH dependent as well. The reduction of the protonation of TPP in high pH resulted in a higher concentration of tripolyphosphate ions [132]. In other words, the higher charge density of TPP at pH of 9 can result in a larger number of binding sites with chitosan polymer when compared with TPP at pH of 4. However, the solution with higher pH also enhanced the competition effect between tripolyphosphate ions and hydroxide ions interacting with protonated chitosan polymers [133]. A significant change induced by pH (TPP) on the sizes and zeta-potentials was not observed in out study.

4.4.2 The impact of MW

The impact of different MWs of anionic molecules on both the size and zeta-potential of NPs were investigated (Table 4.2 and Figure 4.9). TPP with a lower MW (<400Da) and smaller charge density compared to DS, behaving as an anionic bead, was bound with multiple cationic amino groups either from single or several chitosan polymers due to the poly-anionic ions (polyphosphate ion) in TPP. Therefore, the size and zeta-potential of Chi-TPPNPs were largely dependent on the properties of chitosan. The positive zeta-potential of Chi-TPPNPs was contributed by the free amino groups of long chitosan polymer extending towards the surface of the NPs. On the other hand, DS with an average MW 20 times of the MW of TPP, exhibited a higher modification effect on the properties of NPs which was tailored by the volume ratio of Chi /DS.

4.4.3 The impact of volume ratio

The switch of the polarity of the zeta-potentials of Chi-DSNPs was observed when the volume ratio of Chi/DS was less than 5:3, indicating the dominant charge effect produced by the higher volume of DS (5:5 and 5:8). The size of Chi-DSNPs also decreased significantly as the DS volume was increased [134]. Continue decreasing Chi/DS volume ratio from 5:5 to 5:8 did not lead to a significant change of sizes and zeta-potentials of NPs. These results suggest that the cationic amino groups of chitosan polymer were saturated by binding with sulfate groups of DS at the volume ratio of 5:5.

4.4.4 The impact of freeze-drying

Freeze-drying, also known as lyophilization, is a common method to dry and preserve chemicals in industrial applications [135]. A freeze-drying cycle is divided into three steps: freezing, primary drying and secondary drying. The removal of

water from NPs can increase the stability and storage time [136]. However, during the process of freeze-drying, NPs might be challenged with various stresses from the extremely low temperature, vacuum, and ice crystals. The most common cryoprotectants for lyophilization of NPs are sugar based, such as glucose, sucrose, trehalose, and lactose. Trehalose was suggested as a good candidate of cryoprotectant for biomolecules [137]. It serves as a protective layer to substitute water molecules by forming H-bonds with polar groups of the NPs. It is also possible to freeze-dry NPs without the pre-treatment of cryoprotectant, such as poly(ϵ-caprolactone) NPs. Our results (Figure 4.5 C and Figure 4.6 A) showed that the overall shape of NPs was preserved after lyophilization. However, the solubility of NPs after lyophilization was limited, both observed in de-ionized water and PBS, which indicated enhanced inter-/ intramolecular interactions between NPs after freeze-drying (Figure 4.5D and Figure 4.6B). 5% trehalose was used in the freeze-drying of ChiNPs [138].

4.4.5 The impact of drug loading

Our TEM results showed that no obvious morphology and size changes were observed between pre- and post-drug loadings (Figure 4.7). The drug molecules were attached on the ChiNPs via electrostatic interactions. Since the MWs of drug molecules were low (Hy: 160Da and Dex: 400Da), the drug loading might not generate significant impacts on the size of NPs, if the added drug volume is low. However other studies indicated that both zeta-potential and size of NPs were modified by drug loading [27, 134]. ChiNPs were also tested to load genes, peptides, protein drugs, anticancer chemical drugs, and other drugs [121].

4.4.6 The impact of ionic strength

The colloidal homogenous suspension of NPs is maintained by the opposite effects of diffusion/convection and gravitational forces [135]. The concentration gradient is the driving force for the movement of particles from a region of high concentration to a

region of low concentration. During these diffusion processes, particles randomly collide with other molecules in the suspending medium due to the spontaneous thermal motion, referred to as Brownian motion. The collision elevates the chance of mutual interactions between particles and molecules. Gravitational forces counteract with the diffusion force by pulling down the large aggregation of particles and inducing precipitations. Both Brownian motion and gravitational forces are size-dependent. When the particle size is within nano- or micro-size, Brownian motion dominates and maintains the stability of the suspension. However, when counter-ions are introduced into the suspension, the adsorption of counter-ions on the surface of NPs might suppress the ionic repulsion between NPs, causing particle aggregation/agglomeration. The large size of NPs can further enhance the effect of gravitational forces and lead to particle precipitation.

In our work, ChiNP was more stable in the low ionic strength environment where enough ionic repulsions were established by charges of NPs (zeta-potentials were greater than ±25mV, Figure 4.10 and Figure 4.11). After the ionic strength increased (50mM and 150mM PBS), the hydrodynamic size of Chi-TPPNPs significantly increased accordingly (prepared in both pH conditions). These observations were also suggested in Lopez's work [139]. The increase of the sizes and the decrease of the zeta-potentials of Chi-TPPNPs were indicated to be induced by an accumulation of counter-ions on the hydrated layer of the NPs via electrostatic interactions, when NPs were incubated with high ionic strength buffers [127]. The accumulation of counter-ions on the NPs neutralized the charge of the NPs which was observed as the zeta-potential decreased. A reduction of zeta-potential of NPs indicated less repulsion forces between particles which in turn led to a greater chance of the aggregation of individual small particles. As a result, the size of NPs increased which was shown in the data of Chi-TPPNPs. Similar results were observed in the reduction of the zeta-potential (after 24h incubation) of Chi-DSNPs (Figure 4.11). However, no such trend was observed in the size measurement of Chi-DSNPs. The difference of the impact of the ionic strength on the size between Chi-TPPNPs and Chi-DSNPs might

be associated with the MWs of TPP (387Da) and DS (10KDa), which differ by approximately 2 orders of magnitude. The higher MW of DS indicated longer chain length, higher anionic charge density, and stronger binding forces with chitosan polymers, compared with TPP. Nevertheless, the storage of ChiNPs in low ionic strength buffer is suggested to maintain the stability of the NPs suspension in the long term. Chitosan derivatives and PEG-coating were used to improve the performance of NPs by increasing the charge density and the surface roughness which enhances the steric hindrance between NPs [84, 117, 140, 141].

Other factors were also found to influence the formation of NPs, such as: the concentration of acetic acid, the temperature, the stirring speed [127], the ionic strength during synthesis [142], MW and DA of chitosan [140, 143].

4.5 Conclusion

In conclusion, our work investigated the ionic interactions between chitosan polymer with two types of anionic molecules, namely TPP and DS. Chi-NPs were successfully synthesized as sphere NPs. Major factors that affect the properties of ChiNPs were investigated, such as pHs, MWs, volume ratios, purification methods and ionic strengths. In agreement with other studies, the sizes and zeta-potentials of ChiNPs was well preserved if stored in the low ionic strength buffer. Higher ionic strength changed the properties of ChiNPs significantly. However, the size of Chi-DSNPs was less affected. Therefore, we chose Chi-DSNP as the candidate for further in vitro and in vivo studies.

5. THE NEUROPROTECTION BY CHITOSAN NANOPARTICLES (CHI-NPS) - AN IN VITRO AND AN IN VIVO STUDIES

The most important factor associated with a promising medical innovation is if it is performed as expected. There are two general models to test functionality (discussed here as ChiNPs): in vitro and in vivo evaluations. Each of these provides complementary information to each other. For example: (1). An in vitro test can reveal if the therapy has a significant effect on a model cell system. It can give the insights into the mechanism of the action the therapy. However, it does not provide any information regarding the usefulness of the therapy on an animal or a human being. (2). An in vivo study is performed to reveal the effect of a therapy in an animal or a human being. It can provide the knowledge related with behavior recovery, dose adjustment, and side effects which are the key information required for the application of clinical studies. However, it does not provide understanding of the mechanism of the action. Therefore, a proper evaluation of a promising therapy should be performed at both levels of investigations in vitro and in vivo.

In this chapter, we first explored if the neuroprotective effects of ChiNPs can interfere with secondary injury mechanism. We used a specific toxin (hydrogen peroxide) for a specific immortal cell line (BV-2). The beneficial effects of ChiNPs were also tested in a spinal cord injury model. We used a crush/compression model of injury to the mid-thoracid spinal cord of an adult guinea pig. The particular assay we emphasized was the conduction of nerve impulses, lost after the injury, but hopefully recovered after the experimental therapy.

5.1 Introduction

A spinal cord functions as an informational highway to transmit and coordinate both motor and sensory information that is coded via electrical signals in the body. Spinal cord injury (SCI) destroys the passage of the information by mechanically/biochemically damaging the spinal cord tissue [1, 144].

Oxidative stress plays a critical role in many diseases and trauma such as secondary injury in SCI, inflammation, immune-based disease (arthritis, infections) and neurodegenerative disease (Parkinson's Syndrome, Multiple Sclerosis, MS) [10, 21, 23, 145–150]. Oxidative stress describes the imbalance between the potential damage caused by the generation of reactive oxygen species (ROS) and the capability of ROS deactivation by scavengers produced by a biological system. ROS is a collective term that includes oxygen radicals (superoxide anion $O_2^{\cdot -}$ and hydroxyl radicals, $\cdot OH$) and some non-radicals, such as H_2O_2. Free radicals are highly toxic due to active unpaired electron, which can damage many biological molecules, including lipids, proteins, and/or nucleic acids [151]. For instance, the unpaired electron of a free radical can remove electrons from the carbon-carbon double bonds on cell membrane lipids, leading to the initiation of lipid peroxidation (LPO) [152, 153].

As one of the major events in free radical mediated cell injury, LPO can occur in multiple sites simultaneously which results in fatty acid oxidation, lipid cross-linking and/or breakage of covalent links between a membrane glycoprotein and its membrane lipids. Consequently, the transient formation of polarized phospholipid peroxides might create hydrophilic micro-centers due to the higher polarity of peroxides than phospholipids. Therefore, these hydrophilic micro-zones may result in increased membrane permeability [20, 154, 155]. LPO can also produce more radicals or other toxins (aldehydes) as by-products and facilitate positive feed-back, or self-reinforcing, LPO loops. Such aldehydes include the endogenous occurring 4-Hydroxynonenal and acrolein which have been implicated in membrane damage and secondary injury [18, 156, 157].

Further, the non-regulated generation of H_2O_2 is a well-known source of oxidative stress. H_2O_2 is the intermediate product in the conversion of $O_2^{\cdot -}$ into H_2O in the electron transport chain during oxidative phosphorylation in the cell mitochondria. Any disruption of this equilibrium (such as a mechanical stress) can cause activated oxygen by-products ($O_2^{\cdot -}$ and H_2O_2) to overwhelm antioxidant enzymes. H_2O_2 can be further converted into ·OH, in the presence of iron (Fe^{2+}) or other heavy metal ions. ·OH is highly reactive and capable of attacking nearby molecules within nanoseconds [158]. Several studies have documented that high concentration of H_2O_2 results in the disruption of membrane integrity and apoptosis [159–161]. Unfortunately, there is no known direct scavenger to inactivate ·OH due to its extreme reactivity. However, cells are equipped with an inherent anti-oxidant defense system to monitor/scavenge the parent compounds, $O_2^{\cdot -}$ and H_2O_2, as well as other ROSs during the normal oxidative phosphorylation process [162]. This native anti-oxidant defense system include enzymes such as superoxide dismutase (SOD), catalase, glutathione peroxidase (GSHPx) as well as, vitamin E, and glutathione [163]. However, during secondary injury of SCI, the initial damage triggers a production of ROS which quickly depletes the cellular anti-oxidation capability and leaves cells (in our discussion - neural cells) particularly vulnerable to oxidative stress [148, 164]. Exogenous antioxidants (reducing agents) work as direct ROS scavengers and inhibit or prevent oxidative damage induced by ROS. They are often thiols, ascorbic acid, or polyphenols, obtained from a balanced diet or drugs.

Chitin is a natural cationic polysaccharide and can be derived naturally or chemically from certain fungi, insect and crustacean shells. Its derivative, Chitosan, is composed of N-acetyl-glucosamine and glucosamine subunits. Chitosan has been widely used as a biomaterial in food processing, tissue engineering, and in the pharmaceutical industry due to its biodegradability and biocompatibility. The primary amino groups on the glucosamine units of a chitosan polymer partially contribute to various biological activities, such as anti-tumor, antimicrobial, anti-ROS, hemostasis, and as a membrane fusion agent [50–53, 161, 165]. The ability of chitosan to suppress

the production of nitric oxide or ROS stress was reported in murine microglia cell, human umbilical vein endothelial cells, and murine melanoma cells [153, 161, 166]. Chitosan was also suggested to inhibit the production of ROS and LPO by restoring the integrity of membrane lipids following the compression injury in isolated spinal cord segments [26]. Recently, chitosan was also used as a nanomaterial to encapsulate and deliver therapeutic drugs and imaging agents in various biological systems [27, 122, 123, 129, 167, 168]. The advantages of chitosan nanoparticles versus chitosan or other synthetic polymer-based nanomaterials are its inherent bioavailability, biodegradability, biocompatibility, enhanced solubility, reduced hemostasis, and accessibility for modification - such as drug loading and surface modifications.

Our previous work found a dual effect of neuroprotection by both bare chitosan nanoparticles and drug-doped (toxin scavengers) nanoparticles in an acrolein-induced PC12 cell death model. The inhibition of endogenous enzyme leakage and the preservation of viable cells by chitosan nanoparticles were suggested through the restoration of compromised membrane integrity [27].

In this work, we further investigated neuroprotection by chitosan nanoparticles on BV-2 rat microglia challenged by H_2O_2 exposure. This cell injury model is closely associated with the oxidative damage in secondary injury in SCI. The reduction of cell viability and cell proliferation was observed in a time and dose dependent manner after exposure with H_2O_2 at different concentrations . We screened the "rescue" effects of Chitosan-Dextran Sulfate nanoparticles (Chi-DSNPs) without a drug cargo on a H_2O_2 induce BV-2 cell damage at different administration time points and incubation periods. We also investigated the mechanisms of H_2O_2 induced cell death to give new insights on the neuroprotective effects generated by Chi-DSNPs.

We are also interested in the beneficial effects derived from ChiNPs on SCI models in whole animal studies. Experimentally induced standardized compression SCI was performed on sedated guinea pigs. We conducted somatosensory evoked potentials (SSEP) measurements on animals at pre- and post-compression injury conditions. SSEP provided the function of the signal conduction through sensory pathways of

spinal cord. SSEP on the lightly sedated animals after the treatment of ChiNPs was monitored at Day 1, week 1 and week 2.

5.2 Methods and materials

5.2.1 BV-2 cell culture

BV-2 cells are an immortalized mouse microglial cell line that exhibits the morphological and functional characteristics of microglia. The cells were maintained in D1152-Dulbecco's Modified Eagle's Medium (DMEM) supplemented with 0.044M sodium bicarbonate, 10% fetal bovine serum (FBS) and 100U/ml penicillin and 100ug/ml streptomycin (Sigma, A5955). The cells were cultured in a 5%CO2 and 95% air incubator in a humidified cell incubator at 37°C. 0.25×10^5 Cells were seeded in a $75cm^2$ flask. The sub-culture was conducted when 80% confluency was reached, on average, after 3days of cell culture. Culture medium was changed every other day.

5.2.2 Chi-DSNPs and H_2O_2 treatments

For viability measurements, H_2O_2, BV-2 cells were seeded at a density of 1.5E5/well in a 12-well plate overnight. The next day, the medium was replaced with freshly prepared H_2O_2 solutions in culture medium without serum at concentrations of 0, 11, 55, 110μM and cells were cultured for 1h-4h. For viability measurements in response to Chi-DSNPs with the challenge of H_2O_2, the concentration of 5.5μMH_2O_2 was chosen to induce BV-2 cell death for testing the neuroprotective effect of Chi-DSNPs. BV-2 cells were seeded at a density of 0.5E5/well in a 24-well plate overnight. Freshly prepared 1mg/ml, 10ul NPs was administrated at 0 and post-15mins after the addition of H_2O_2. Cell viability was measured at the end of a 2h incubation using a trypan blue exclusion test. For proliferation measurements in response to Chi-DSNPs, BV-2 cells were seeded at a density of 1E4/well in a 96-well plate overnight to achieve cell attachment to the bottom of the well. Cell medium with serum was replaced with diluted

NP suspension at a concentration of 0, 0.1,0.2, 0.5mg/ml, 100μl. For proliferation measurements in response to H_2O_2, cell medium with serum was replaced with H2O2 at 0, 0.05, 0.1, 0.2, and 0.3mM for 20h. For proliferation measurements in response to Chi-DSNPs with the challenge of H_2O_2, cells were pre-treated with 0.2mg/ml, 100μl Chi-DSNPs for 4h before incubating with 0.05mM H_2O_2. In these experiments, cell proliferation was measured using a WST-assay. The detail information of WST assay can be found in the following.

5.2.3 Trypan blue dye exclusion test

Medium was carefully removed and cells were gently rinsed once with warm 1X PBS. Cells were incubated with 0.2% trypan blue, diluted with 1X PBS, for 2mins. Then, trypan blue solution was removed and replaced with 1X PBS. Necrotic cells were stained with trypan blue and appeared as dark spheres. Viable cells were not stained and appeared as bright spheres.

5.2.4 WST-1 cell proliferation assay

Cell proliferation was tested with a WST assay (Cayman). The assay is based on the conversion of WST-1 reagent into formazan salts by cellular mitochondrial enzyme dehydrogenases in viable cells. The absorption was measured by a microplate reader. 10% (v/v) WST-1 agent was added to each sample well and a background control well (no cells present, only cell medium). After 2h incubation at 37°C in the dark, the absorption of each well was measured in a multi-well plate reader at 450nm. The final data was calculated by subtracting the background signal from the absorption of sample wells. Four experiments were conducted, quadruplicate for each treatment.

5.2.5 Phase contrast imaging

BV-2 cells were allowed to reach confluency in the 75cm^2 flask. Then, cells were harvested and seeded at 1E5/well in a 12-well plate. After overnight incubation, cells attached well on the bottom of the well. Medium was replaced with H_2O_2 at 0, 0.05, 0.1, and 5.5mM. Cells were placed in a temperature and humidity controlled culture chamber was connected to an Olympus IX81 Microscope System. Phase contrast images were taken at a time interval of 30mins for 20h. Sequential images were taken at fixed positions enabled by the multi-dimentional acquisition (MDA) program of the microscope's software.

5.2.6 Annexin V-FITC apoptosis detection

Early apoptotic cell death was detected by annexin V-FITC apoptosis probe (Abcam). After the initiation of cell apoptosis, membrane phosphatidylserine (PS) is translocated to the surface of the cell membrane from the inner surface of the plasma membrane. The binding between PS and its high affinity protein annexin V will stain the apoptotic cells with a convenyional FITC green fluorescent probe which is pre-conjugated with the annexin V protein. Cells that have lost membrane integrity will show red staining with propidium iodine (PI) throughout the nucleus and a halo of green staining (FITC) on the cell plasma membrane surface.

BV-2 cells were allowed to reach confluency in the 75cm2 flask. Then, cells were harvested and seeded at 1E5/well in 12well plates. Cells were exposed to H_2O_2 at 0, 0.05, 0.1, and 5.5mM to induce cell death. The adherent cells were trypsined gently and washed once with 500ul of 1X binding buffer. Cells were incubated with 5ul Annexin V-FITC and 5ul (50mg/ml) of PI for 5mins in the dark at room temperature. Cells were centrifuged gently and re-suspend in 200ul 1X binding buffer. 100ul cell suspensions were placed on a glass slide and mounted with a coverslip. Images were taken by a (Nickon Diaphot 300 Microscope) at the incubation time of 0h and 4h for

H_2O_2 (5.5mM) and 0h and 20h for H_2O_2 (0, 0.1, 0.05mM) with a dual filter set for FITC and PI.

5.2.7 Compression injury in vivo

All animals used in this study were handled in accordance with, and prior approval by, the Purdue University Animal Care and Use Committee (PACUC). In this study, every effort was made to reduce the number and suffering of the animals used. The compression injury procedure can be found in the manuscript of Borgens 2002. Adult female guinea pigs (Hartley strain) weighted in a range of 300 to 400mgs were anesthetized with a intramuscular injection of Ketamine 60mg/kg, followed by xylazine 10mg/kg. An adequate anesthesia throughout the procedure was confirmed by a lack of response from a toe-pinch test. The aseptic surgery procedure was performed. Briefly, the dorsal aspect of the anesthetized guinea pigs was shaved by an electric clipper. Betadine and 70% alcohol were applied and wiped off at shaved areas subsequently. After identify the approximate area at T13 level, a one-segment laminectomy procedure was performed to expose the spinal cord under a stereoscope. The 15s-compression injury was induced by using a pair of modified forceps possessing a spacer of 0.8mm. The previous experiments demonstrated that the compression induced as described above can generate a complete block of SSEP conduction. The muscle around the laminectomy was stitched together with a 3-0 prolene suture. The skin was closed with Michel wound clips 7.5mm each. A 3ml of sterile lactated ringers and carproten was injected subcutaneously to the animals. Then, animals were kept warm by placing under a heat lamp until fully recovered and moved to Purdue Animal Housing Facility where they received daily care.

5.2.8 ChiNPs treatment

The synthesis of ChiNPs can be referred to Chapter 4. ChiNPs were freshly prepared prior to each experiment. 1mg/ml particles were mixed well in sterile lactated

ringer solution and subcutaneously injected at the nape of the neck of the animals 30mins after the compression injury. The control groups were administrated with 1mg/ml silica NPs subcutaneously as well.

5.2.9 Somatosensory Evoked Potential (SSEP) recording

The measurements of SSEP on lightly sedated guinea pigs were used to evaluate the function recovery of evoked potential conduction pre- and post- spinal cord compression injury with the single administration of ChiNP suspension. The SSEP recording procedure can be found in the manuscripts of Borgens [24,25]. The presence or absence of SSEP through the lesion was used as the criteria to study the performance of therapeutic effect of ChiNPs. Guinea pigs were intramuscular injected with a mixture of ketamine 20mg/kg and xylazine 4mg/kg. Needle electrodes were placed subcutaneously on the lightly sedated guinea pigs [49]. A first pair of stimulating pin electrodes was inserted in the left hind-leg near the tibial nerve. A second pair of stimulating electrodes was inserted in the ipsilateral foreleg near the medial nerve and the abdomen. A pair of recording electrodes were inserted at the right side and the front of the head, slightly left to the right eye. Two neural circuits were established. The first one was the test circuit. Stimulation was conducted through the lesion, from the tibial nerve to the contralateral side of the sensory cortex. The second one was the control circuit. Stimulation was by-pass the lesion, from the medial nerve to the contralateral side of the cortex. A switch box was designed to switch the stimulating signal between tibial nerve and medial nerve without replacing electrodes. A Nihon Kohden Neuropack 2 Stimulator/Recorder was used to generate the stimulation and receive the evoked potential signals. The stimulation frequency was 200 HZ. The magnitude of the stimulation signal was adjusted until the twitching movement surrounding the stimulation electrodes almost invisible. A complete blockage of evoked potentials in the test circuit indicated a successful compression injury on the spinal cord. A recovery of evoked potentials through the compression lesion on the

spinal cord, recorded at the contralateral sensory cortex, from the stimulation of the hind-legs, was suggested as a function recovery of electrophysiological conduction in spinal cord injured animals. Evoked potentials were measured on the normal, post-injury, Day1, Week1, and Week2 after stimulated at the tibial and median nerves respectively. The evoked potential was recorded as a average waveform of three measurements. Each measurement was generated by averaging 120 recordings.

5.2.10 Materials

WST-1 assay was purchased from Cayman Chemical company. Annexin V-FITC apoptosis detection Kits was purchased from Abcam. BV-2 cells were a gift from Wen Gao, Center for Paralysis Research (CPR). Adult female guinea pigs were purchased from Hilltop and housed at Purdue animal holding facility. Ketamine and xylazine were purchase from Purdue Veterinary School Pharmacy. Nihon Kohden Neuropack 2 Stimulator/Recorder (SSEP recorder) is located at CPR. Olympus IX81 and Nikon Diaphot 300 Microscope is located at Doyle Laboratory at Purdue University. Other chemicals and agents were purchased from Sigma-Aldrich.

5.2.11 Statistics

All data points were represented as means±standard deviation. Statistical analysis was conducted using one-way ANOVA for comparison among more than 2 groups, Tukey-Kramer Multiple Comparisons test for comparison between experiment groups and Fisher's exact test for in vivo evaluations (InStat software). Other values were accepted as being statistically significant if the P value was less than 0.05.

5.3 Results

5.3.1 Time and dose dependent cell death induced by H_2O_2

We first assessed the cell viability of BV-2 cells with 1h incubation of H_2O_2 at different concentrations (0, 11, 55, 110μM). As shown in Figure 5.2, H_2O_2 greater than 55μM induced more than 90% cell death within the 1st hour. Furthermore, BV-2 cell death with 11μM H_2O_2 was monitored within a window of 0-4h.

5.3.2 Time and dose dependent inhibition of cell proliferation induced by H_2O_2

H_2O_2 induced an inhibition of BV-2 cell proliferation within a window of 20h measured with the WST-1 assay (Figure 5.3). Expansion of a viable cell population always results in an increase in the activity of the mitochondrial enzyme dehydrogenases, which as a consequence , leads to an increase of the signal intensity. As expected, cell proliferation was suppressed as the concentration of H_2O_2 increased. When the concentration of H_2O_2 was more than 0.2mM, no further decrease of cell proliferation was detected with WST assay.

5.3.3 The effect of Chi-DSNPs on cell proliferation

As discussed above the effect of Chi-DSNPs on BV-2 cell proliferation was measured with WST-1 assay (Table 2). It was observed that cell proliferation within 20h was not affected significantly by Chi-DSNPS up to 0.5mg/ml ($P>0.05$). There was a mild trend for a reduction in cell proliferation, indicating a potential stress caused by high concentrations of Chi-DSNPs on cell functions. As Chi-DSNPs concentration was increased to 1mg/ml, cells were more susceptible to H_2O_2 challenge (data not shown) which further confirmed our hypothesis of stress induced by NPs.

Table 5.1

The effect of Chi-DS NPs on cell proliferation. Cell proliferation was not affected by the incubation of Chi-DSNPs for 20hs at different concentrations (0, 0.1, 0.2, 0.5mg/ml). A trend of reduction of cell proliferation was noticed as the concentration of Chi-DSNPs was increasing. However, no significant difference was observed between different treatments (P>0.05).

Chi-DSNPs(mg/ml)	0.5	0.2	0.1	Medium (0)
Cell Proliferation (Arbitrary Unit)	1.873±0.26	1.97±0.32	1.995±0.27	2.073±0.33

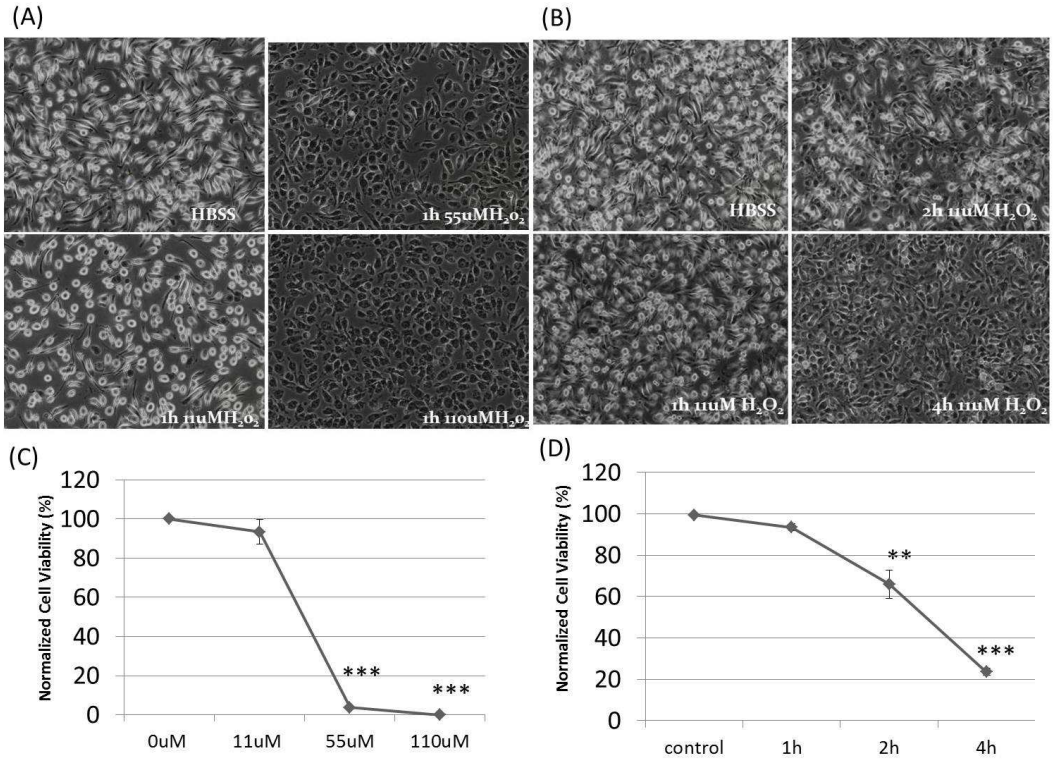

Fig. 5.1. BV-2 cell viability challenged by H_2O_2. Dose and time dependent cell death were observed when BV-2 cells incubated with different concentrations and periods of H_2O_2. Viable cells were shown with various morphologies and white halos. Non-viable cells were appeared as dark spheres after treated with Tyrpan Blue. (A) Time dependent cell death of BV-2 cells incubated 1h with 0, 11, 55, 110μMH_2O_2. (B) Dose dependent cell death of BV-2 cells incubated 11μMH_2O_2 for 0-4h. (C) The quantitative data of time dependent cell death. (D) The quantitative data of dose dependent cell death. All data was normalized and compared with control groups. Data was represented as mean±S.D. **P<0.05, ***P<0.01.

5.3.4 The effect of Chi-DSNPs on cell viability challenged by H_2O_2

Enhancement of BV-2 cell viability by the administration of Chi-DSNPs at 0min and 15mins after incubation with 5.5mM H_2O_2 was measured by the trypan blue dye exclusion test. Results (Figure 5.4) showed that a 2.5h incubation period, H_2O_2 induced almost 60% cell death in medium treated groups (P<0.001), whereas 5μm-

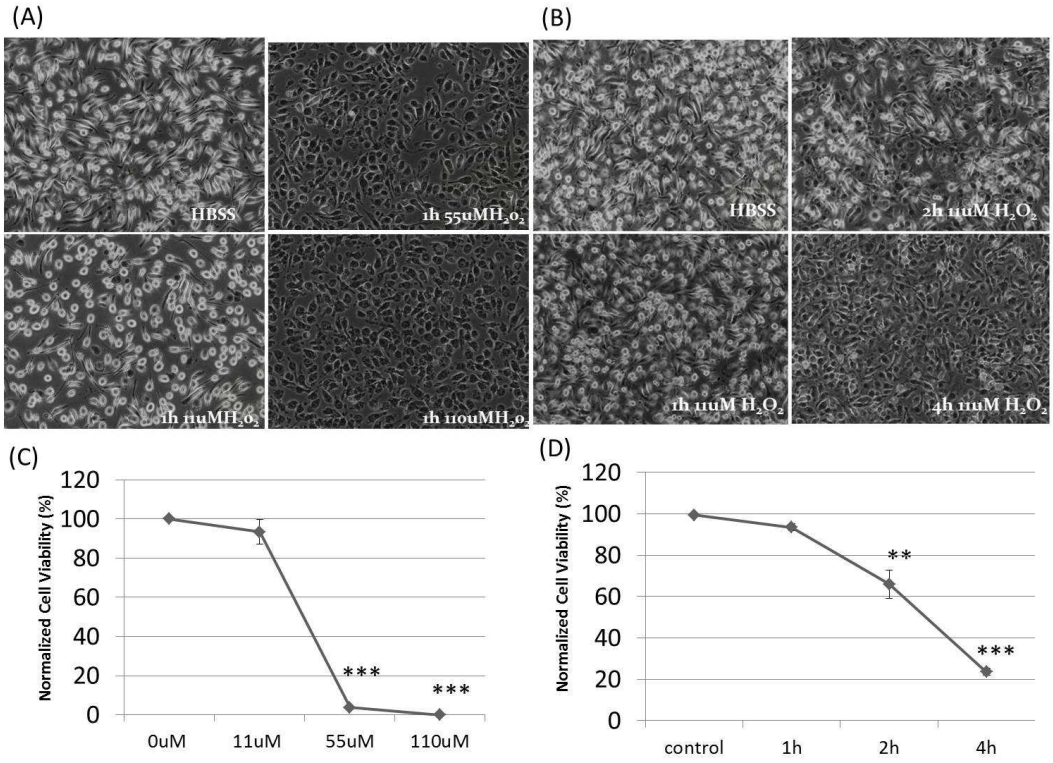

Fig. 5.2. BV-2 cell viability challenged by H_2O_2. Dose and time dependent cell death were observed when BV-2 cells incubated with different concentrations and periods of H_2O_2. Viable cells were shown with various morphologies and white halos. Non-viable cells were appeared as dark spheres after treated with Tyrpan Blue. (A) Time dependent cell death of BV-2 cells incubated 1h with 0, 11, 55, 110μMH_2O_2. (B) Dose dependent cell death of BV-2 cells incubated 11μMH_2O_2 for 0-4h. (C) The quantitative data of time dependent cell death. (D) The quantitative data of dose dependent cell death. All data was normalized and compared with control groups. Data was represented as mean±S.D. **P<0.05, ***P<0.01.

filtered Chi-DSNPs preserved approximately 20% extra viable cells on average (P<0.01). A significant difference of these protective effects on the timing of the administration of CHI-DSNPs between 0min and 15mins (P>0.05) was not detected. Additionally, post-30min treatment of BV-2 cells with Chi-DSNPs did not provide a beneficial effect (data not shown).

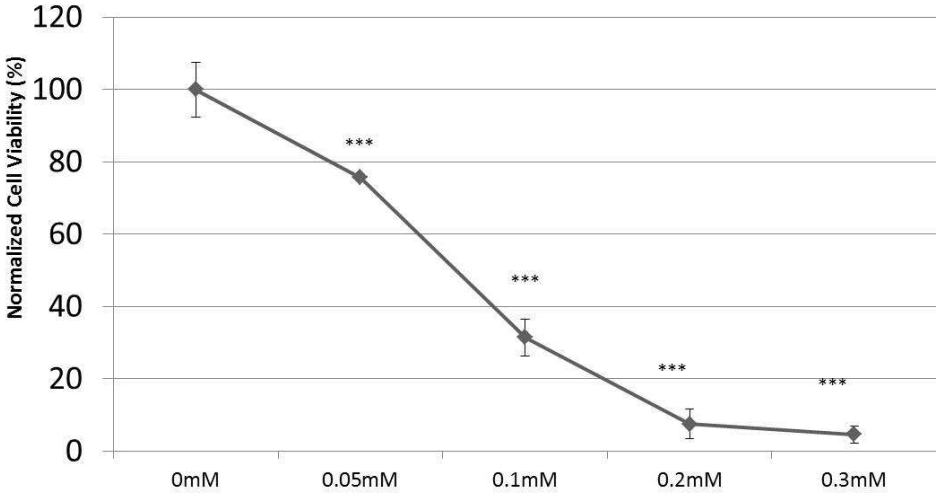

Fig. 5.3. The inhibition of BV-2 cell proliferation induced by the Incubation of H_2O_2 for 20hs. H_2O_2 induced the inhibition of cell proliferation in all studied concentrations (***P<0.001). The inhibition of cell proliferation was suggested to be dose-dependent. All H_2O_2 treated groups were normalized and compared with the control group (0mM H_2O_2). Data was represented as mean±S.D.

5.3.5 The effect of Chi-DSNPs on cell proliferation challenged by H_2O_2

To investigate the effect of Chi-DSNPs on H_2O_2 induced inhibition of cell proliferation at 20 hours, mitochondrial enzyme activity was measured by the WST-1 assay. Figure 5.5 shows that there stastically significant difference between the medium and 5μm filtered Chi-DSNPs pre-treated healthy control groups was not detected (P>0.05). This suggested that 0.2mg/ml NPs was well tolerated in BV-2 cell culture. On the other hand, 0.05mM H_2O_2 induced an approximate 25% inhibition of cell proliferation compared to healthy controls (5μm-np and medium; P<0.01). The administration of pre-4h incubation of Chi-DSNPs (1.2μm and 5μm-filtered) showed some enhancement in cell proliferation subsequent to challenge by H_2O_2 (P>0.05). However, this enhancement was still significantly lower than healthy controls (P<0.05).

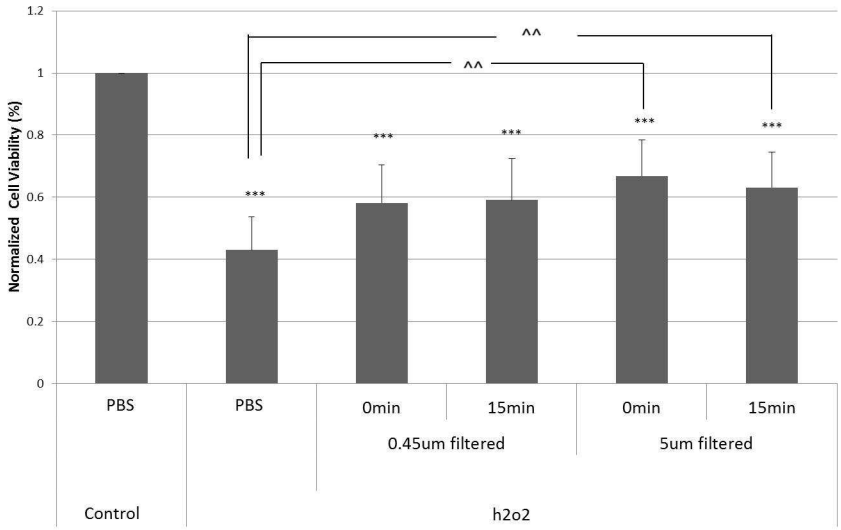

Fig. 5.4. The neuroprotection by Chi-DSNPs on H_2O_2 challenged BV-2 Cells. Data was normalized and compared with control (control-PBS) groups. H_2O_2 significantly decreased the proliferation rate of BV-2 cells compared with control groups (control-PBS). (***P<0.001). The administration of 5μm filtered group Chi-DSNPs, both at 0min and post 15min, enhanced cell viability significantly compared with H_2O_2-PBS treated group (^^P<0.01). All data was represented mean±SD.

It was observed that a statistical difference between H_2O_2-1.2μm Chi-DSNPs and medium-5μm Chi-DSNPs was not reached (P>0.05).

5.3.6 Morphological analysis of BV-2 cells challenged by low and high H_2O_2

The morphology of BV-2 cells was automatically recorded at 1h interval in a temperature and humidity controlled culture chamber using a computer-managed phase contrast microscope. The images of cells after H_2O_2 treatment at 0h, 2.5h and 18h were selected to evaluate any changes in cell morphology. In healthy control groups (Figure 5.6). A-C), cells appeared as adherent with elongated processes and a normal rate of proliferation. In 0.05mM H_2O_2 group (D-J), the morphology of cells

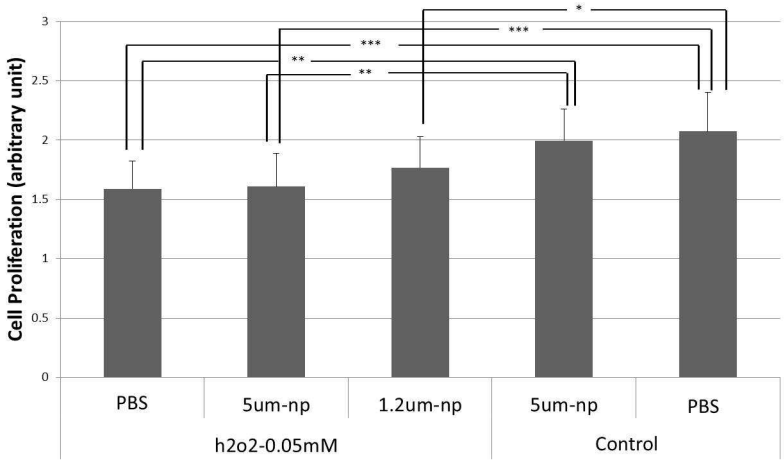

Fig. 5.5. The neuroprotection by Chi-DSNPs on H_2O_2 challenged BV-2 Cells. Cell proliferation was inhibited significantly by long-exposure of H_2O_2, compared with control groups (control-PBS). No significant difference was detected between control groups (PBS and NP treated groups) ($P>0.05$). A small increasing of cell proliferation was observed between H_2O_2-1.2μm-np group, which compared with H_2O_2 group, however the significant difference was not detected. No significant difference was observed between 1.2μm-np group and the control group (groups treated with NPs). Data was represented as mean± SD. * $P<0.05$, **$P<0.01$, ***$P<0.001$. All data was represented mean±SD.

was distorted after 4h incubation . In(F), multiple dead cells formed clumps were observed. In high magnification images(data not shown), the surface of cells became very irregular and globular intrusions were observed. In 5.5mM hydrogen peroxide group (G-I), cells started retracting their processes after 1h incubation. Some small blebs were formed and swelling of cytoplasm was also observed (data not shown). Eventually, these cells appeared to be dark indicating near or actual death. Multiple small bright spots were detected in some single dead cell, suggesting there were holes on these particular membranes (I). Nevertheless, the overall shape of the cells was still approximately spherical.

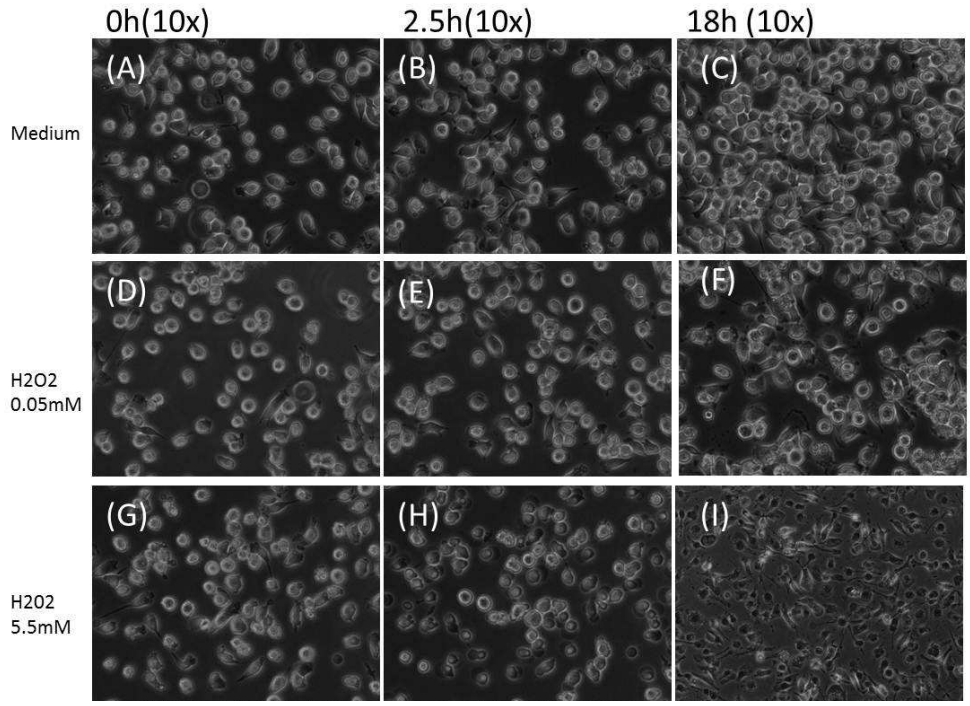

Fig. 5.6. The morphology changes of BV-2 cells induced by H_2O_2. Phase contrast images of BV-2 cells incubated with different H_2O_2 concentrations (0, 0.05, and 5.5mM) at 0h, 2.5h and 18h. (A)-(C) Medium control. (B-F) H_2O_2 0.05mM. (G-I) H_2O_2 5.5mM. Healthy cells appeared as spheres with white halos (A-E, G). Dead cells appeared as dark ones (H-I). (F) injured or non-viable cells formed clusters.

5.3.7 Fluorescence imaging of BV-2 cell death induced by low and high H_2O_2

The mode of BV-2 cell death was analyzed by dual-fluorescence staining, which combined FITC-Annexin-V (staining of phosphatidylserine on the membrane) with Propidium Iodine (PI) (intercalating with DNA base pairs). PI is membrane impermeant. Once the dye enters the cell membrane cytosol and binds with nucleic acids, the fluorescent intensity is enhanced by 20-30 fold [169]. Since the loss of membrane integrity is a pathological hallmark of necrotic cell death, only necrotic cells fluorescence red due to PI staining. [170]. Necrotic cells were stained with both PI (in

the nucleus) and FITC (on the membrane) whereas apoptotic cells were stained only with FITC (on the membrane) [171]. In Figure 5.7 (A-C) only one cell was detected to be stained with FITC-annexin-V/PI. Photomicrographs D-F show that BV-2 cells treated with 5.5mM H_2O_2 were stained bright red PI on the nucleus and some FITC on the membrane, which suggests necrosis as the major mechanism of cell death. We did not detect any cells stained only with FITC-suggesting that these cells did not undergo apoptotic cell death. Interestingly, the treatment of 0.1mM (G-I) and 0.05mM H_2O_2 (J-L) resulted in the reduction of annexin-V/PI stained cells, but also led to cells stained only with FITC. The majority of these dead cells were stained with FITC only, which indicated that long exposure to a low dose of H_2O_2 induced mostly apoptotic cell death, combined with some necrosis.

5.3.8 SSEP

SSEP of all animals were recorded and monitored prior to the compression injury, immediately post-injury, in Day 1, in Week 1 and in Week 2. The representative records of SSEP at different time points in ChiNP treated groups were shown in Figure 5.8. After the compression injury, the SSEP conduction through the lesion was blocked and a "flat signal" was recorded. However, the SSEP conduction through the median nerve-cortex circuit was intact. The preserved SSEP in the control circuit demonstrated the normal electrophysiological function above the lesion area. In all 16 ChiNP treated animals, 4 of these died prior to the final physiological measurement. In the remaining ChiNP treated animals, a small signal was recorded in Week 1 and an increased signal was observed in week 2. Instead of complicating evaluation by periodic scoring, we statistically compared only those animals that survived until the end of the study. This difference between "controls"-no SSEP signals and "experimentals"- the presence of SSEP signals was strikingly statistically significant ($P<0.001$).

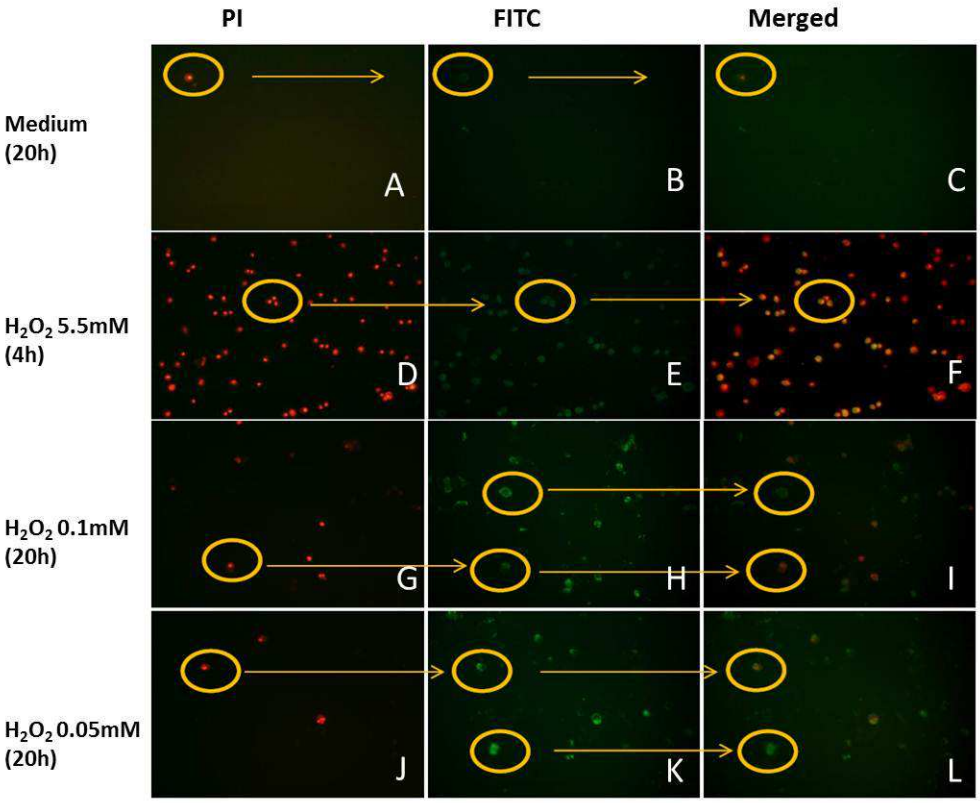

Fig. 5.7. Fluorescence images of BV-2 cells challenged with H_2O_2. Only one cell in the image was observed to be stained by PI and FITC which indicated the high cell viability in the medium-control group (A-C). Cells incubated with H_2O_2 (5.5mM-4h) resulted in mainly necrotic cell death (stained by PI or PI and FITC, shown as red or yellow dots). However, cells incubated with H_2O_2 (0.05mM-20h and 0.1mM-20h) resulted in mainly apoptotic cell death (stained by FITC only, shown as green dots). PI and FITC signal was represented as red and green color, respectively. Cells with yellow color indicated the co-stain of PI/FITC dyes. (A-C) medium control-20h, (D-F) 5.5mM-4h, (G-I) 0.1mM-20h, (J-L) 0.05mM-20h.

5.4 Discussion

5.4.1 The choice of microglia cells

Our previous study showed that chitosan nanoparticles exhibited neuroprotective effects in a acrolein-challenged PC12 cell model [27]. PC12 cells are widely used

as a model system for neuronal studies. In this work, we extend the investigation of potential protective effects of chitosan nanoparticles on neuroglia cells. The neuroprotection of glial cells has significant therapeutic impact as well as practical advantages: 1). Neuroglia cells are supporting cells which are critical for the survival and function of neurons [164, 172, 173]. The co-culture of glia and neurons indicate that glial cells can protect neurons by directly releasing glutathione into the extracellular environment - helping to maintain antioxidant levels sufficient to protect against ROS mediated damage. Neurons cultured in glial conditioned medium were also capable of up-regulating the r-glutamylcysteine synthetase (rGCS) gene whose activity is a rate-limiting step in de novo glutathione synthesis. 2). Moreover Glia cells have been shown to be more resistant than neurons to oxidative stress induced by H_2O_2 [148].

CNS neuroglia cells include macroglia (astrocytes, oligodendrocytes, radial glia, and ependymal cells) and microglia cells [174,175]. In SCI, the activation of astrocytes can result in a pathological gliosis suggested to create a harsh environment for axon regeneration. Oligodendrocytes form the myelin sheaths around axons and are vulnerable to oxidative attack. Microglia are resident tissue macrophages of CNS. They act as the initial innate immune response following CNS injuries. In SCI, the role of microglia can be protective and/or destructive [173, 176–178]. Activated microglia can give rise to microglia/ macrophages which release pro-inflammatory cytokines and proteases after SCI and it is considered as the destructive effect. On the other hand, microglia can be polarized into M2 macrophages to promote neural repair during the intermediate stages of SCI.

In this work, we used BV-2 cell line, an immortalized rat microglial cell line, which shares properties with activated microglial cells, such as antigen profile (LPS triggered TNF-alpha release) and a phagocytic capacity [179, 180]. The major advantages of using cell lines other than primary cells are: 1) immortal cells are convenient for culture and passage. 2) as an immortal cell line, they lead to significantly reproducible results whereas using primary cells might generate variable results due to the impurity of the cells. The downside of using cell line is that the response activated in a cell line

might not be as close as if it is generated from the primary cells, particularly if the research focus is a particular molecular/biochemcial pathway. Instead, the underlying mechanism of H_2O_2 induced apoptotic cell death is shared across many different cell types, including endothelial cells (EC), melanoma, macroglia, and microglia cell lines [153,161,166], which is characterized by a initiation of apoptotic cascade signals, such as caspase-3 and the activation of mitogen-activated protein kinases (MAPKs). Therefore, using BV-2 cell lines was validate to investigate the neuroprotection by ChiNPs on a H_2O_2 induced cell death model.

5.4.2 Understanding the role of H_2O_2 in SCI

H_2O_2 is widely used as an oxidative stress molecule in many injury and neurodegenerative models. Liu DX et al (1999) reported a significant elevation of intracellular level of H_2O_2 30 mins after a weight drop induced SCI and lasted over 11h in this rat SCI model [181]. In his work, H_2O_2 was suggested to be derived from $O_2^{\cdot -}$. The post-activation and long lasting increase of H_2O_2 indicated that it was not an immediate response to SCI, which consequently, confirmed the role of H_2O_2 in secondary injury of SCI.

Here, we established an H_2O_2 induced ROS cell death model using different H_2O_2 concentrations and incubation periods. The purpose of constructing different profiles of H_2O_2 induced cell damage was to find the concentration range that can mimic the ROS-induced cell damage seen after SCI, and secondly to investigate the neuroprotective ranges for Chi-DSNPs. ROS-SCI induced cell death is a combination of necrosis and apoptosis [10, 182–184], depending on concentrations and incubation times of H_2O_2. Our new results show that short exposure (1-4h) of high doses H_2O_2 (11-110μM) induced a time or/and dose dependent necrotic cell death (Figure 5.2); whereas long exposure (20h) of low doses H_2O_2 (0.05-0.1μM) results in mostly apoptotic cell death (Figure 5.7) as well as a significant suppression of cell proliferation

(Figure 5.3) [185]. The selection of H_2O_2 concentration was based on our preliminary data (data not shown) and previous work [153, 161, 166].

We observed that more than 80% necrotic cell death at 4h after incubation with 11mM H_2O_2. The elevation of hydroxyl radicals was also observed in the same period in a weight drop-induced SCI animal model [183, 186]. It was also found that the administration of H_2O_2 induced the reduction of labile iron pools, indicating enhanced conversion of H_2O_2 into hydroxyl radicals catalyzed by iron. However, Liu only monitored induced cell death after 20h of SCI and more immediate evaluations were not conducted. Considering the elevation timing of hydroxyl radicals in Liu's work and H_2O_2 induced cell death (revealed here), a concentration of 11 mM is likely too high to produce a pathologically relevant cell death in an experimentally induced SCI study. Therefore, we reduced the concentration of H_2O_2 to a more realistic 5.5 mM to gauge the protective effects by Chi-DSNPs.

5.4.3 Understanding the Chi-NP results

Our results show that 5.5mM Chi-NP protected microglia cells from hydrogen peroxide (2.5h) (Figure 5.4). The neuroprotective effects of Chi-NP can be deduced from lipid interactions with the chitosan polymer. Chitosan can significantly "seal" the membrane breaches/holes produced by mechanical forces [26,27]. H_2O_2 can induce LPO, resulting in increased membrane permeability. Considering the presence of H_2O_2 in the bathing medium, cellular membranes are the first cell component to be damaged. Our results also suggest that the larger sized (5μm-filtered) Chi-DSNPs had a stronger protective effect than the smaller size (0.45μm-filtered) of NPs. One possible reason might be associated with the availability of the number of chitosan polymers and the hydrophilic radius of the NPs themselves. Compared with small Chi-NP, the larger ones incorporate a higher amount of chitosan polymers - which in turn can react in a more robust fashion and occupy a larger surface area with multiple membrane lipids.

We also studied the results of a 20h incubation of 0.05mM hydrogen peroxide on BV-2 cells. No significant improvement of cell proliferation was observed between control and Chi-NP treated groups. At first glance, our "rescue" experiments had unexpected results. In order to investigate the reason, we conducted a morphological analysis in bright field and a cell death study with annexin-V/PI stainings. The morphological analysis of BV-2 cells induced in two H_2O_2 conditions showed very different results (Figure 5.6). Cells in the high concentration of H_2O_2 (5.5mM) retracted their processes but the overall morphology was still preserved. However, cells in the low concentration of H_2O_2 (0.05mM) formed clusters where irregular and globular intrusions were observed. Results (Figure 5.7) from fluorescence staining confirmed increasing occurrence of apoptotic cell death (FITC staining) in 0.05mM H_2O_2. Both fluorescence staining and bright field imaging suggested that the outcomes observed in "rescue" experiments can be explained by cells dying from either apoptosis or necrosis. Actually, necrosis, apoptosis or a combination of the two is commonly observed in H_2O_2 induced cell death [10,159,182–184]. Therefore, our data supports the notion that H_2O_2 at low dosage but at long incubation time likely leads to apoptosis. High dosages of toxin, but with very short incubation times are more associated with necrosis. Neuroprotection by Chi-NP in "rescuing" cells from necrosis is might be due to the a physical interactions of chitosan polymer with compromised membrane lipids [26,27]. This was observed in 5.5mM H_2O_2 treatments. In 0.05mM, even though the low concentration of H_2O_2 was not immediately as "toxic" as at higher concentrations in the acute phase (0-4h), this level triggered apoptotic cell death which is not reversible.

Other studies also suggest the anti-oxidant effects of a pre-incubation with chitosan, but with different periods, ranging from 30mins to 24h. We do not wish to follow this line of investigation as it is impracticable outside of the laboratory and may not reveal any useful insights into mechanisms of action and/or integration of the polymer in injury or disease. The beneficial effects of chitosan also depended on the MW of chitosan, cell types tested, and the nature of "challenge" toxins [153,166].

The uptake of chitosan / Chi-NP by A549 cells was observed in a dose and time-dependent way [187]. We emphasize however that anti-oxidant therapy has never been useful outside of animal laboratory models of CNS injury [10]. While in the acute necrotic cell death, a hypothesized anti-oxidant effect might not be sufficient to neutralize H_2O_2 and dampen so-called ROS mediated damage. However, it is just as likely that direct treatments with potent antioxidants may not prove beneficial either. The accepted mechanism for an inhibition of necrosis is via the sealing effect of poloxamers, poloxamines, PEG, and Chitosan followed by spontaneous membrane assembly in regions of defect [1, 10, 22, 26]. It was also suggest that the incidence of apoptotic cell death in chronic CNS injuries is grossly exaggerated [10].

5.4.4 Comparisons of SSEP recovery after compression injury with different treatments (Chi-NPs, Saline and Silica NPs)

In this work, the presence or absence of SSEP through the lesion was used as the criteria to study the performance of therapeutic effect of ChiNPs. Our results showed that no recovery was observed in the silica NPs treated groups and the saline treated groups (in our previous studies [25]. On the other hand, the conduction in ChiNP treated groups was shown to start some level of recovery in 2 weeks of the administrations of NPs.

Since SSEP mainly monitors the sensory function at the dorsal column of the spinal cord, other functional tests might be also conducted in the future to provide the effect of ChiNPs in the perspective of motor function. The cutaneous trunci muscle reflex (CTM) was used as a tool to evaluate behavioral recovery in rats and guinea pigs [144]. CTM reflex is a reflexive contraction of the skin of the back, stimulated by a light physical touch of the skin. Different from SSEP, CTM reflex involves both sensory and motor circuitries. Details of the anatomical basis of CTM reflex can be found in Borgens 2003 [1]. Successful applications of CTM reflex was observed in SCI guinea pig studies [21, 22].

5.4.5 The in vivo biodistribution and nanotoxicity of ChiNPs

As the advantages of nanomedicine compared with the delivery of bulk materials have been increasingly recognized in recent years, the investigations of biodistribution and nanotoxicity of nanomedicine also increases [56, 188–191]. The biodistribution of ChiNPs has been studied in many routes of administrations and organs: intravenous, ocular, oral, pulmonary and liver [192]. Even though these NPs are all based on chitosan polymer, the variety of size and surface properties allow them to have various activities in vivo [193]. The accumulation of NPs in the body was influenced by many effects: (1) the retention effect due to the leaky vascular structure and the poor lymphatic drainage system in tumors [168]; (2) the mucoadhesion effect due to the interaction between chitosan and the mucus layer of the ocular mucosa [194, 195]; (3) the elimination effect due to the clearance by the reticuloendothelial organs (liver) and the filtration organ (kidney) [167]. The toxicity of ChiNPs were also studied in bare NPs [128, 143], in gene delivery (siRNA and DNA) [196, 197], and drug delivery [198]. Overall, the application of ChiNPs in cell and animal studies is suggested to be safe [192]. Our future work is to investigate the biodistribution of ChiNPs in SCI animal models and elucidate the actions of ChiNPs after the intravenous administration.

5.5 Conclusion

In conclusion, Chi-NPs partially spared cells from necrotic cell death which was induced by acute H_2O_2 incubation. The mechanism of the neuroprotection by Chi-NPs might be associated with the interaction between chitosan polymer and membrane lipids which in turn facilitated the membrane restoration. Our in vivo study showed that the immediate subcutaneous administration of Chi-NPs results in some level of the conduction of SSEP 1 week after the compression spinal injury performed in guinea pigs.

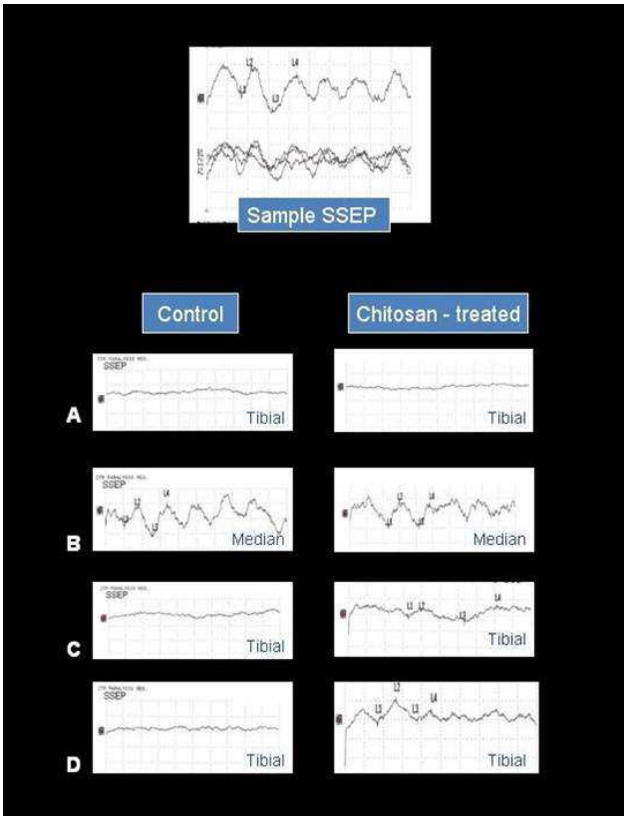

Fig. 5.8. Somatosensory evoked potential recordings in control and injured guinea pig spinal animals. The top panel (sample SSEP) consists of a single and three overlapped measurements of SSEP. The single waveform is a representative record of SSEP collected in a normal animal, which was an average of 3 overlapped traces (each, the average of 120 consecutive measurements, shown at below) The lower panel (Control and Chitosan-treated) presented averaged signals: SSEPs from a control animal (on the left) and from a Chi-NPs treated animal (on the right). A. The eliminations of SSEPs were observed through the lesion in both animals (control and Chi-NP treated) after the compression injury on the cord. B. The readings of intact SSEP were obtained from median nerve stimulation/recording in both animals throughout the observation period. Note the appearance of weak SSEP recorded in only the ChiNPs treated animal in week 1 (C, on the right) and week 2 (D, on the right). However, SSEP in the Control animal was shown as a "flat" line throughout the observation period (C, D, both on the left) which indicated the absence of the signal conduction through the lesion. The time base is 10 ms per division, with an amplitude of 1.25 uV per division.

6. CONCLUSIONS

6.1 Conclusions

In this thesis, we presented data of the affinity of TMR-PSiNPs at the injured sites of spinal cord tissues. We fabricated ChiNPs based on an ionic gelation method and investigated the neuroprotective effects by chitosan and ChiNPs in SCI associated cell, tissue and animal models. The experimental findings and interpretations were summarized below:

1. Using an ex vivo compression model, PSiNPs were shown to accumulate significantly at the damage sites of the spinal cord tissues ($P<0.05$). The fluorescent intensity of TMR-PSiNPs was shown to be inversely proportional to the distance from the site of the compression injury. The fluorescent intensity of TMR-PSiNPs decreased significantly in intact regions, compared with the compression site. SEM results were consistent with the result from fluorescence images. SEM results suggested that larger amount of PSiNPs was located at the damage site compared with the intact sites.

2. Using ex vivo compression and transection models, chitosan polymer was suggested to facilitate the restoration of membrane integrity by suppressing the random exchange of molecules across the membrane breaches. The incubation of compressed spinal cord segments with chitosan inhibited significantly the leakage of LDH compared with PBS treated control ones ($P<0.05$). In addition, the incubation of transected spinal cord segments with chitosan excluded the internalization of TMR probes ($P<0.05$), compared with PBS treated ones.

3. A significant difference of the effects of the neuroprotection based on DAs and MWs of chitosan was not observed ($P>0.05$). The preference of FITC-chitosan

(DA0%) on the damage sites of the spinal cord segments was not observed as well ($P>0.05$).

4. Two types of ChiNPs were successfully constructed: ChiDSNPs and ChiTPP-NPs, based on an ionic gelation method. ChiNPs appeared as spheres.

5. The bimodal size distribution was observed in both types of NPs (Chi-TPPNPs: 20-40nm and 100-200nm; Chi-DSNPs: 40-60nm and 200-300nm).

6. The sizes and zeta potentials of NPs were associated with the volume ratio of chitosan / DS and chitosan / TPP. As the volume of TPP or DS increases, the size of NPs decreases, whereas stronger binding forces between oppositely charged polymers were suggested. Particularly, the zeta-potential of MC-DSNPs in de-ionized water was reversed from positive to negative, as Chi/DS ratios decreased from 5:3 to 5:8.

7. A significant impact of pH on the formation of ChiTPPNPs was not observed. ChiTPPNPs were formed successfully at both pHs of TPP (4.3 and 9.1). ChiDSNPs were only formed at pH of DS (4.6). However, no NP but polymer aggregations were synthesized at high pH of DS ($pH>6$).

8. ChiNPs were stable when incubated in the buffer with low ionic strength (less than 0.1 XPBS). The incubation of MC-TPPNPs in the buffer with high ionic strength (more than 0.5 XPBS) induced a size increase (5 times) and a decrease of zeta-potential (80%) ($P<0.05$), These changes indicated the aggregation of MC-TPPNPs in the high ionic strength environment. The zeta-potential of MC-DSNPs was decreased significantly as well in the high ionic strength ($P<0.05$). However, a significant change of size was not observed in MC-DSNPs.

9. Using H_2O_2 challenged BV-2 cell models, the neuroprotection by Chi-NPs was suggested to rescue cells undergoing necrotic cell death.

10. Cell death and the inhibition of cell proliferation induced by H_2O_2 were concentration and time depedent. BV-2 cells incubating with a lower (0.05mM) concentration of H_2O_2 for a long period of time (22h) produced mainly apoptotic cell death. BV-2 cells incubating with a higher (5.5mM) concentration of H_2O_2 for a short period of time (2-4h) resulted in mainly necrotic cell death.

11. Using an in vivo compression injury model, the subcutaneous administration of Chi-NPs restored partially the conduction of SSEP after 1 week of NPs' injection, while the control groups treated with silica NPs or saline still showed no recovery of function. The conduction of SSEP was blocked completely after the compression injury performed.

Our studies have showed that the application of chitosan successfully blocked the exchange of molecules through the membrane breaches which were produced by mechanical forces. The application of Chi-NPs dampened the cytotoxicity of hydrogen peroxide, rescued BV-2 cells from necrotic death and restored the sensory signal conduction through the lesion. In addition, the affinity of PSiNPs at the injured spinal tissues indicated that PEG can be used to target damaged cells. Our studies did not find a DA and MW dependent neuroprotective effect by chitosan. We also learned that the properties of Chi-NPs were significantly affected by high ionic strength.

6.2 Future Work

SSEP is a sensory functional test which evaluates the sensory signal conduction through the spinal cord. Other functional tests, such as the motor functional test, cutaneous trunci muscle (CTM) reflex, need to be included to complete the understanding of the neuroprotective effects of ChiNPs in whole animal studies. Studies of the biodistribution and the metabolism of Chi-NPs will also allow us to get more information of the effect of Chi-NPs in the human body. Considering the affinity of PEG at the membrane damage and the biodegradability and the neuroprotective effects by chitosan and Chi-NPs, PEG-chitosan complex can be fabricated to combine both targeting and neuroprotective effects. The beneficial effect of PEG-chitosan complex can be investigated in CNS models.

LIST OF REFERENCES

LIST OF REFERENCES

[1] R. Borgens in *Restoring function to the injured human spinal cord* (R. Borgens, ed.), 2003.

[2] "Centers for disease control and prevention." `www.cdc.gov`.

[3] P. Anderson, "Cns/aans guidelines discourage steroids in spinal injury.," 2013.

[4] M. Hadley and B. Walters, "Guidelines for the management of acute cervical spine and spinal cord injuries," *Neurosurgery*, vol. 72, no. 1-259, 2013.

[5] D. Baptiste and M. Fehlings, "Pharmacological approaches to repair the injured spinal cord," *J. Neurotrauma.*, vol. 23, pp. 318–334, 2006.

[6] C. Tator, "Review of treatment trials in human spinal cord injury: issues, difficulties and recommendations.," *Neurosurgery*, vol. 59, pp. 982–987, 2006.

[7] A. Blight, "Miracles and moleculesprogress in spinal cord repair," *Nat. Neurosci.*, vol. 5, no. 1051-1054, 2002.

[8] R. P. Bunge, "Glial cells and the central myelin sheath.," *Physiol. Rev.*, vol. 48, no. 1, pp. 197–251, 1968.

[9] C. Tator, "Clinical manifestations of acute spinal cord injury.," *American association of neurological surgeons*, pp. 15–26, 1995.

[10] R. Borgens and P. Liu-Snyder, "Understading secondary injury," *Q. Rev. Biol.*, vol. 87, no. 2, pp. 89–127, 2012.

[11] G. Meer, D. Voelker, and W. Feigenson, "Membrane lipids: where they are and how they behave," *Nat. Rev. Mol. Cell Bio.*, vol. 9, pp. 112–124, 2008.

[12] H. McNally and R. Borgens, "Three-dimensional imaging of living and dying neurons with atomic force microscopy," *J. Neurocytol.*, vol. 33, pp. 251–258, 2004.

[13] H. Yawo and M. Kuno, "Calcium dependence of membrane sealing at the cut end of the cockroach giant axon," *J. Neurosci. Res.*, vol. 5, no. 6, pp. 1626–1632, 1985.

[14] K. Arnold, A. Herrmann, K. Gawrisch, and L. Pratsch, "Water-mediated effects of peg on membrane properties and fusion," in *Molecular Mechanisms of Membrane Fusion* (S. Ohki, D. Doyle, T. Flanagan, S. Hui, and E. Mayhew, eds.), pp. 255–272, 1988.

[15] X. Y. Xie and J. N. Barrett, "Membrane resealing in cultured rat septal neurons after neurite transection: evidence for enhancement by ca^{2+}-triggered protease activity and cytoskeletal disassembly," *J. Neurosci.*, vol. 11, pp. 3257–3267, 1991.

[16] R. Steinhardt, "The mechanisms of cell membrane repair: A tutorial guide to key experiments," *Ann. N.Y. Acad. Sci.*, vol. 1066, pp. 152–165, 2005.

[17] K. Barbee, "Mecanical cell injury," *Ann. N.Y. Acad. Sci.*, vol. 1066, pp. 67–84, 2005.

[18] K. Uchida, M. Kanematsu, Y. Morimitsu, T. Osawa, N. Noguchi, and E. Niki, "Acrolein is a product of lipid peroxidation reaction: Formation of free acrolein and its conjugate with lysine residues in oxidized low density lipoproteins," *J. Biol. Chem.*, vol. 273, no. 26, pp. 16058–16066, 1998.

[19] J. Lee, G. Zipfel, and D. Choi, "The changing landscape of ischaemic brain injury mechanisms," *Nature*, vol. 399 suppl., pp. A7–A14, 1999.

[20] J. Wong-Ekkabut, Z. Xu, W. Triampo, I. Tang, D. Tieleman, and L. Monticelli, "Effect of lipid peroxidation on the properties of lipid bilayers: a molecular dynamics study.," vol. 93, pp. 4225–4236, 2007.

[21] R. Borgens and S. R., "Immediate recovery from spinal cord injury through molecular repair of nerve membranes with polyehylene glycol," *FASEB*, vol. 14, pp. 27 – 32, 2000.

[22] R. Borgens and D. Bohnert, "Rapid recovery from spinal cord injury after subcutaneously administered polyethylene glycol," *J. Neurosci. Res.*, vol. 66, pp. 1179 – 1186, 2001.

[23] R. Borgens, "Cellular engineering: molecular repair of membranes to rescue cells of the damaged nervous system.," *Neurosurgery*, vol. 49, no. 2, pp. 370–380, 2001.

[24] R. Borgens, R. Shi, and D. Bohnert, "Behavioral recovery from spinal cord injury following delayed application of polyethylene glycol," *J. Exp. Biol.*, vol. 205, no. 1, pp. 1–12, 2002.

[25] C. T., S. R., I. A., and B. R.B., "Functional silica nanoparticle-mediated neuronal membrane sealing following traumatic spinal cord injury," *J. Neurosci. Res.*, vol. 88, pp. 1433–1444, 2010.

[26] Y. Cho, R. Shi, and R. B. Borgens, "Chitosan produces potent neuroprotection and physiological recovery following traumatic spinal cord injury," *J. Exp. Biol.*, vol. 213, no. 9, pp. 1513–1520, 2010.

[27] Y. Cho, R. Shi, and R. Ben Borgens, "Chitosan nanoparticle-based neuronal membrane sealing and neuroprotection following acrolein-induced cell injury," *J. Bio. Eng.*, vol. 4, no. 1, p. 2, 2010.

[28] Y. Cho, R. Shi, R. Borgens, and A. Ivanisevic, "Functionalized mesoporous silica nanoparticle-based drug delivery system to rescue acrolein mediated cell death," *Nanomedicine*, vol. 3, pp. 507–519, 2008.

[29] J. Silver and H. Miller, "Regeneration beyond the glial scar," *Nature*, vol. 5, pp. 146–156, 2004.

[30] L. Olson, "Medicine: Clearing a path for nerve growth," *Nature*, vol. 416, pp. 589–590, 2002.

[31] W. Maddrey, "Drug-induced hepatotoxicity," *J. Clin. Gastroenterol.*, vol. 39, pp. S83–89, 2005.

[32] "Clinicaltrials.gov." `clinicaltrials.gov`.

[33] S. Wang, K. Wang, and W. Wang, "Mechanisms underlying the riluzole inhibition of glutamate release from rat cerebral cortex nerve terminals (synaptosomes)," *Neuroscience*, vol. 125, no. 1, pp. 191 – 201, 2004.

[34] H. Zimmerman, "Miscellaneous drugs and diagnostic chemicals," in *Hepatotoxicity: The adverse effects of drugs and other chemicals on the liver* (H. Zimmerman, ed.), 1999.

[35] M. Fehlings, "Editorial: recommendations regarding the use of methylprednisolone in acute spinal cord injury: making sense out of the controversy.," *Spine*, vol. 26, pp. S56–S57, 2001.

[36] M. Brackem, M. Shepar, and W. e. a. Collins, "A randomized, controlled trial of methylprednisolone or naloxone in the treatment of acute spinal cord injury study.," *New Engl. J. Med.*, vol. 322, pp. 1405–1411, 1990.

[37] J. Xu, G. Fan, S. Chen, Y. Wu, X. Xu, and C. Hsu, "Methylprednisolone inhibition of tnf-alpha expression and nf-kb activation after spinal cord injury in rats," *Mol. Brain Res.*, vol. 59, no. 2, pp. 135 – 142, 1998.

[38] A. Khoshnevisan, A. Mardani, and S. Kamali, "An overview of pharmacological approaches for management and repair of spinal cord injuries," *Iran. J. Psychiatry*, vol. 5, pp. 119–127, 2010.

[39] A. Blesch and M. Tuszynski, "Neurotrophic factor therapy: NGF, BDNF and NT-3," in *Encyclopedia of Neuroscience* (L. R. Squire, ed.), pp. 1093 – 1100, Oxford: Academic Press, 2009.

[40] P. Menon, D. Muresanu, A. Sharma, H. Mossler, and H. Sharma, "Cerebrolysin, a mixture of neurotrophic factors induces marked neuroprotection in spinal cord injury following intoxication of engineered nanoparticles from metals," *CNS Neurol. Disord. Drug Targets*, vol. 11, pp. 40–9, 2012.

[41] E. Bradbury, R. Moon, L. D. F.and Popat, V. R. King, G. S. Bennett, P. N. Patel, J. W. Fawcett, and S. McMahon, "Chondroitinase abc promotes functional recovery after spinal cord injury," *Nature*, vol. 416, pp. 636–640, 2002.

[42] S. Hannila and M. Filbin, "The role of cyclic AMP signaling in promoting axonal regeneration after spinal cord injury," *Expl. Neurol.*, vol. 209, no. 2, pp. 321 – 332, 2008.

[43] P. Dergham, B. Ellezam, C. Essagian, H. Avedissian, W. Lubell, and L. Mckerracher, "Rho signaling pathway targeted to promote spinal cord repair," *J. Neurosurg.*, vol. 22, pp. 6570–6577, 2002.

[44] D. Cadotte and M. Fehlings, "Spinal cord injury: A systematic review of current treatment options," *Clin. Orthop. Relat. R.*, vol. 469, no. 3, pp. 732–741, 2011.

[45] P. Laverty, A. Leskovar, G. Breur, J. Coates, R. Bergman, W. Widmer, J. Toombs, S. Shapiro, and R. Borgens, "A preliminary study of intravenous surfactants in paraplegic dogs: polymer therapy in canine clinical SCI," *J. Neurotrauma.*, vol. 21, pp. 1767–1777, 2004.

[46] A. Koob and R. Borgens, "Polyethylene glycol treatment after traumatic brain injury reduces β-amyloid precursor protein accumulation in degeneration axons.," *J. Neurosci. Res.*, vol. 83, pp. 1558–1563, 2006.

[47] J. Luo, R. Borgens, and R. Shi, "Polyethylene glycol immediately repairs neuronal membranes and inhibits free radical production after acute spinal cord injury," *J. Neurol. Chem.*, vol. 83, pp. 471–480, 2002.

[48] J. Luo, R. Borgens, and R. Shi, "Polyethylene glycol improves function and reduces oxidative stress in synaptosomes following spinal cord injury," *J. Neurotrauma.*, vol. 21, pp. 994–1007, 2004.

[49] Y. Cho, R. Shi, R. Borgens, and A. Ivanisevic, "Repairing the damaged spinal cord and brain with nano medicine," *Small*, vol. 4, pp. 1676–1681, 2008.

[50] J. Berger, M. Reist, J. Mayer, O. Felt, and R. Gurny, "Structure and interactions in chitosan hydrogels formed by complexation or aggregation for biomedical applications," *Eur. J. Pharm. Biopharm.*, vol. 57, no. 1, pp. 35 – 52, 2004.

[51] "Chitin/chitosan: modifications and their unlimited application potential-an overview," *Trends Food Sci. Tech.*, vol. 18, no. 3, pp. 117 – 131, 2007.

[52] I. Aranaz, M. Mengibar, R. Harris, I. Paios, B. Miralles, N. Acosta, G. Galed, and A. Heras, "Functional characterization of chitin and chitosan.," *Current Chemical Biology*, vol. 3, pp. 203–230, 2009.

[53] "Biodegradation, biodistribution and toxicity of chitosan," *Adv. Drug Deliver. Rev.*, vol. 62, no. 1, pp. 3 – 11, 2010.

[54] A. Aderem and D. M. Underhill, "Mechanisms of phagocytosis in macrophages.," *Annu. Rev. Immunol*, vol. 17, no. 1, p. 593, 1999.

[55] J. A. Champion and S. Mitragotri, "Role of target geometry in phagocytosis," *P. Natl. Acad. Sci.*, vol. 103, no. 13, pp. 4930–4934, 2006.

[56] S. McNeil, "Unique benefits of nanotechnology to drug delivery and diagnostics," in *Characterization of Nanoparticles Intended for Drug Delivery* (S. McNeil, ed.), vol. 697 of *MIMB*, pp. 3–8, Humana Press, 2011.

[57] Q. Zhang, N. Iwakuma, P. Sharma, C. Moudgil, B.M.and Wu, J. McNeill, H. Jiang, and S. Grobmyer, "Gold nanoparticles as a contrast agent for in vivo tumor imaging with photoacoustic tomography," *Nanotechnology*, vol. 20, no. 39, p. 395102, 2009.

[58] L. Rosen, J.E.and Chan, D. Shieh, and F. X. Gu, "Iron oxide nanoparticles for targeted cancer imaging and diagnostics," *Nanomed. Nanotechnol.*, pp. 275–290, 2012.

[59] Q. Zhao, L. Wang, R. Cheng, L. Mao, R. Arnold, E. Howerth, Z. Chen, and S. Platt, "Magnetic nanoparticle-based hyperthermia for head and neck cancer in mouse models," *Theranostics*, vol. 2, pp. 113–121, 2012.

[60] I. I. Slowing, B. G. Trewyn, S. Giri, and V. S.-Y. Lin, "Mesoporous silica nanoparticles for drug delivery and biosensing applications," *Adv. Funct. Mater.*, vol. 17, no. 8, pp. 1225–1236, 2007.

[61] J. Harrison, C. Bartlett, P. K. Cowin, G.and Nicholls, C. Evans, T. Clemons, I. A. Zdyrko, B.and Luzinov, A. R. Harvey, K. S. Iyer, S. A. Dunlop, and M. Fitzgerald, "In vivo imaging and biodistribution of multimodal polymeric nanoparticles delivered to the optic nerve," *Small*, vol. 8, no. 10, pp. 1579–1589, 2012.

[62] S. Chvatal, Y.-T. Kim, A. Bratt-Leal, H. Lee, and R. Bellamkonda, "Spatial distribution and acute anti-inflammatory effects of methylprednisolone after sustained local delivery to the contused spinal cord," *Biomaterials*, vol. 29, no. 12, pp. 1967 – 1975, 2008.

[63] V. Reukov, V. Maximov, and A. Vertegel, "Proteins conjugated to poly(butyl cyanoacrylate) nanoparticles as potential neuroprotective agents," *Biotechnol. Bioeng.*, vol. 108, no. 2, pp. 243–252, 2011.

[64] N. D. Jeffery, S. C. McBain, J. Dobson, and D. M. Chari, "Uptake of systemically administered magnetic nanoparticles (MNPS) in areas of experimental spinal cord injury (SCI)," *J. Tissue Eng. Regen. Med.*, vol. 3, no. 2, pp. 153–157, 2009.

[65] R. Juliano, "Nanomedicine: is the wave cresting?," *Nat. Rev. Drug Discov.*, vol. 12, pp. 171–172, 2013.

[66] M. E. Schwab, "Repairing the injured spinal cord.," *Science*, vol. 295, no. 5557, pp. 1029 – 1031, 2002.

[67] H. Meiri, M. Spira, and I. Parnas, "Membrane conductance and action potential of a regenerating axonal tip," *Science*, vol. 211, no. 4483, pp. 709–712, 1981.

[68] S. W. Burgess, T. J. McIntosh, and B. R. Lentz, "Modulation of poly(ethylene glycol)-induced fusion by membrane hydration: importance of interbilayer separation," *Biochem.*, vol. 31, no. 10, pp. 2653–2661, 1992.

[69] B. Lentz, "Polymer-induced membrane fusion: potential mechanism and relation to cell fusion events," *Chem. Phys. Lipids*, vol. 73, no. 12, pp. 91 – 106, 1994.

[70] J. Lee and B. Lentz, "Evolution of lipid structures during model membrane fusion and the relation of this process to cell membrane fusion," *Biochem.*, vol. 36, no. 21, pp. 6251–6259, 1997.

[71] K. Kao, F. Constabel, M. Michayluk, and O. Gamborg, "Plant protoplast fusion and growth of intergeneric hybrid cells," *Planta*, vol. 120, pp. 215 – 227, 1974.

[72] Q. Ahkong, J. Howell, J. Lucky, F. Safwat, M. Davey, and E. Cocking, "Fusion of hen erythrocytes with yeast protoplasts induced by polyethylene glycol.," *Nature*, vol. 5503, pp. 66–67, 1975.

[73] B. Lentz, "Peg as a tool to gain insight into membrane fusion," *Eur. Biophys. J.*, vol. 36, no. 4-5, pp. 315–326, 2007.

[74] S. Singer and G. Nicolson, "The fluid mosaic model of the structure of cell membranes," *Science*, vol. 175, no. 4023, pp. 720–731, 1972.

[75] P. Liu-Snyder, M. P. Logan, R. Shi, D. T. Smith, and R. B. Borgens, "Neuroprotection from secondary injury by polyethylene glycol requires its internalization," *J. Exp. Biol.*, vol. 210, no. 8, pp. 1455–1462, 2007.

[76] J. Donaldson, R. Shi, and R. Borgens, "Polyethylene glycol rapidly restores physiological functions in damaged sciatic nerves of guinea pigs," *Neurosurgery*, vol. 1, pp. 147–56, 2002.

[77] A. Koob, B. Duerstock, C. Babbs, Y. Sun, and R. Borgens, "Intravenous polyethylene glycol inhibits the loss of cerebral cells after brain injury," *J. Neurotrauma.*, vol. 22, pp. 1092–1111, 2005.

[78] J. Brent, "Current management of ethylene glycol poisoning," *Drugs*, vol. 61, pp. 979–988, 2002.

[79] E. Caravati, A. Erdman, G. Christianson, A. Manoguerra, L. Booze, A. Woolf, K. Olson, P. Chyka, E. Scharman, P. Wax, D. Keyes, and W. Troutman, "Ethylene glycol exposure: an evidence-based consensus guideline for out-of-hospital management," *Clin. Toxicol. (Phila)*, vol. 43, pp. 327–345, 2005.

[80] S. Schneiderman, J. Farber, and R. Baserga, "A simple method for decreasing the toxicity of polyethylene glycol in mammalian cell hybridization," *Somat. Cell Genet.*, vol. 5, no. 2, pp. 263–269, 1979.

[81] G. Szabo, A. Kiss, and L. Trn, "Permeabilization of lymphocytes with polyethylene glycol 1000. discrimination of permeabilized cells by flow cytometry," *Cytometry*, vol. 3, no. 1, pp. 59–63, 1982.

[82] A. Cole and R. Shi, "Prolonged focal application of polyethylene glycol induces conduction block in guinea pig spinal cord white matter," *Toxicol. in Vitro*, vol. 19, no. 2, pp. 215 – 220, 2005.

[83] R. Webster, V. Elliott, B. Park, D. Walker, and P. Hankin, M.and Taupin, "PEG and PEG conjugates toxicity: towards an understanding of the toxicity of PEG and its relevance to PEGylated biologicals," in *PEGylated Protein Drugs: Basic Science and Clinical Applications* (F. Veronese, ed.), Milestones in Drug Therapy, pp. 127–146, Birkhauser Basel, 2009.

[84] F. Veronese and G. Pasut, "PEGylation, successful approach to drug delivery," *Drug Discov. Today*, vol. 10, no. 21, pp. 1451 – 1458, 2005.

[85] S. Maskarinec, G. Wu, and K. C. LEE, "Membrane sealing by polymers," *Ann. N.Y. Acad. Sci.*, vol. 1066, no. 1, pp. 310–320, 2006.

[86] B. Chen, M. Zuberi, R. B. Borgens, and Y. Cho, "Affinity for, and localization of, PEG-functionalized silica nanoparticles to sites of damage in an ex vivo spinal cord injury model," *J. Bio. Eng.*, vol. 6, no. 1, pp. 1–10, 2012.

[87] H. Winterhalter, M.and Brner, S. Marzinka, R. Benz, and J. Kasianowicz, "Interaction of poly(ethylene-glycols) with air-water interfaces and lipid monolayers: investigations on surface pressure and surface potential.," *Biophys. J.*, vol. 69, pp. 1372–1381, 1995.

[88] J. Maskarinec, S.A.and Hannig, R. Lee, and K. Lee, "Direct observation of poloxamer 188 insertion into lipid monolayers," *Biophys. J.*, vol. 82, no. 3, pp. 1453–1459, 2002.

[89] A. Abuchowski, J. R. McCoy, N. C. Palczuk, T. van Es, and F. F. Davis, "Effect of covalent attachment of polyethylene glycol on immunogenicity and circulating life of bovine liver catalase.," *J. Biol. Chem.*, vol. 252, no. 11, pp. 3582–6, 1977.

[90] A. Abuchowski, T. van Es, N. C. Palczuk, and F. F. Davis, "Alteration of immunological properties of bovine serum albumin by covalent attachment of polyethylene glycol.," *J. Biol. Chem.*, vol. 252, no. 11, pp. 3578–81, 1977.

[91] J. Jokerst, T. Lobovkina, R. Zare, and S. Gambhir, "Nanoparticle PEGylation for imaging and therapy," *Nanomedicine (Lond.)*, vol. 6, pp. 715–728, 2011.

[92] T. Niidome, M. Yamagata, Y. Okamoto, A. Y., H. Takahashi, T. Kawano, Y. Katayama, and Y. Niidome, "Peg-modified gold nanorods with a stealth character for in vivo applications," *J. Control. Release.*, vol. 114, no. 3, pp. 343 – 347, 2006.

[93] A. Faure, S. Dufort, V. Josserand, P. Perriat, J. Coll, S. Roux, and O. Tillement, "Control of the in vivo biodistribution of hybrid nanoparticles with different poly(ethylene glycol) coatings," *Small*, vol. 5, pp. 2565–2575, 2009.

[94] C. S. Fishburn, "The pharmacology of PEGylation: Balancing PD with PK to generate novel therapeutics," *J. Pharm. Sci.*, vol. 97, no. 10, pp. 4167–4183, 2008.

[95] J. Yan, M. Estvez, J. Smith, K. Wang, X. He, L. Wang, and W. Tan, "Dye-doped nanoparticles for bioanalysis," *Nano Today*, vol. 2, no. 3, pp. 44 – 50, 2007.

[96] "Chitin as a biomaterial," in *Polymeric Biomaterials: Medicinal and Pharmaceutical Applications* (S. Dumitriu and V. Popa, eds.), 2013.

[97] L. Nair and C. Laurencin, "Biodegradable polymers as biomaterials," *Prog. Polym. Sci.*, vol. 32, no. 8-9, pp. 762 – 798, 2007.

[98] L. Berger and R. Weiser, "The beta-glucosaminidase activity of egg-white lysozyme," *Biochim. Biophys. Acta*, vol. 26, no. 3, pp. 517–521, 1957.

[99] E. Khor, "Chitin as a biomaterial," in *Chitin: Fulfilling a biomaterials promise* (E. Khor, ed.), 2001.

[100] G. I. A. (GIA), "Global chitin derivatives market to reach US$63 billion by 2015." `www.prweb.com/releases/chitin_chitosan/derivatives_glucosamine/prweb4603394.htm`.

[101] F. Quemeneur, M. Rinaudo, and B. Pepin-Donat, "Influence of molecular weight and ph on adsorption of chitosan at the surface of large and giant vesicles," *Biomacromolecules*, vol. 9, no. 1, pp. 396–402, 2008.

[102] "Synthesis of a fluorescent chitosan derivative and its application for the study of chitosan-mucin interactions," *Carbohyd. Polym.*, vol. 38, no. 2, pp. 99 – 107, 1999.

[103] M. Roberts, M. Bentley, and J. Harris, "Chemistry for peptide and protein pegylation," *Adv. Drug Deliver. Rev.*, vol. 54, pp. 459–476, 2002.

[104] A. Pavinatto, F. J. Pavinatto, A. Barros-Timmons, and N. Osvaldo, "Electrostatic interactions are not sufficient to account for chitosan bioactivity," *ACS Appl. Mater. Interfaces*, vol. 2, no. 1, pp. 246–251, 2010.

[105] F. J. Pavinatto, A. Pavinatto, L. Caseli, D. S. dos Santos, T. M. Nobre, M. E. D. Zaniquelli, and O. N. Oliveira, "Interaction of chitosan with cell membrane models at the air-water interface," *Biomacromolecules*, vol. 8, no. 5, pp. 1633–1640, 2007.

[106] F. J. Pavinatto, L. Caseli, A. Pavinatto, D. S. dos Santos, T. M. Nobre, M. E. D. Zaniquelli, H. S. Silva, P. B. Miranda, and O. N. de Oliveira, "Probing chitosan and phospholipid interactions using langmuir and langmuir-blodgett films as cell membrane models," *Langmuir*, vol. 23, no. 14, pp. 7666–7671, 2007.

[107] D. Chattopadhyay and M. Inamdar, "Aqueous behaviour of chitosan," *International Journal of Polymer Science*, 2010.

[108] N. Fang, V. Chan, H. Mao, and K. W. Leong, "Interactions of phospholipid bilayer with chitosan: Effect of molecular weight and ph," *Biomacromolecules*, vol. 2, no. 4, pp. 1161–1168, 2001.

[109] G. Tsai and W. Su, "Antibacterial activity of shrimp chitosan against escherichia coli," *J. Food Protect.*, vol. 62, no. 3, pp. 239–243, 1999.

[110] B. Baldrick, "The safety of chitosan as a pharmaceutical excipient," *Regul. Toxicol. Pharm.*, vol. 56, no. 3, pp. 290 – 299, 2010.

[111] F. Danhier, O. Feron, and V. Prat, "To exploit the tumor microenvironment: Passive and active tumor targeting of nanocarriers for anti-cancer drug delivery," *J. Control. Release.*, vol. 148, no. 2, pp. 135 – 146, 2010.

[112] M. Terrones, "Sceince and technology of the twenty-first century: synthesis, properties, and applications of carbon nanotubes," *Ann. Rev. Mater. Res.*, vol. 33, pp. 419–501, 2003.

[113] B. Kairdolf, A. Smith, T. Stokes, M. Wang, A. Young, and S. Nie, "Semiconductor quantum dots for bioimaging and biodiagnostic applications," *Annu. Rev. Anal. Chem.*, vol. 6, pp. 143–162, 2013.

[114] C. W. Evans, M. J. Latter, D. Ho, S. A. M. A. Peerzade, T. D. Clemons, S. A. Fitzgerald, M.and Dunlop, and K. S. Iyer, "Multimodal and multifunctional stealth polymer nanospheres for sustained drug delivery," *New J. Chem.*, vol. 36, pp. 1457–1462, 2012.

[115] D. Owens and N. Peppas, "Opsonization, biodistribution, and pharmacokinetics of polymeric nanoparticles," *Int. J. Pharm.*, vol. 307, no. 1, pp. 93 – 102, 2006.

[116] A. Parodi, N. Quattrocchi, A. L. van de Ven, C. Chiappini, M. Evangelopoulos, J. O. Martinez, B. S. Brown, I. K. Khaled, S. Z. andYazdi, M. V. Enzo, L. Isenhart, M. Ferrari, and E. Tasciotti, "Synthetic nanoparticles functionalized with biomimetic leukocyte membranes possess cell-like functions," *Nat. Nanotechnol.*, vol. 8, pp. 61–68, 2003.

[117] H. Koo, M. S. Huh, I. Sun, S. H. Yuk, K. Choi, K. Kim, and I. Kwon, "In vivo targeted delivery of nanoparticles for theranosis," *Accounts Chem. Res.*, vol. 44, no. 10, pp. 1018–1028, 2011.

[118] K. Choi, K. Min, J. Na, K. Choi, K. Kim, J. Park, I. C. Kwon, and S. Jeong, "Self-assembled hyaluronic acid nanoparticles as a potential drug carrier for cancer therapy: synthesis, characterization, and in vivo biodistribution," *J. Mater. Chem.*, vol. 19, pp. 4102–4107, 2009.

[119] D. Lee, R. Lockey, and S. Mohapatra, "Folate receptor-mediated cancer cell specific gene delivery using folic acid-conjugated oligochitosans," *J. Nanosci. Nanotechno.*, vol. 6, no. 9-1, 2006", pages =.

[120] J. Benesch and Tengvall.P., "Blood protein adsorption onto chitosan," *Biomaterials*, vol. 23, no. 12, pp. 2561 – 2568, 2002.

[121] J. J. Wang, Z. W. Zeng, R. Z. Xiao, T. Xie, G. L. Zhou, X. Zhan, and S. L. Wang, "Recent advances of chitosan nanoparticles as drug carriers," *Int. J. Nanomed.*, vol. 2011, pp. 765–774, 2011.

[122] H. Peniche and C. Peniche, "Chitosan nanoparticles: a contribution to nanomedicine," *Polym. Int.*, vol. 60, no. 6, pp. 883–889, 2011.

[123] J. Park, G. Saravanakumar, K. Kim, and I. Kwon, "Targeted delivery of low molecular drugs using chitosan and its derivatives," *Adv. Drug Deliver. Rev.*, vol. 62, no. 1, pp. 28 – 41, 2010.

[124] A. Bernkop-Schnurch and S. Dnnhaupt, "Chitosan-based drug delivery systems," *Eur. J. Pharm. Biopharm.*, vol. 81, no. 3, pp. 463 – 469, 2012.

[125] K. Bowman and K. Leong, "Chitosan nanoparticles for oral drug and gene delivery," *Int. J. Nanomed.*, vol. 1, no. 2, pp. 127–128, 2006.

[126] M. Garcia-Fuente and M. Alonso, "Chitosan-based drug nanocarriers: Where do we stand?," *J. Control. Release.*, vol. 161, no. 2, pp. 496 – 504, 2012.

[127] W. Fan, W. Yan, Z. Xu, and H. Ni, "Formation mechanism of monodisperse, low molecular weight chitosan nanoparticles by ionic gelation technique," *Colloid. Surface B*, vol. 90, no. 0, pp. 21 – 27, 2012.

[128] A. Nasti, N. Zaki, P. Leonardis, S. Ungphaiboon, P. Sansongsak, M. Rimoli, and N. Tirelli, "Chitosan/tpp and chitosan/tpp-hyaluronic acid nanoparticles: Systematic optimisation of the preparative process and preliminary biological evaluation," *Pharm. Res.*, vol. 26, no. 8, pp. 1918–1930, 2009.

[129] X. Shu and K. Zhu, "A novel approach to prepare tripolyphosphate/chitosan complex beads for controlled release drug delivery," *Int. J. Pharm.*, vol. 201, no. 1, pp. 51 – 58, 2000.

[130] X. Shu and K. Zhu, "The influence of multivalent phosphate structure on the properties of ionically cross-linked chitosan films for controlled drug release," *Eur. J. Pharm. Biopharm.*, vol. 54, no. 2, pp. 235 – 243, 2002.

[131] A. Almond and J. K. Sheehan, "Predicting the molecular shape of polysaccharides from dynamic interactions with water," *Glycobiology*, vol. 13, no. 4, pp. 255–264, 2003.

[132] B. Zinder, J. Hertz, and H. R. Oswald, "Kinetic studies on the hydrolysis of sodium tripolyphosphate in sterile solution," *Water Res.*, vol. 18, pp. 509–512, 1984.

[133] F. Mi, S. Shyu, S. Lee, and T. Wong, "Kinetic study of chitosan-tripolyphosphate complex reaction and acid-resistive properties of the chitosan-tripolyphosphate gel beads prepared by in-liquid curing method," *J. Polym. Sci. Pol. Phys.*, vol. 37, no. 14, pp. 1551–1564, 1999.

[134] Y. Chen, V. Mohanraj, F. Wang, and H. Benson, "Designing chitosan-dextran sulfate nanoparticles using charge ratios," *AAPS PharmSciTech*, vol. 8, no. 4, pp. 131–139, 2007.

[135] W. Abdelwahed, G. Degobert, S. Stainmesse, and H. Fessi, "Freeze-drying of nanoparticles: Formulation, process and storage considerations," *Adv. Drug Deliver. Rev.*, vol. 58, no. 15, pp. 1688 – 1713, 2006.

[136] F. Franks, "Freeze-drying of bioproducts: putting principles into practice," *Eur. J. Pharm. Biopharm.*, vol. 45, no. 3, pp. 221 – 229, 1998.

[137] L. Crowe, D. Reid, and J. Crowe, "Is trehalose special for preserving dry biomaterials?," *Biophys. J.*, vol. 71, 1996.

[138] R. Fernandez-Urrusuno, D. Romani, P. Calvo, J. Vila-Jato, and M. Alonso, "Development of a freeze-dried formulation of insulin-loaded chitosan nanoparticles. in vitro characterization and evaluation of insulin nasal absorption in vivo," *STP Pharma. Sci.*, vol. 9, pp. 429–436, 1999.

[139] T. Lopez-Leon, E. Carvalho, B. Seijo, and J. Ortega-Vinuesa, "Physicochemical characterization of chitosan nanoparticles: electrokinetic and stability behavior," *J. Colloid. Interf. Sci.*, vol. 283, no. 2, pp. 344 – 351, 2005.

[140] F. Andrade, F. Goycoolea, D. Chiappetta, and J. Neves, "Chitosan-grafted copolymers and chitosan-ligand conjugates as matrices for pulmonary drug delivery," *International Journal of Carbohydrate Chemistry*, vol. 2011, no. 4, 2011.

[141]

[142] H. Jonassen, A. Kjoniksen, and M. Hiorth, "Effects of ionic strength on the size and compactness of chitosan nanoparticles," *Colloid. Polym. Sci.*, vol. 290, no. 10, pp. 919–929, 2012.

[143] M. Huang, E. Khor, and L. Lim, "Uptake and cytotoxicity of chitosan molecules and nanoparticles: effects of molecular weight and degree of deacetylation," *Pharm. Res.*, vol. 21, no. 2, pp. 344–353, 2004.

[144] A. Blight and R. Borgens, "Morphometric analysis of a model of spinal cord injury in guinea pigs, with behavioral evidence of delayed secondary pathology," *J. Neurosurg.*, vol. 103, no. 2, pp. 156 – 171, 1991.

[145] B. Juurlink and P. Paterson, "Review of oxidative stress in brain and spinal cord injury: suggestions for pharmacological and nutritional management strategies," *J. Spinal Cord Med.*, vol. 21, pp. 309–334, 1998.

[146] F. Facchinetti, V. Dawson, and T. Dawson, "Free radicals as mediators of neuronal injury," *Cell. Mol. Neurobiol.*, vol. 18, no. 6, pp. 667–682, 1998.

[147] L. Wood, P. Gibson, and M. Garg, "Biomarkers of lipid peroxidation, airway inflammation and asthma," *Eur. Respir. J.*, vol. 21, no. 1, pp. 177–186, 2003.

[148] Y. Iwata-Ichikawa, E.and Kondo, I. Miyazaki, M. Asanuma, and N. Ogawa, "Glial cells protect neurons against oxidative stress via transcriptional upregulation of the glutathione synthesis," *J. Neurol. Chem.*, vol. 72, no. 6, pp. 2334–2344, 1999.

[149] J. Bains and C. Shaw, "Neurodegenerative disorders in humans: the role of glutathione in oxidative stress-mediated neuronal death," *Brain Res. Rev.*, vol. 25, no. 3, pp. 335 – 358, 1997.

[150] Z. Jia, H. Zhu, J. Li, X. Wang, H. Misra, and Y. Li, "Oxidative stress in spinal cord injury and antioxidant-based intervention," *Spinal Cord*, vol. 50, pp. 264 – 274, 2012.

[151] E. Hall and J. Braughler, "Free radicals in cns injury," *Res. Publ. Assoc. Res. Nerv. Ment. Dis.*, vol. 71, pp. 81 – 105, 1993.

[152] A. Farooqui and L. Horrocks, "Lipid peroxides in the free radical pathophysiology of brain diseases," *Cell. Mol. Neurobiol.*, vol. 18, no. 6, pp. 599–608, 1998.

[153] H. Liu, W. Li, G. Xu, X. Li, X. Bai, P. Wei, C. Yu, and Y. Du, "Chitosan oligosaccharides attenuate hydrogen peroxide-induced stress injury in human umbilical vein endothelial cells," *Pharmacol. Res.*, vol. 59, no. 3, pp. 167 – 175, 2009.

[154] R. Recknagel, E. Glende, and A. Hruszkewycz, "Chemical mechanisms in carbon tetrachloride toxicity," in *Free radicals in biology* (W. Pryor, ed.), 1977.

[155] L. Goodglick and A. Kane, "Membrane perturbation by asbestos fibers and disease," in *Cellular membrane: A key to disease processes* (S. Ohnishi and T. Ohnishi, eds.), 1992.

[156] K. Uchida, "4-hydroxy-2-nonenal: a product and mediator of oxidative stress," *Prog. Lip. Res.*, vol. 42, no. 4, pp. 318 – 343, 2003.

[157] S. A. Baldwin, R. Broderick, D. Osbourne, G. Waeg, D. A. Blades, and S. W. Scheff, "The presence of 4-hydroxynonenal/protein complex as an indicator of oxidative stress after experimental spinal cord contusion in a rat model," *J. Neurosurg.*, vol. 88, no. 5, pp. 874–883, 1998.

[158] "A detailed interpretation of OH radical footprints in a tbp-dna complex reveals the role of dynamics in the mechanism of sequence-specific binding," *J. Mol. Biol.*, vol. 304, no. 1, pp. 55 – 68, 2000.

[159] K. Irani, "Oxidant signaling in vascular cell growth, death, and survival: A review of the roles of reactive oxygen species in smooth muscle and endothelial cell mitogenic and apoptotic signaling," *Circ. Res.*, vol. 87, no. 3, pp. 179–183, 2000.

[160] K. K. Griendling and G. A. FitzGerald, "Oxidative stress and cardiovascular injury: Part i: Basic mechanisms and in vivo monitoring of ros," *Circulation*, vol. 108, no. 16, pp. 1912–1916, 2003.

[161] H. Liu, J. He, W. Li, Z. Yang, Y. Wang, X. Bai, C. Yu, and Y. Du, "Chitosan oligosaccharides protect human umbilical vein endothelial cells from hydrogen peroxide-induced apoptosis," *Carbohyd. Polym.*, vol. 80, no. 4, pp. 1062 – 1071, 2010.

[162] R. Floyd and J. Carney, "Free radical damage to protein and dna: mechanisms involved and relevant observations on brain undergoing oxidative stress.," *Ann. Neurol.*, vol. 32, pp. S22–27, 1992.

[163] Cadenas and Enrique, "Basic mechanisms of antioxidant activity," *Biofactors*, vol. 6, no. 4, pp. 391–397, 1997.

[164] R. Dringen, B. Pfeiffer, and B. Hamprecht, "Synthesis of the antioxidant glutathione in neurons: Supply by astrocytes of cysgly as precursor for neuronal glutathione," *J. Neurosurg.*, vol. 19, pp. 562–569, 1999.

[165] Y. Du, L. Wang, H. Yuan, X. Wei, and F. Hu, "Preparation and characteristics of linoleic acid-grafted chitosan oligosaccharide micelles as a carrier for doxorubicin," *Colloid. Surface B*, vol. 69, no. 2, pp. 257 – 263, 2009.

[166] E. Mendis, M. Kim, N. Rajapakse, and S. Kim, "An in vitro cellular analysis of the radical scavenging efficacy of chitooligosaccharides," *Life Sci.*, vol. 80, no. 23, pp. 2118 – 2127, 2007.

[167] "Self-assembled nanoparticles based on glycol chitosan bearing hydrophobic moieties as carriers for doxorubicin: In vivo biodistribution and anti-tumor activity," *Biomaterials*, vol. 27, no. 1, pp. 119 – 126, 2006.

[168] "Effect of polymer molecular weight on the tumor targeting characteristics of self-assembled glycol chitosan nanoparticles," *J. Control. Release.*, vol. 122, no. 3, pp. 305 – 314, 2007.

[169] D. Arndt-Jovin and T. Jovin, "Fluorescence labeling and microscopy of dna.," *Method. Cell Biol.*, vol. 30, pp. 417–448, 1989.

[170] U. Cevik and T. Dalkara, "Intravenously administered propidium iodide labels necrotic cells in the intact mouse brain after injury," *Cell Death Differ.*, vol. 10, pp. 928–929, 2003.

[171] H. Sawai and N. Domae, "Discrimination between primary necrosis and apoptosis by necrostatin-1 in annexin v-positive/propidium iodide-negative cells," *Biochem. Bioph. Res. Co.*, vol. 411, no. 3, pp. 569 – 573, 2011.

[172] D. Rowitch and A. R. Kriegstein, "Developmental genetics of vertebrate glial-cell specification," *Nature*, vol. 468, pp. 214 – 222, 2010.

[173] S. David and A. Kroner, "Repertoire of microglial and macrophage responses after spinal cord injury," *Nat. Rev. Neurosci.*, vol. 12, pp. 388 – 399, 2011.

[174] C. Eroglu and B. A. Barres, "Regulation of synaptic connectivity by glia," *Nature*, vol. 468, pp. 223–231, 2010.

[175] B. A. Barres, "The mystery and magic of glia: A perspective on their roles in health and disease," *Neuron*, vol. 60, pp. 430– 440, 2008.

[176] Y. Yin, M. T. Henzl, B. Lorber, T. Nakazawa, T. T. Thomas, F. Jiang, R. Langer, and L. I. Bnowitz, "Oncomodulin is a macrophage-derived signal for axon regeneration in retinal ganglion cells," *Nat. Neurosci.*, vol. 9, pp. 843 – 852, 2006.

[177] "Macrophage polarization in tumour progression," *Semin. Cancer Biol.*, vol. 18, no. 5, pp. 349 – 355, 2008.

[178] K. Horn, S. A. B., A. L. H., N. Rooijen, and J. Silver, "Another barrier to regeneration in the cns: Activated macrophages induce extensive retraction of dystrophic axons through direct physical interactions," *J. Neurosurg.*, vol. 28, pp. 9330–9341, 2008.

[179] V. Bocchini, R. Mazzolla, R. Barluzzi, E. Blasi, and H. Sick, P. Kettenmann, "An immortalized cell line expresses properties of activated microglial cells," *J. Neurosci. Res.*, vol. 31, no. 4, pp. 616–621, 1992.

[180] B. Stansley, J. Post, and K. Hensley, "A comparative review of cell culture systems for the study of microglial biology in alzheimer's disease," *J. Neuroinflamm.*, vol. 9, p. 115, 2012.

[181] D. Liu, J. Liu, and J. Wen, "Elevation of hydrogen peroxide after spinal cord injury detected by using the fenton reaction," *Free Radical Bio. Med.*, vol. 27, no. 3-4, pp. 478 – 482, 1999.

[182] G. Fragoso, A. Martinez-Bermudez, H. Liu, A. Khorchid, S. Chemtob, W. Mushynski, and G. Almazan, "Developmental differences in h2o2-induced oligodendrocyte cell death: role of glutathione, mitogen-activated protein kinases and caspase 3," *J. Neurol. Chem.*, vol. 90, pp. 392–404, 2004.

[183] F. Bao and D. Liu, "Hydroxyl radicals generated in the rat spinal cord at the level produced by impact injury induce cell death by necrosis and apoptosis: protection by a metalloporphyrin," *Neuroscience*, vol. 126, no. 2, pp. 285 – 295, 2004.

[184] M. Crowe, J. Bresnahan, S. Shuman, J. Masters, and M. Beattie, "Apoptosis and delayed degeneration after spinal cord injury in rats and monkeys," *Nat. Med.*, vol. 3, pp. 73–76, 1997.

[185] P. K. Mander, A. Jekabsone, and G. C. Brown, "Microglia proliferation is regulated by hydrogen peroxide from nadph oxidase," *J. Immunol.*, vol. 176, no. 2, pp. 1046–1052, 2006.

[186] D. Liu, J. Liu, D. Sun, and J. Wen, "The time course of hydroxyl radical formation following spinal cord injury: the possible role of the iron-catalyzed haber-weiss reaction.," *J. Neurotrauma.*, vol. 21, pp. 805–816, 2004.

[187] M. Huang, Z. Ma, E. Khor, and L. Lim, "Uptake of fitc-chitosan nanoparticles by a549 cells," *Pharm. Res.*, vol. 19, no. 10, pp. 1488–1494, 2002.

[188] E. Baran, N. Ozer, and V. Hasirci, "In vivo half life of nanoencapsulated L-asparaginase," *J. Mater. Sci. Mater. Med.*, vol. 13, no. 12, pp. 1113–1121, 2002.

[189] R. Duncan, "The dawning era of polymer therapeutics," *Nat. Rev. Drug Discov.*, vol. 2, pp. 347 – 360, 2003.

[190] "The role of solid nanoparticle technology in the parenteral delivery of poorly water-soluble drugs," *Int. J. Pharm.*, vol. 284, pp. 109 – 122, 2004.

[191] S. Stern and S. McNeil, "Nanotechnology safety concerns revisited," *Toxicol. Sci.*, vol. 101, no. 1, pp. 4–21, 2008.

[192] X. Wei, Z. Zhang, and Z. Qian, "Pharmacokinetics and in vivo fate of drug loaded chitosan nanoparticle," *Curr. Drug Metab.*, vol. 13, pp. 364–371, 2012.

[193] J. Grossman and S. McNeil, "Nanotechnology in cancer medicine," *Phys. Today*, vol. 65, pp. 38–42, 2012.

[194] A. Gorle and S. Gattani, "Development and evaluation of ocular drug delivery system," *Pharm. Dev. Technol.*, vol. 15, no. 1, pp. 46–52, 2010.

[195] N. Li, C. Zhuang, M. Wang, X. Sun, S. Nile, and W. Pan, "Low molecular weight chitosan-coated liposomes for ocular drug delivery: In vitro and in vivo studies," *Drug Deliv.*, vol. 19, no. 1, pp. 28–35, 2012.

[196] W. Lai and M. Lin, "Nucleic acid delivery with chitosan and its derivatives," *J. Control. Release.*, vol. 134, pp. 158–168, 3008.

[197] K. Corsi, F. Chellat, L. Yahia, and J. Fernandes, "Mesenchymal stem cells, MG63 and HEK293 transfection using chitosan-dna nanoparticles," *Biomaterials*, vol. 24, no. 7, pp. 1255 – 1264, 2003.

[198] K. Janes, M. Fresneau, and A. Marazuela, "Chitosan nanoparticles as delivery systems for doxorubicin," *J. Control. Release.*, vol. 73, no. 23, pp. 255 – 267, 2001.

VITA

VITA

Bojun Chen was born on January 10, 1984 in Beijing, China. In 2002, she enrolled in Capital Medical University in Beijing, majored in Biomedical Enginneering. She received a Bachelor of Engineering degree in 2006. She was also elected in the post-graduate recommendation for master science program in Capital Medical University in Beijing, majored in Biophysics. She received a Master of Science degree in 2009. In August 2009, she came to the United States to begin her graduate study in Department of Basic Medical Sciences at Purdue University. She joined the family of Center for Paralysis Research in Veterinary Medicine and co-advised by Dr. Borgens and Dr. Li. She focused on the neuroprotective effects of chitosan and chitosan nanoparticles on spinal cord injury. She expects to graduate from Purdue with a Ph.D. degree in December 2013.